Membranes for virus removal by size exclusion

Dissertation

zur Erlangung des akademischen Grades eines

Doktors der Naturwissenschaften

– Dr. rer. nat. –

vorgelegt von

Peter Kosiol

geboren in Oppeln, Polen

Lehrstuhl für Technische Chemie II

der

Universität Duisburg-Essen

2018

Die vorliegende Arbeit wurde im Zeitraum von Dezember 2013 bis Januar 2018 im Arbeitskreis von Prof. Dr. Mathias Ulbricht am Lehrstuhl für Technische Chemie II der Universität Duisburg-Essen in Kooperation mit der Fa. Sartorius-Stedim Biotech GmbH angefertigt.

Gutachter: Prof. Dr. Mathias Ulbricht, Prof. Dr.-Ing. Stefan Panglisch
Vorsitzender: Prof. Dr. Rainer Meckenstock
Disputation am: 05.07.2018

Hiermit versichere ich, dass ich die vorliegende Arbeit mit dem Titel

“Membranes for virus removal by size exclusion”

selbst verfasst und keine außer den angegebenen Hilfsmitteln und Quellen benutzt habe, und dass die Arbeit in dieser und ähnlicher Form noch bei keiner anderen Universität eingereicht wurde.

Göttingen, 29.01.2018

Danksagung

Als Erstes gilt mein besonderer Dank Prof. Dr. Mathias Ulbricht für die anregenden Diskussionen und eine stets hervorragende Betreuung während meiner Promotion. Desweiteren möchte ich Prof. Dr.-Ing. Stefan Panglisch für die Übernahme des Zweitgutachtens sowie Prof. Dr. Rainer Meckenstock für die Übernahme des Vorsitzes der Prüfungskommission danken.

Ein ganz herzlicher Dank gilt Dr. Björn Hansmann und Dr. Volkmar Thom von der Firma Sartorius, die mir eine Promotion mit einem spannenden Thema im Unternehmen ermöglicht haben und mir stets mit Rat und Tat zur Seite standen.

Außerdem danke ich all meinen Kollegen von der Firma Sartorius für ein hervorragendes Arbeitsklima, viel Spaß und eine schöne Zeit im Labor. Ganz besonders möchte ich dabei Swetlana Macht, Magnus Warnke und Ralf Wittmeier aus der Virusfiltrationsgruppe sowie Miriam Börger, Pia-Vanessa Lehman, Andreas Schwerdt und Tabea Streil aus dem Phagenlabor danken. Ebenso danke ich den übrigen Doktoranden und Studenten aus dem Arbeitskreis Ulbricht sowie von Sartorius, darunter Alexander Helling, Matthias Müller und Jan Schwellenbach, für die zahlreichen und anregenden Diskussionen.

Einen ganz besonderen Stellenwert hatten für mich die Studenten, die ich im Rahmen von Praktika und Abschlussarbeiten betreuen durfte. Dafür möchte ich Jakob Brandt, Jannik Dippel, Catharina Kahrs, Jörn Kietz, Marie-Theres Müller, Phillip Schodder und Nicole Seehase für ihren besonderen Einsatz meinen Dank aussprechen.

Abschließend danke ich meiner Familie und insbesondere Alexandra Kentsch, die mich stets unterstützt und für die nötige Ablenkung und Ausgleich gesorgt haben.

Kurzzusammenfassung

Moderne biopharmazeutische Prozesse schließen eine umfassende Strategie zur Virusabreicherung ein, um die Gefahr von Viruskontaminationen von Arzneimitteln zu verringern und damit die Sicherheit von Patienten zu gewährleisten. Neben der Testung von Ausgangsmaterialien und der finalen Arznei, ist es für Herstellprozesse basierend auf Säugetierzelllinien von Behördenseite erforderlich, dass mindestens zwei orthogonale Prozessschritte für die Inaktivierung oder Abreicherung von endogenen bzw. zufälligen Viren implementiert sind. Über die letzten drei Dekaden hinweg hat sich die auf Größenausschluss basierende Virusfiltration unter Verwendung von porösen Membranen im Dead-End-Betrieb als Industriestandard etabliert.

Membranen zur Virusfiltration bestehen aus komplexen porösen Strukturen, die in der Lage sind kleine Viren, wie das Parvovirus mit einem Durchmesser von 18-24 nm, mindestens zu 99.99 % abzureichern. Gleichzeitig ist eine Transmission von typischen Produktspezies, zu denen monoklonale Antikörper vom IgG-Typ gehören und Durchmesser von 9-12 nm aufweisen, von mehr als 95 % erforderlich. Aus diesen ähnlichen Größenordnungen resultiert eine besonders anspruchsvolle Trennaufgabe, die diese Membranen zu erfüllen haben.

Neben dem obligatorischen Virusrückhaltevermögen sind aus applikativer Sicht die Wasser- bzw. Pufferpermeabilität sowie die Robustheit gegenüber Verblockung die entscheidenden Eigenschaften von Membranen zur Virusfiltration. Aus materialwissenschaftlicher Perspektive sind diese Eigenschaften eng mit der Porengrößenverteilung in der trennaktiven Schicht, dem Porengrößengradienten entlang der Membrandicke sowie den Charakteristika der Membranoberfläche verbunden.

Im Allgemeinen beschäftigt sich die vorliegende Arbeit mit der Methodenentwicklung sowie der Anwendung dieser Methoden zur Charakterisierung struktureller Membraneigenschaften wie der Porengrößenverteilung und dem Porengrößengradienten. Desweiteren wurde eine Auswahl kommerzieller sowie nicht-kommerzieller Membranen zur Virusfiltration hinsichtlich Virusrückhalt sowie Robustheit gegenüber Verblockung untersucht. Die so ermittelten applikativen Membraneigenschaften werden in der vorliegenden Arbeit ins Verhältnis zu den strukturellen Eigenschaften der Membranen gesetzt. Hieraus werden mechanistische Konzepte zur Wirkungsweise von Membranen zur Virusfiltration insbesondere bezüglich Verblockung und Virusrückhaltung abgeleitet und diskutiert.

Table of contents

1 Introduction

Modern biopharmaceutical processes implement comprehensive virus clearance strategies to minimize the threat of viral contamination of drugs and ensure patient safety. Besides testing of source materials and the finally formulated drug, manufacturing processes based on mammalian cell lines are required by the regulatory agencies to include at least two dedicated orthogonal unit operations for the inactivation or removal of endogenous or adventitious viruses [1]. Throughout the last three decades, size exclusion based virus filtration using porous membranes in dead-end mode has become an industry standard known for its reliability and robustness to clear viruses while not affecting product quality and allowing high product recovery [2–4].

Virus filtration membranes (VFMs) have complex porous structures capable of retaining small viruses such as parvoviruses having 18-24 nm in diameter [1] by at least 99.99 % corresponding to a $\log_{10}$ reduction value (LRV) >= 4. At the same time, typical product molecules like monomeric IgG-type monoclonal antibodies, having diameters of 9-12 nm [5], need to be transmitted by more than 95 %. Exhibiting pore sizes (nominally 20 nm) within the same magnitude of both product and contaminant species renders the separation task that VFMs fulfil intensely sophisticated. For comparison, other size-based unit operations utilizing membranes, such as microfiltration, separate species differing by at least one order of magnitude in hydrodynamic diameter.

This high demand for selectivity renders the development and manufacturing of VFMs a challenging task. Besides the obligatory virus retention performance, the main application relevant performance characteristics of a VFM are the water/buffer permeability and the fouling robustness. From a material scientific perspective, these application characteristics are closely linked to the pore size distribution (PSD) in the separation-active layer (SAL), the pore size gradient (PSG) along the membrane thickness and the characteristics of the membrane surface.

In general, the present thesis focuses on method development and application of analytical techniques capable of determining structural membrane properties such as the PSD and PSG. Further, commercial and non-commercial VFMs are characterized by their virus retention performance and fouling robustness using representative virus models and feed streams.

Particular attention is paid on relating membrane properties and application performances. Thereby, mechanistical concepts for the mode of operation are derived and discussed.

In **paper 1** (cf. section 3.1), a technique utilizing the filtration of gold nanoparticles (GNPs) for the determination of PSDs for a set of commercial and non-commercial VFMs is presented and discussed. Further, these results on the PSDs are related towards the virus retention performance of the VFMs investigated.

Paper 2 (cf. section 3.2) focuses on PSGs, also determined by using GNPs, of a very similar set of VFMs. The fouling mechanism of a model antibody containing feed stream is investigated and the fouling robustness of the VFMs using this antibody is related to their PSGs.

Paper 3 (cf. section 3.3) provides a comprehensive Design of Experiment (DoE)-based investigation on the virus retention mechanisms as a function of membrane characteristics as well as solution and process conditions. Furthermore, filtration results are supported by biophysical characterization of the virus and non-virus containing feed streams with respect to particle size distributions.

1.1 Current scientific knowledge

1.1.1 Threat of virus contaminations and state-of-the-art virus clearance in biopharmaceutical industry

Biopharmaceutical drugs derived from mammalian cell cultures (e.g. recombinant proteins, monoclonal antibodies) or human plasma (e.g. coagulation factors, intravenous immunoglobulin (IVIG)) suffer from a potential risk of virus contamination [1,2,6]. Such contaminations can originate from contaminated master cell banks (endogenous virus) or be introduced by contaminated source materials (adventitious virus) [1]. Although few events of virus contaminations were reported in the last decades and detected in time prior to administering these drugs to patients [7,8], these incidents had far reaching consequences for the implicated pharmaceutical companies and their patients. Two reported contamination events with Vesivirus 2117 at Genzyme in 2008 and 2009 led to shortages of the two key drugs Cerezyme and Fabrazyme caused by plant shutdowns and extensive decontamination processes [7,9,10]. Patients were affected by rationing of these drugs, which in case of Cerezyme, the only drug available for treatment of Gaucher disease, had an impact on patient treatment. Consequences were of disastrous extent for Genzyme. Besides loss of patient confidence, economic damage ran into hundreds of millions of dollars und put the company under close supervision by the regulatory agencies [10].

To mitigate risks of virus contaminations that might lead to far reaching consequences, guidelines by the health authorities [1,2,11] require comprehensive viral clearance strategies. These strategies consist of testing of the master cell banks or blood and plasma donors, raw materials, unprocessed and processed bulk material for presence of viruses. In addition, downstream processes are required to incorporate at least two dedicated orthogonal unit operations for the removal of viruses and/or inactivation of viral infectivity. The capabilities of each virus removal/inactivation unit operation need to be demonstrated during process development stage prior to manufacturing. For this purpose, down-scale virus clearance studies are conducted using the individual process intermediates under process related conditions together with representative viruses. According to FDA guideline ICH Q5A, viruses "... should be chosen to resemble viruses which may contaminate the product and to represent a wide range of physico-chemical properties in order to test the ability of the system to eliminate viruses in general" [1]. Therefore, viruses typically selected for clearance studies include large, enveloped viruses such as murine leukemia virus (MuLV, 80-110 nm, retrovirus)

as accepted model for endogenous viruses and small, non-enveloped viruses such as parvoviruses (18-24 nm) [1] as worst case for inactivation and filtration trials. Unit operations applied for virus clearance can be divided into techniques based on inactivation and removal. These unit operations differ with respect to their efficacy and robustness towards different types of viruses. Virus inactivation approaches by solvent/detergent, low pH and high temperature treatment suffer from limited efficacy against non-enveloped viruses [2,12]. Virus removal techniques based on interactions such as ion-exchange chromatography lack robustness with respect to process conditions and efficacy can be highly dependent on the individual virus species and its surface characteristics [2,12]. However, size exclusion based virus removal using VFMs is known as an effective and robust unit operation for virus clearance. This results from its capability of removing all viruses independent of their surface characteristics and including challenging small viruses of high resistance towards physico-chemical treatment [2,12]. Most recently, new VFMs became commercially available for application in upstream processing in order to prevent entry of viruses into the bioreactor by contaminated cell culture media [13].

1.1.2 History and application of virus filtration membranes

From technological perspective, polymeric VFMs with complex networks of interconnected pores emerged in the late 1980s/early 1990s from significantly older, already existing types of membranes such as dialysis, ultrafiltration and microfiltration membranes [14,15].

In 1989, data was published proving the capability for substantial size exclusion based retention of LRV >= 6 for human immunodeficiency virus (80-130 nm [2]) by porous, polymeric membranes resulting in no detectable infectivity in the filtrates while exhibiting significant transmission of albumin and γ-globulin [14]. The same year, these cellulosic hollow fiber membranes were commercialized by Asahi Chemical Ind. Co. Ltd., a company with focus on dialysis membranes, under the trademark Planova™ for virus filtration of pharmaceutical blood and plasma products [14]. Related to dialysis membranes, such membranes are characterized by a sponge-like pore structure showing a rather shallow PSG, consisting of a multitude (100-200) of retentive pore layers in the SAL (Fig. 1, left) [14,16].

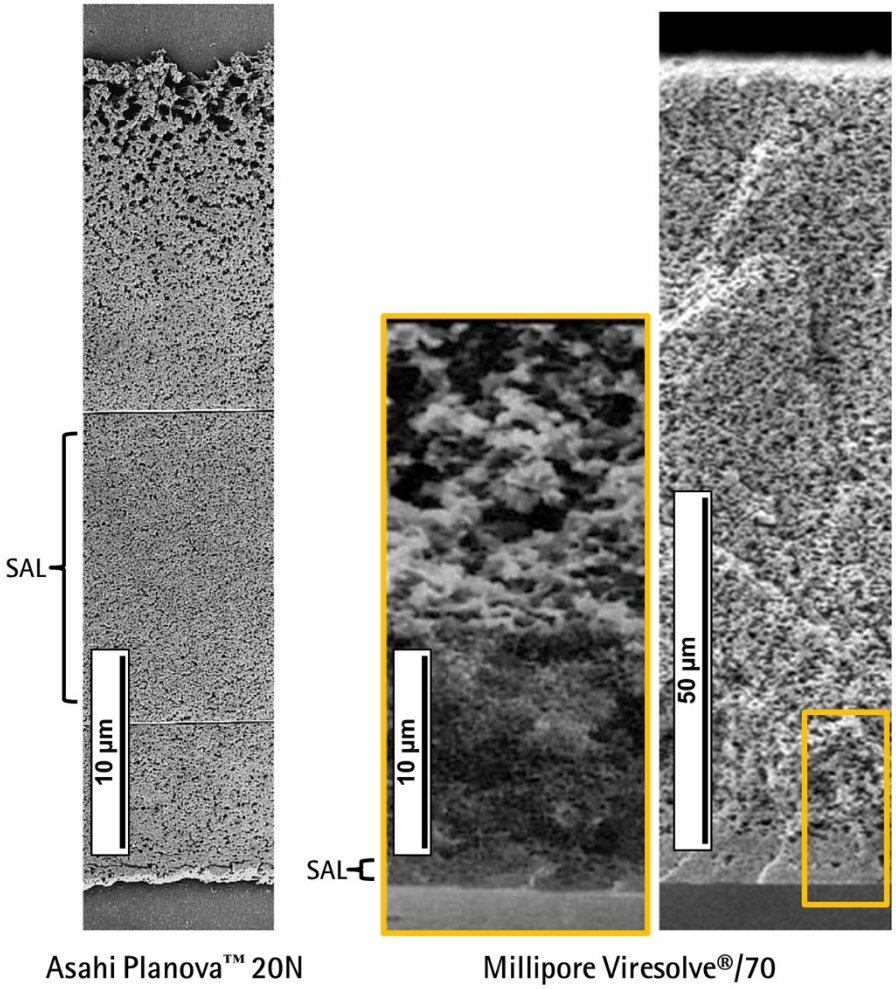

Fig. 1. Scanning electron microscopy images of cross-sections of early VFMs Asahi Planova™ 20N (left) and Millipore Viresolve®/70 (middle and right) adapted from [15,17].

A very different approach was taken by Millipore Corp. in 1992, developing VFMs derived from ultrafiltration membranes (UFMs) under the Viresolve® trademark [15]. Pore structures are sponge-like and exhibit steep PSGs with a thin, skin-like SAL (Fig. 1, middle and right). Special considerations have been taken by Millipore Corp. to reduce the presence of abnormally large pores (defects) in the SAL, which were attributed to be responsible to low retention performance of "typical" UFMs [15]. Also, in order to improve fouling robustness, these membranes made of polyvinylidene fluoride (PVDF) incorporated a surface modification. As unique feature, this membrane was developed for tangential flow filtration (TFF) for which the membrane was oriented with the SAL facing upstream towards the feed (Fig. 2, right).

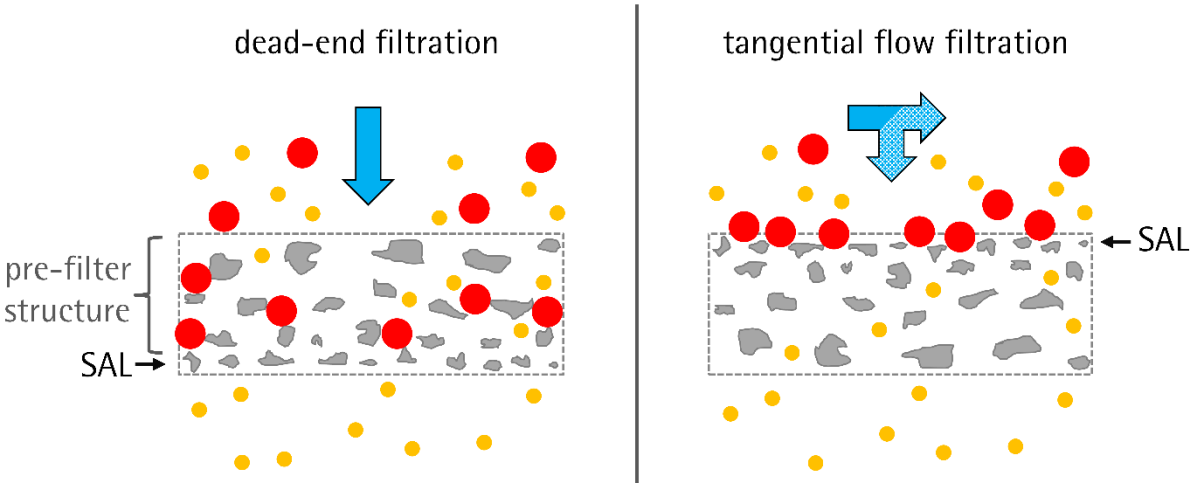

Fig. 2. Schematic illustration of dead-end (left) and tangential flow filtration (right). Blue arrows indicate the flow direction.

Today, VFMs are developed and manufactured by Asahi Kasai Medical, Merck-Millipore, Pall and Sartorius-Stedim Biotech and made from polyethersulfone (PES), PVDF and regenerated cellulose (RC) by phase inversion processes. For purpose of fouling robustness, PES and PVDF VFMs are typically surface modified by proprietary techniques.

VFMs are often classified by the virus size or type of virus they have to retain. Early VFMs were developed to retain large viruses > 50 nm such as retroviruses (80-110 nm), where the demand for selectivity was moderately high [18]. With further improvements of selectivity, small virus retentive membranes became available, capable of retaining all viruses > 18 nm like parvoviruses (18-24 nm) as worst-case model [4]. While providing high selectivity, VFMs associated to the first generation of small virus retentive membranes, developed before the early 2000s, were reported to lack retention robustness and occasionally result in significant parvovirus breakthroughs [18,19]. Retention robustness was significantly improved for the recent second generation. Often, small virus retentive membranes, nominally being rated as 20 nm filters, are denoted as parvovirus retentive VFMs.

Furthermore, some of the early VFMs were intended for use in TFF mode. Single-use VFMs operated in dead-end mode have become industry standard due to advantages such as ease of use, ease of validation and economics (Fig. 2, left) [20]. For reasons of fouling robustness, all VFMs have a more or less distinct PSG. In case of VFMs used in dead-end mode, membranes are oriented with the SAL away from the feed. In such orientation the porous structure before the SAL can act as pre-filter protecting the SAL from fouling (Fig. 2, left) [21].

In a downstream process virus filtration is typically located close to end of the process before the final concentration and buffer exchange (UF/DF), where the process intermediate is already of high purity and fouling is minimized (Fig. 3) [22].

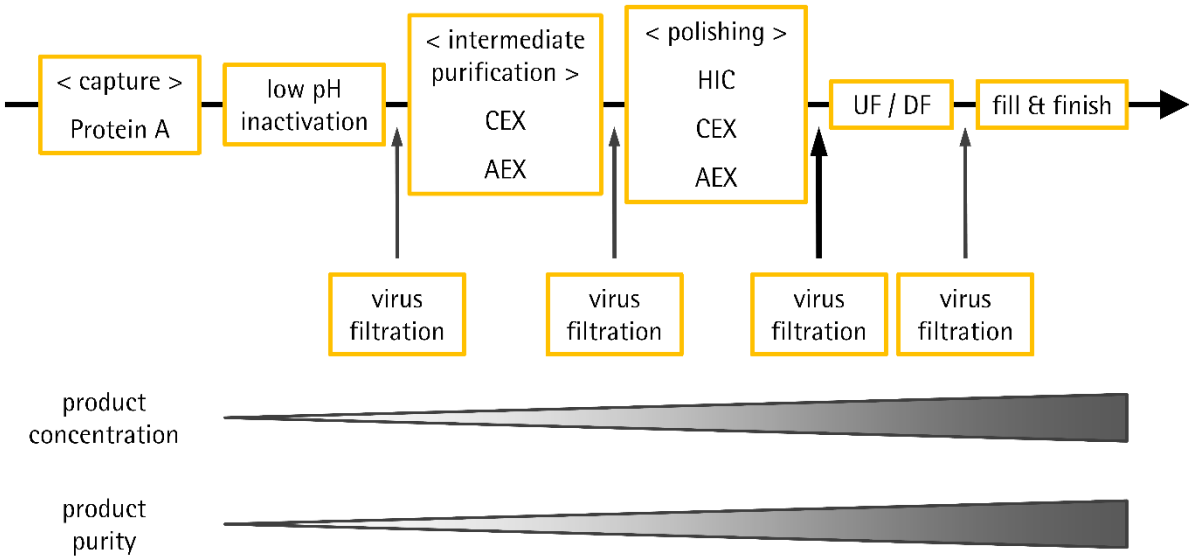

Fig. 3. Conventional sequence of unit operations in downstream antibody production including typical positions for the virus filtration unit operation adapted from [22].

1.1.3 Significance and characterization of the virus filtration membrane structure

Porous membranes with complex 3-dimensional structures of interconnected pores can be characterized with respect to their material properties such as structure and surface properties as well as by their application performance such as permeability, virus retention and fouling robustness (Fig. 4).

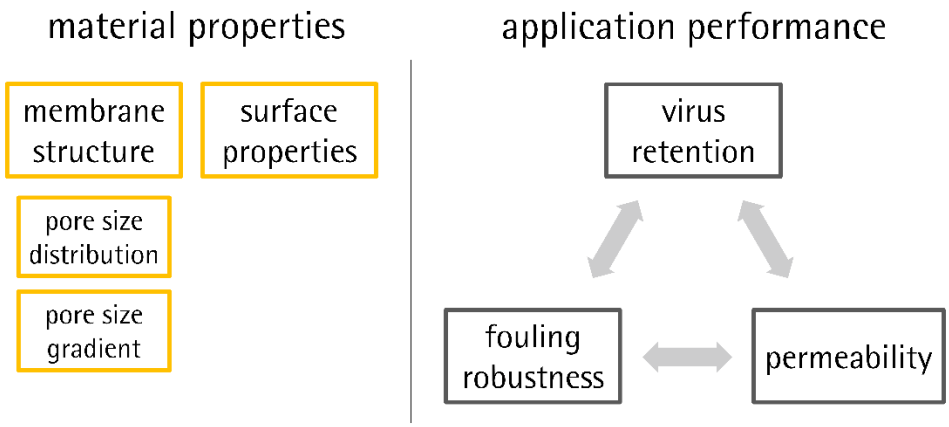

Fig. 4. Overview over most relevant membrane properties and application performance characteristics.

Today it is well accepted that size exclusion is the primary separation mechanism of VFMs, although interactions are discussed in literature to be potentially contributing [4]. Therefore, this thesis focuses on the development and application of techniques specifically applicable for determination of structural properties of VFMs. Special focus is paid on the determination of pore sizes with respect to the PSD within the SAL as well as the PSG along the membrane thickness, also in literature referred to as membrane symmetry. More general and comprehensive literature addressing membrane characterization including surface properties can be found elsewhere [23–26].

Pore size distribution

Size exclusion has proven to facilitate the necessary high selectivity for separation of viruses and biopharmaceutical product molecules and is therefore considered to be mainly dependent on the PSD in the SAL of the membrane [4]. Such a high selectivity is achieved by a narrow and defined PSD, which can typically be well described by a log-normal distribution function [27,28]. In comparison to other membranes used in downstream processing such as UFMs, VFMs are assumed to have a very narrow PSD [29,30]. Also in contrast to UFMs, the SAL of a VFM usually consists of a multitude of pore layers which reduces the risk of few abnormally large pores causing severe loss in virus retention performance [17,31,32]. While the first generation of parvovirus VFMs has suffered from low robustness regarding virus retention [32], occasionally exhibiting severe parvovirus breakthrough, the latest second generation of VFMs has proven significantly increased retention robustness [19].

A major challenge to link membrane structure properties of very different VFMs to their performance properties is the lack of material independent techniques to characterize membrane pores in the size range of 5-50 nm. Deeper knowledge of structural properties of VFMs could provide the basis for developing a better mechanistic understanding of both, virus retention and fouling behaviour.

Well-established displacement techniques for determination of PSDs within the SAL like gas-liquid displacement porometry (GLDP) as well as mercury porosimetry suffer from severe limitations. Required pressures for phase displacement are too high (>> 10 bar) for polymeric 20 nm rated VFMs and typically lead to compaction and alteration of the pore structure during the measurement [33].

Liquid-liquid displacement porometry (LLDP), a more recent displacement technique, utilizes the lower interfacial tension between two liquids compared to a typical interfacial tension between a gas and a liquid phase, resulting in lower applied pressures required for displacement. An illustration of the LLDP procedure is given in Fig. 5.

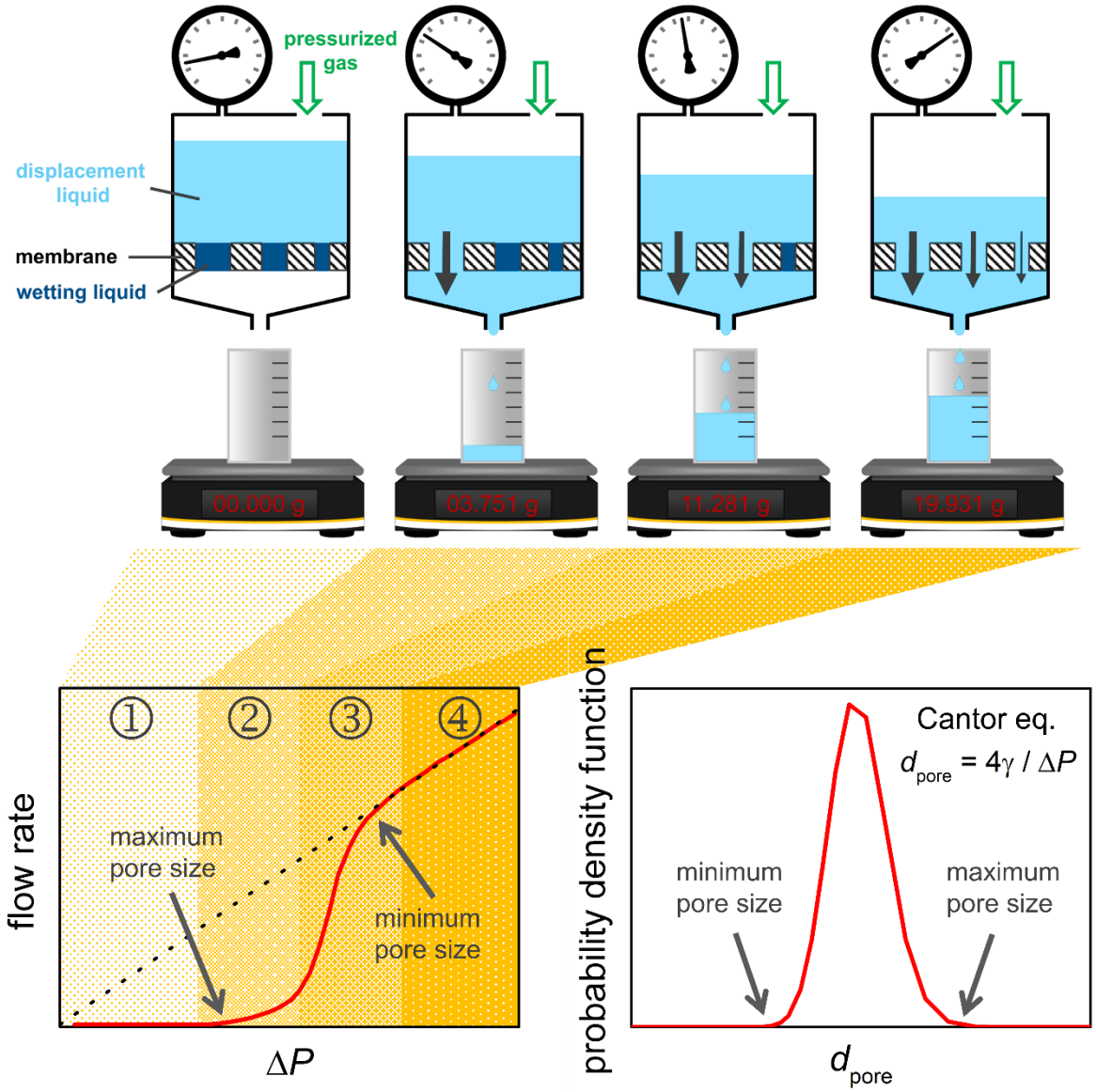

Fig. 5. Schematic illustration of the LLDP procedure (top), plot of typical measurement data (bottom left) and resulting pore size distribution (bottom right). The Cantor equation was utilized to translate the transmembrane pressure ΔP into a pore diameter d_{pore} by using the interfacial tension γ.

Due to the lower pressures applied, LLDP has been demonstrated to be applicable to VFMs [27,34]. The two studies showed a correlation between LLDP results and virus retention for homologous VFMs, differing only in pore size. However, by applying the same procedure to

different VFMs with respect to material, surface chemistry and PSG, Giglia et al. [27] observed deviations from the previously obtained correlation with regard to virus retention. Although being applicable to VFMs in general, the strength of LLDP is to determine PSDs of homologous membranes only differing with respect to the PSD within the SAL. Comparative LLDP studies of VFMs made from different materials, with different pore size gradients and surface properties are challenging for various reasons [35]. Typical 2-phase systems utilized for LLDP consist of water/alcohol [36] or water/polyethylene glycol/ammonium sulfate [37] mixtures. Alcohol containing systems can cause significant swelling of PES membranes leading to erroneous results [38] or even structural damaging of the membrane [39] while other materials like PVDF exhibit only negligible swelling with the same alcohols. As polyethylene glycol is known to strongly interact with PES [40], measured pore sizes might not be accurate and might be dependent on contact time of the membrane with the polymer-rich phase. In addition to the variation of membrane base materials, VFMs usually are surface modified exhibiting different surface chemistries, depending on the manufacturer and the specific modification methods used [4]. This leads to additional interactions between the membranes and the 2-phase systems, making interpretations of results for a variety of VFMs difficult. LLDP can also suffer from low reproducibility for identifying the maximum pore size, caused by measuring flow rates significantly above the base line flow rate already at pressures much below the expected bubble-point of the individual membrane [36]. This is especially relevant as the maximum pore size, in contrast to the mean and minimum pore size, was found to be the most predictive result from LLDP towards virus retention [34]. In a previous study, the correlation between maximum pore size determined by LLDP and virus retention using *Pseudomonas aeruginosa* bacteriophage PP7 as model virus for a variety of commercial VFMs was found to be quite low as depicted in Fig. 6 (R^2 = 0.33) [35].

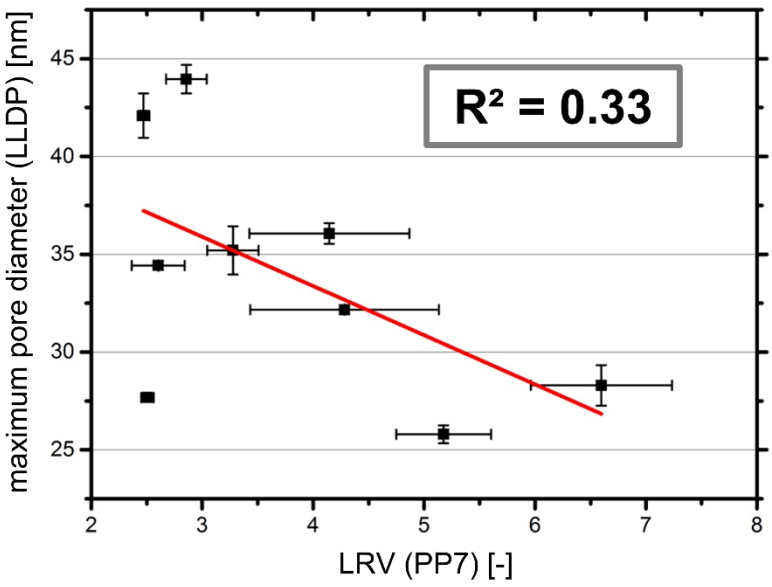

Fig. 6. Correlation of maximum pore diameter determined by LLDP with virus retention reproduced from [35].

Although scanning electron microscopy (SEM) is successfully applied for the determination of pore sizes in the range of VFMs, quantitative applications are mostly limited to track-etched membranes or other membranes, having the separation-active pores visible on the outermost membrane surface [36]. The SAL of VFMs is often located deeper within the membrane structure, necessitating the preparation of cross-sections, which on the other hand can cause artefacts (e.g. by compaction or smearing). In addition, the measurement of pore sizes by image analysis of 2-dimensional pictures is challenging, as VFMs have complex pore networks. A different approach is based on retention of solutes of known size in course of filtration experiments to gain insights into PSDs. Typical solutes can be linear, branched or circular polymers (e.g. dextran [41–43], polyethylene glycol/polyethylene oxide [43–45], deoxyribonucleic acid (DNA) [46]) or rigid spherical particles (e.g. inorganic nanoparticles made from noble metals [47–49]). While the application of linear polymers, such as dextrans, to determine PSDs has become a standard technique for UFMs, results obtained for VFMs are more difficult to interpret, as the results are strongly dependent on PSGs and membrane orientation, which the authors contributed to internal concentration polarization [41]. Susanto et al. also observed and discussed adsorption of dextrans on PES membranes, leading to membrane fouling, i.e. flux decline and changed retention [50]. It has been further demonstrated that circular plasmid DNA with 350 nm in hydrodynamic diameter can penetrate pores of 10 nm in size due to stretching of the molecule, an effect which is also

amplified by higher transmembrane pressures, leading to further increased DNA transmission [46]. This effect could also occur to linear polymers that form spherical coil-like structures in solution, leading to inaccurate determination of the largest pore, which is most relevant for virus retention [43]. The “PDA Technical Report No. 41 - Virus Filtration”, a major guideline for virus filtration, states dextran retention not to correlate with virus/phage retention [20].

Rigid spherical particles on the other hand have proven to be highly applicable for examination of virus retentive properties of VFMs. Helling et al. investigated retention properties of microfiltration membranes and VFMs with a set of particles exhibiting different Young’s moduli ranging from < 1.2 MPa for bacteria up to > 310 MPa for bacteriophage PP7 and polystyrene latex beads [51]. They found that for soft particles like bacteria retention can decline with higher transmembrane pressure caused by deformation and squeezing through of the particles. Retention of particles having a significantly higher stiffness like bacteriophage PP7 and latex beads was observed to be constantly high within the investigated pressure range up to 10 bar. Deformation and squeezing through of GNPs with even significantly higher Young’s moduli of 100 GPa [52] during filtrations using VFMs is therefore unlikely. Besides their stiffness, GNPs are commercially available in a wide range of sizes from below 5 nm up to several hundreds of nanometers. The spherical shape, low size dispersity and high optical absorption in the visible spectrum of GNPs are very favourable attributes for solute retention experiments. Depletion of GNPs in a solution in course of filtration experiments can be easily measured up to a LRV of 3 using a standard UV-Vis spectrophotometer. Thus GNPs have been applied in the development of the first commercial VFMs made of RC and used as virus model for filtration experiments [16,48,53]. In biopharmaceutical manufacturing GNPs are used for physical post-use integrity testing of VFMs, as the retention of GNPs correlates with virus retention [20,54]. For integrity testing, however, the retention performance for a single particle size, usually 20 nm for parvovirus retentive VFMs, is determined, which gives only limited insights into the actual PSD of the membrane. Arkhangelsky et al. reported the use of GNPs and silver nanoparticles in separate filtration experiments using different sized particles with various membranes made from cellulose acetate (CA), PES, PVDF, polycarbonate (PC) or ceramics [43,47]. The authors were able to determine PSDs only of some of the membranes tested by using GNPs. They observed limitations of this technique to gain information on the pore structure of membranes made of PES and CA, which was caused by high affinity of the particles towards the specific membrane materials and was related to higher membrane

hydrophobicity. Adsorption of metal nanoparticles, increasing the observed retention efficiency of polymeric membranes and thereby superimposing the size exclusion properties, has also been observed by other groups [49,55,56]. One way to overcome unwanted adsorption of GNPs is the surface functionalization of GNPs using protective ligands. Although some ligands have proven to significantly reduce adsorption of GNPs on certain membrane materials, their efficiency to suppress adsorption is highly specific towards the individual membrane material and therefore not universally applicable [49]. Another way to reduce GNP adsorption was reported by Wei and Liu for the separation of GNPs by size exclusion chromatography, where adsorption of GNPs to the stationary phase has been an issue [57,58]. By addition of an anionic surfactant, namely sodium dodecyl sulfate (SDS), to the mobile phase adsorption was significantly reduced. The authors explained this observation by an interaction between the stationary phase material (polystyrene-divinylbenzene) and SDS. The presence of SDS was claimed to have no significant influence on the particle size. Furthermore a post-use integrity testing procedure for VFMs made from hydrophilized synthetic polymers has been patented using metal nanoparticles in complex solvents comprising of an anionic polymer together with at least one non-ionic surfactant and/or a water-soluble polymer containing a pyrrolidone group in order to reduce interfering adsorption of the nanoparticles [59].

Pore size gradient

In contrast to UFMs, which have thin SALs of single digit microns thickness and support structures having pore sizes that are magnitudes larger compared to the ones within the SALs, VFMs can have thick SALs with up to 30 µm thickness, consisting of a multitude of pore layers, contributing to the high selectivity [17,60,61]. While UFMs have very steep PSGs, commercially available VFMs exhibit a wide range of PSGs from UF-like steep to very shallow (cf. Fig. 1). Some early VFMs on the market were derived from UFMs exhibiting similar membrane structures. For UFMs and UF-like VFMs operated in TFF mode with the SAL facing towards the feed, the support structure acts mainly as mechanical support for the thin SAL and does not contribute to the fouling resistance (cf. Fig. 2, right). Some studies using these early commercial, UF-like structured VFMs, intended for application in TFF mode, investigated the impact of membrane orientation on fouling behaviour [21,62,63]. The authors of these studies found significantly increased performance with respect to fouling resistance when the

membranes were oriented with the SAL facing away from the feed. In such orientation, the mode of operation, either dead-end or TFF, had no impact on fouling robustness. The performance increase was attributed to the porous membrane support structure, acting as a depth pre-filter (cf. Fig. 2, left). This pre-filtration effect protects the SAL from fouling by “trace levels of submicron-sized particles” [62]. Nowadays all commercially available VFMs are used in the orientation with the SAL facing away from the feed. Those VFMs are also designed for dead-end use.

The effectivity of the support structure acting as a pre-filter is highly dependent on the actual PSG. Commercial VFMs having an UF-like steep PSG offer high water permeability. Their thin SAL is the main contributor to the overall hydraulic resistance of the membrane. Due to the steep PSG, only a small section of the membrane in close proximity to the SAL has pore sizes in the range of IgG protein aggregates, which are probably < 40 nm [64], resulting in low depth pre-filter capacities and higher susceptibility towards fouling. Accumulation of foulants being retained by size exclusion closely to the SAL of microfiltration membranes having steep PSGs was visualized by using confocal scanning laser microscopy [65,66]. VFMs with shallow PSGs have typically lower water permeability as a larger part of the membrane structure contributes to the hydraulic resistance. This can increase processing times which negatively impacts the productivity of such VFMs. Apart from that, such membranes are known to often show higher robustness against fouling, which might be attributed to the fact, that a larger part of the membrane structure is capable of retaining the fouling species. Track-etched membranes typically have cylindrical pores and therefore no PSG. Such membranes are very rarely used in biopharmaceutical processes due to their high susceptibility towards fouling with aggregate containing protein feed streams. An overview of commercial VFMs including a very qualitative classification regarding their PSGs (“membrane pore symmetry”) was given by Miesegaes et al. (Table I) [4].

Table I. Marketed VFMs (as of 2013) reproduced from [4].

Filter Vendor	Filter Brand	Virus Target Class[a]	Mode[b]	Membrane Pore Symmetry	Layers	Membrane Chemistry
Millipore	Viresolve NFR	Retro	DFF	Asymmetric	Triple layer	Hydrophilic polyethersulfone (PES)
	Viresolve NFP	Parvo	DFF	Asymmetric	Triple layer	Hydrophilic polyvinylidene fluoride (PVDF)
	Viresolve 70	Parvo	TFF	Asymmetric	Single layer	Hydrophilic PVDF
	Viresolve 180	Retro	TFF	Asymmetric	Single layer	Hydrophilic PVDF
	Viresolve Pro	Parvo	DFF	Asymmetric	Double layer	Hydrophilic PES
Sartorius Stedim Biotech	Virosart CPV	Parvo	DFF	Symmetric	Double layer	Hydrophilic PES
Pall	Ultipor VF grade DV50	Retro	DFF	Symmetric	Triple layer	Hydrophilic acrylate-modified PVDF
	Ultipor VF grade DV20	Parvo	DFF	Symmetric	Double layer	Hydrophilic acrylate-modified PVDF
	Pegasus grade LV6	Retro	DFF	Symmetric	Double layer	Hydrophilic acrylate-modified PVDF
	Pegasus grade SV4	Parvo	DFF	Symmetric	Double layer	Hydrophilic acrylate-modified PVDF
Asahi Kasei	Planova 35N	Retro	DFF/TFF[c]	Asymmetric	Hollow fiber	Hydrophilic cuprammonium regenerated cellulose
	Planova 20N	Parvo	DFF/TFF	Asymmetric	Hollow fiber	Hydrophilic cuprammonium regenerated cellulose
	Planova 15N	Parvo	DFF/TFF	Asymmetric	Hollow fiber	Hydrophilic cuprammonium regenerated cellulose
	Planova BioEX	Parvo	DFF/TFF	Asymmetric	Hollow fiber	Modified PVDF

[a] "Target virus class" can be a subjective concept based on the application and product type (i.e. biotech vs plasma product). Some large virus retentive filters can retain viruses smaller than retroviruses. Consultation with filter vendors is warranted if clearance of a particular virus is a process requirement.
[b] DFF, direct flow filtration; TFF, tangential flow filtration.
[c] Can be configured by end users to run in either mode.

PSGs that exhibit pore sizes reflecting the particle size of foulants could help to utilize a large extent of the total membrane structure to retain fouling species in order to maximize the depth pre-filter capacity while keeping the hydraulic resistance as low as possible achieving highest possible permeability. Determining the PSG is an especially challenging task with view on applicability of methods towards the high diversity of membrane materials and surface chemistries that commercial VFMs exhibit [4].

Utilizing high resolution imaging techniques such as scanning or transmission electron microscopy (SEM/TEM) to investigate membrane cross-sections already provides good qualitative impressions of membrane structures and related PSGs. Quantitative analysis using SEM/TEM is significantly more challenging [67] and often limited to determination of pore sizes on the outermost membrane surface [68] rather than within the inner membrane

structure. Samples of membrane cross-sections need to be prepared carefully by freeze fracturing or microtomy avoiding artefacts that alter the pore structure (e.g. by compaction or smearing). In contrast to track-etched membranes with cylindrical pores, VFMs have a complex sponge-like pore structure with highly interconnected pores. Quantitative image analysis of such structures requires binarization of grayscale images which is a very subjective procedure with resulting pore sizes highly dependent on the individual operator [67]. For the evaluation of two-dimensional images, also simplifications with respect to the definition of the term “pore size” are required. Ziel et al. proposed a computer-aided method to determine PSGs of 0.2 µm rated microfiltration membranes measuring the distances of the pore voids using “equidistant lines parallel to the (outer) membrane surface and perpendicular to the flow direction in the membrane” (= mean free path length) as depicted in Fig. 7 [69].

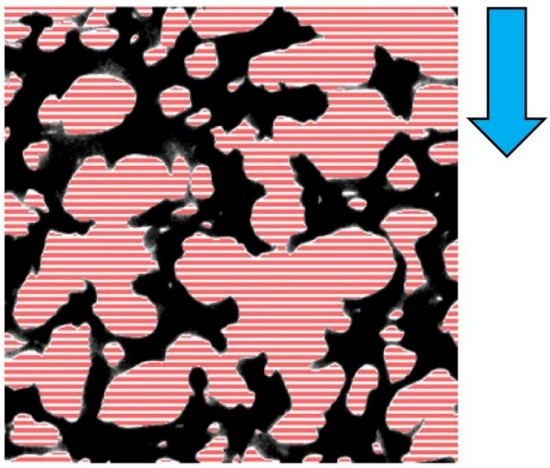

Fig. 7. Cross-section of a segment of a microfiltration membrane after processing by the image analysis algorithm from Ziel et al. adapted from [69]. Red lines feature the free path lengths identified by the algorithm. The blue arrow indicates the flow direction in the membrane.

While the PSG throughout the whole cross-section was determined quite well, the magnitude of the mean free path lengths was significantly larger than 0.2 µm, even in the SAL. This is related to the simplified definition of the mean free path length which can be determined from a single two-dimensional image of a membrane cross-section. For a proper quantitative description of the porous structure, additional information on the third dimension is required. This information can be obtained by more sophisticated techniques such as X-ray computed tomography [70,71] or serial slicing and imaging of cross-sections using electron microscopy in combination with 3D reconstruction of the membrane structure [72,73]. However, these

techniques are time consuming and require specialized and expensive equipment in addition to high computational demands dealing with large amount of data. In addition, although spacial resolution of X-ray computed tomography improved over the last years, resolution is still too low in order to resolve the structures of VFMs.

Similar to the determination of PSDs, solute retention experiments can also provide information on the PSG. Using monodispersed, fluorescently-labelled bacteriophages, it was observed by confocal scanning laser microscopy that these particles accumulate at a certain depth of a VFM (Fig. 8) [74–76].

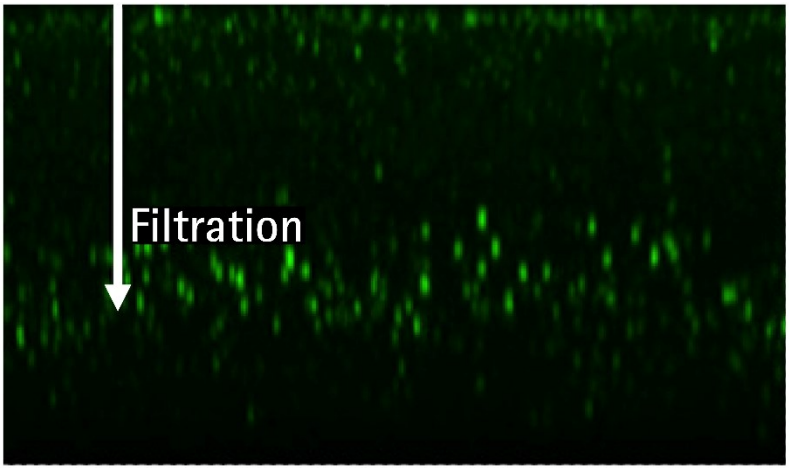

Fig. 8. Cross-section of a VFM after filtration with a feed containing fluorescently-labelled bacteriophage PP7 adapted from [74]. The image was obtained by confocal scanning laser microscopy and shows accumulated PP7 mostly in a distinct membrane section in the lower half of the membrane. The white arrow indicates the flow direction in the membrane.

As the pore size narrows towards the filtrate-side of a typical VFM, particles are efficiently retained when the pores sizes become similar or smaller than the size of the particle. Thereby, information is gained on the pore size at this depth of the membrane. Besides investigation of virus retention mechanisms, using viruses for structural characterization of membranes has several disadvantages. Viruses have to be handled with increased precaution (e.g. biosafety level facility). For variation of virus sizes, which is a necessity for determining the PSG, different virus species have to be used. Virus species can also differ with respect to their surface properties, which can result in interfering adsorptive retention [77,78].

Using rigid and spherical model particles of non-biological origin, such as GNPs, has the advantage that such particles are available in a broad size range having the same or different surface properties if needed. Limited to VFMs made from RC, GNPs of different size have

already been used to qualitatively describe the PSGs [16,17,48]. Within this studies cross-sections of the VFMs were prepared after filtration with GNPs. Accumulation of GNPs at a certain depth of the membrane was observed, causing a local change of membrane colour and membrane composition, which was visible by light and electron microscopy. Relating the size of the GNPs retained to their position in the membrane has provided insights into the PSG. While these studies were conducted with VFMs made from RC, exhibiting no significant GNP adsorption, adsorptive interaction can be a serious issue with other relevant materials such as PES, as already discussed for the determination of the PSD using GNPs.

1.1.4 Virus retention mechanisms

Although it is now well accepted that virus retention is dominated by size exclusion, other factors than virus size and PSD might contribute to the overall level of retention [4]. In general, factors are manifold and can be categorized by VFM-, feed stream- and process-related. A summary of factors influencing virus retention is given in Table II.

Table II. Summary of factors potentially influencing virus retention.

VFM-related	Feed stream-related	Process-related
PSD	virus size	mode of filtration (dead-end, TFF)
PSG	virus surface (charge, hydrophobicity, ...)	transmembrane pressure / flow rate
membrane orientation	virus concentration	flow interruptions (number, duration)
number of membrane layers	pH	volume-to-area ratio / total virus load
surface chemistry (charge, hydrophobicity, ...)	ionic strength	
surface roughness	product size	
	product surface (charge, hydrophobicity, ...)	
	additives (surfactants, ...)	

To substantiate size exclusion as main retention mechanism, Peinador et al. observed that virus retention correlates with the maximum pore diameter, which they determined by using LLDP [34]. Furthermore, Giglia et al. predicted LRVs of commercial and non-commercial VFMs for different sized viruses based on LLDP data taking account of the entire PSD [27]. Good

correlation between predicted and measured virus retention was found for convection-dominated flow conditions during virus filtration.

In contrast to retention mechanisms of soft pathogens such as mycoplasma or common bacteria using microfiltration membranes, where deformation of the pathogen at high transmembrane pressure was found to be a cause for pathogen breakthrough, viruses such as bacteriophage PP7 exhibit a by magnitudes higher stiffness preventing virus breakthrough at elevated transmembrane pressures [51].

However, it has been shown that virus retention can additionally be influenced by other mechanisms, which are feed stream- and process-related. Flux decay as a result of fouling, caused by either product-related foulants or by the virus spike, was shown to have a very significant negative impact on the virus retention of the first-generation VFMs [32,79]. This observation was explained by selective pore plugging of the small retentive pores deviating the convective flux into larger non-retentive pores [79]. Kreil et al. investigated the impact of antibody-virus interaction on the virus retention of 35 nm VFMs [80]. The authors observed a significant virus reduction for a 20 nm B19V parvovirus by 5 $\log_{10}$ during a pre-filtration step using a 0.1 µm rated filter, when virus specific antibodies were present that could aggregate with the virus. Others observed pH and ionic strength to have an impact on virus retention, which they attributed to non-specific electrostatic interactions between membrane and virus as well as between product molecule and virus [76,81].

Furthermore, it has been first published in 2011 that flow interruptions (FIs) can reduce virus retention levels of VFMs [82]. Since then, it has repeatedly been observed that the virus retention for different types of VFMs decreased, when the filtration was resumed after a temporary FI [60,75,83]. Depending on the VFM and the experimental conditions applied in these studies, the virus concentrations in the filtrate fraction directly after the FI were found to be 10 to 1000-fold higher after a temporary FI. However, in most cases the decreased level of retention was reversible and recovered for later fractions [75,76,84–86]. From mechanistical perspective it is assumed that the decreased level of virus retention results from Brownian motion of the virus particles during the FI or under low flow conditions [87,88]. Under normal flow conditions, the virus particles are forced through the pore network until reaching pores small enough to be capable of size exclusion (Fig. 9 A)). Virus particles are constrained to these retentive pores by the convective flow, reducing their mobility based on diffusive movement (Fig. 9 B)). In contrast, under low or no flow conditions, the constraint of

captured particles to the retentive pores is reduced or lacking completely, resulting in a diffusive movement that allows previously retained virus particles to cover a certain distance within the pore network (Fig. 9 C)). Due to the log-normal PSD of the membrane, these virus particles have a certain chance to reach larger non-retentive pores. When the filtration is then resumed and a typical convective flow reinstated, the majority of virus particles, which again reached retentive pores, will be constrained to these. The smaller share of virus particles that had reached non-retentive pores can pass through these further downstream into the VFM until either being re-captured in a deeper zone or even transmitted through the membrane, leading to a higher virus concentration in the filtrate.

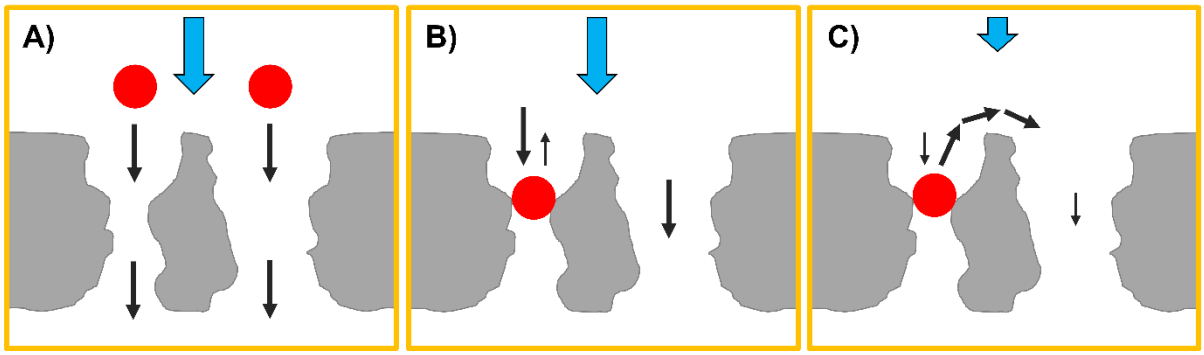

Fig. 9. Schematic illustrations of virus particles in a porous medium such as a VFM at normal (long blue arrows) and low/no (short blue arrow) flow conditions adapted from [87]. A) Virus particles moving under normal flow conditions into a small, retentive pore (left particle) and through a larger non-retentive pore (right particle). B) Virus particle constrained to a retentive pore due to high convective flow. C) Previously retained virus particle from B) can move back in porous network under low/no flow condition due to Brownian motion resulting in an additional chance to reach a non-retentive pore.

A diffusion-based mechanism of virus reorganization during a FI is further supported by observing impacts of solution viscosity [85,88] and the duration of the FI [85] as both affect the distance that can be covered by the virus particles by diffusion. Furthermore, it has been reported that retention after a FI can be influenced by pH and ionic strength, which was attributed to electrostatic interactions between virus, membrane and product molecule [76]. It is assumed that attractive electrostatic interactions between the virus and the inner membrane surface could cause an additional constrain for virus particles.

Commercial VFMs from different brands, even different VFM types from a single brand, have shown significant differences in retention performance and robustness [32,75,84,85].

1.1.5 Membrane fouling

A broad variety of new drug formats is currently under development by numerous biopharmaceutical companies, introducing a larger diversity of molecule properties and impurity profiles [89–91]. While robust virus retention contributes to patient safety of drugs, fouling robustness reduces the expenditure of time and money for process development and improves the economics of this unit operation carried out by a single-use approach. In contrast to unit operations employing multi-use filtration membranes, such as ultrafiltration, improved fouling robustness can significantly reduce the required amount of membrane area and lower the costs for consumables.

IgG-type antibodies, a major class of biopharmaceutical molecules to which most of the commercial monoclonal antibodies belong and which are the main component of IVIG [92], exhibit hydrodynamic diameters of 9-12 nm for aggregate free solutions [5]. VFMs, which are expected to transmit such product molecules by > 95 %, are reported to have only slightly larger mean pore diameters of 12-17 nm [27]. Typical product related membrane foulants, e.g. protein aggregates, often are in the size range of parvoviruses and effectively foul the membrane due to pore blocking. Studies of Barnard et al. using monoclonal antibodies revealed that trace amounts of protein aggregates ($1x10^{-4}$ % of the total mass of protein in solution) in the size range of 20-40 nm are sufficient to cause significant flux decay during virus filtration [64]. Furthermore, Brown et al. determined the size range of dimers up to pentamers of IgG-type monoclonal antibodies to be 16-23 nm with respect to their hydrodynamic diameter, which is very similar to the reported size range for parvoviruses [93].

Although obvious that fouling can originate from size exclusion of larger foulants, fouling by adsorptive mechanisms is also often discussed for membranes applied for biopharmaceutical processes [25,94–98]. Bolton et al. found the fouling species of IVIG to consist “of monomeric IgG variants containing more exposed hydrophobic surfaces” rather than aggregated IgG molecules, which was further supported by Villain [94,99].

Furthermore, shear stress caused by laminar flow distribution within the pore structure is hypothesized to induce denaturation/aggregation of proteins contributing to fouling [25]. Scientific results on that matter are very rare and limited to microfiltration membranes, indicating a higher relevance of interaction of proteins with the membrane surface causing denaturation/aggregation [98]. Even if non-membrane-related, simplified model systems (e.g. stir bar in solution, mixer, Couette cell) for generating sheer stress are used, results are

inconclusive between the different studies on whether denaturation/aggregation was caused by sheer stress and/or interaction with other surfaces [100–105]. In addition, concentration polarization phenomena leading to a decreased permeability with increased driving force, mostly known from UFMs, were also reported for VFMs [21,63,106]. Other smaller impurities like product fragments, host cell proteins and DNA can also cause fouling due to adsorption to the membrane [107].

One strategy to maximize the throughput of the virus filtration step is to locate the unit operation close to the end of the downstream purification process, where the feed typically has already a high purity (Fig. 3) [22]. Another strategy involves the specific optimization of the unit operations upstream of the virus filtration to further reduce impurities [108].

Adsorptive pre-filters exist that have proven to significantly reduce fouling of VFMs [64,93,94]. Such filters can remove foulants by either hydrophobic or electrostatic interaction.

From membrane manufacturer's perspective, development of VFMs achieving high fouling robustness involves a twofold strategy. For one part of the strategy, the membrane surface (including inner and outer surface) has to be rendered inert towards attractive interactions with feed components, so that accumulation of certain species from the feed stream and pore plugging is reduced. This can be achieved already by selection of low interacting base materials like RC [109] or by means of surface modification of higher interacting base materials such as PES [96,110–112]. For further reading, numerous publications can be found dealing with anti-fouling surface modification of membranes [26,113–115]. More specifically, surface modification in context of VFMs was investigated by L. Villain [99]. For the other part of the strategy, structural optimization of the VFMs is involved. Therefore, special focus is paid on the PSG, utilizing the membrane structure to act as a depth pre-filter to protect the SAL from foulants (cf. section 1.1.3).

1.2 Summary of gaps in current scientific knowledge

Due to the proprietary nature of the manufacturing processes of commercial VFMs, each membrane type is unique, differing with respect to the PSD, PSG and surface chemistry [4]. As a result, also broad variations with respect to application performance such as virus retention and fouling robustness have been observed [32,75,109,116]. Therefore, a deeper understanding between membrane properties and application performance is of high importance in order to develop the next generation of robust high performance VFMs.

In general, published investigations focusing on membrane properties and/or application performance of VFMs are often limited to a smaller set of commercial membranes and seldom include non-commercial variations. Hence, holistic insights spanning the wide variety of properties that commercial VFMs already exhibit are very rare. Deduction of universal trends from different publications is often not feasible and/or outcomes not conclusive, which can be a result from very individual experimental conditions between the studies such as compositions of feed streams or virus spike.

Briefly, the gaps in the current scientific knowledge on VFMs and their application can be divided into the lack of

- methods for quantitative structural characterization of PSDs and PSGs that are independent of the membrane surface chemistry and other membrane properties,
- holistic understanding of virus retention mechanisms as function of VFM-, feed stream- and process-related properties and
- understanding of fouling mechanisms and their relation towards PSGs.

As discussed in section 1.1.3, a variety of techniques exists (e.g. porometry/porosimetry, SEM, solute retention) that are capable to quantitatively determine PSDs of porous membranes. So far, broad applicability of these methods towards VFMs is limited by factors that are depending e.g. on the membrane material/surface chemistry, PSGs and sample preparation, rendering these techniques not necessarily to correlate with virus retention. Size exclusion-based GNP retention experiments, being close to application mode of operation, are successfully applied for RC membranes [16,48,53], which show no significant attractive interactions, while attractive interactions interfere with PSD determination for other membrane materials/surface chemistries [43,47,49,55,56].

A very similar gap exists for the quantitative determination of PSGs where existing techniques suffer from major drawbacks. Image analysis of TEM/SEM images is prone to generation of artefacts during sample preparation and also requires harsh simplifications with respect to the definition of the pore size, often causing overestimation of pore sizes [67,69]. X-ray computed tomography, having the necessary resolution, is very time consuming, low throughput and requires expensive equipment [70,71]. Estimations of pore sizes across the thickness of the membrane by localization of retained particles/solutes of defined size are often aggravated by adsorptive retention and therefore results are mostly limited to membranes made of RC [16,17,48].

Virus retention as most important application performance characteristic is investigated in numerous studies, focusing mostly on different feed compositions and effects of FI. With respect to membrane properties, these studies typically use commercial VFMs without deeper consideration and characterization of membrane properties. For instance, the root cause for the lack of virus retention robustness of the first generation of VFMs is poorly understood. Also, adsorptive contributions by the VFM towards the retention under normal flow conditions and after FI have not been investigated so far. Holistic studies investigating a larger number of parameters and quantifying their impact by statistical means, even determining possible interactions between parameters, are rare.

Besides virus retention, fouling robustness is of high importance for the economy of the unit operation. Very little has been published on improvement of fouling robustness of VFMs by means of membrane development. However, it was pointed out by several studies that the porous structure of VFMs located between the feed facing site and the SAL acts a depth pre-filter protecting the more sensitive SAL from foulants [62,63]. So far, no studies investigated the depth pre-filter structure in more detail, especially with respect to the PSG. In addition, studies determining the fouling mechanism and identifying the fouling species of IVIG, found subsets of more hydrophobic and monomeric IgG antibodies to be the cause for fouling rather than IgG aggregates [94,99]. The study by Villain applied fractionation by hydrophobic interaction chromatography (HIC) in combination with size exclusion chromatography (SEC) [99]. Fractions containing more hydrophobic species exhibited higher extent of fouling but did not show any higher amounts of aggregates. It was hypothesized that reversible aggregates could be disrupted during SEC and therefore not detected properly. A more recent investigation by Rayfield et al. using dynamic light scattering (DLS) to characterize feed

streams for virus filtration indicated that DLS might be more predictive towards identifying fouling feed streams than classical SEC (without inline DLS detector) due to its high sensitivity towards detection of aggregated species in their native environment [117].

2 Scope of the research

The present thesis focuses on improving the understanding of the mode of operation of VFMs. As first objective, analytical techniques were developed that are capable of determining structural membrane properties in a quantitative manner, overcoming the drawbacks of existing techniques such as low applicability towards a broad range of membrane materials/surface chemistries. Due to the size exclusion based principle of operation, special focus was paid on analysis of structural membrane properties, especially with respect to the PSD and the PSG. For this purpose, a technique based on the retention of different sized GNPs was adapted from literature and its applicability extended towards other membrane materials than RC. As commercially available VFMs exhibit a high diversity regarding pore structures and materials/surface chemistries, a broad panel of these membranes was selected for the structural investigations complemented by additional UFMs and model VFMs.

As second objective, these membranes were characterized by their virus retention performance using bacteriophage PP7 and well as by their fouling robustness using IVIG. In greater depth, the fouling mechanism of IVIG, including the identification of the fouling species, was elucidated. Furthermore, virus retention performance was evaluated in context of PSDs, while fouling robustness was evaluated in context of PSGs providing mechanistical insights. **Paper 1** (cf. section 3.1) focuses on determination of PSDs and virus retention and **paper 2** (cf. section 3.2) on PSGs and fouling, respectively.

As third objective, in **paper 3** (cf. section 3.3) virus retention mechanisms were investigated within a holistic, DoE-based approach as a function of membrane characteristics, solution and process conditions. A unique feature of this study is the use of model VFMs having specifically designed PSDs and protein binding capacities as measure for the interaction of proteins with the membrane, which is presumably also valid for the interaction between non-enveloped viruses and the membrane. Besides the solution characteristics pH, salt concentration/conductivity and protein concentration, also the absence/presence of FI has been examined. Furthermore, filtration results are supported by biophysical characterization of the virus and non-virus containing feed streams with respect to particle size distributions.

2 Scope of the research

3 Publications

3.1 Determination of pore size distributions of virus filtration membranes using gold nanoparticles and their correlation with virus retention (paper 1)

P. Kosiol, B. Hansmann, M. Ulbricht, V. Thom,

Determination of pore size distributions of virus filtration membranes using gold nanoparticles and their correlation with virus retention,

J. Memb. Sci. 533 (2017) 289–301.

doi: 10.1016/j.memsci.2017.03.043.

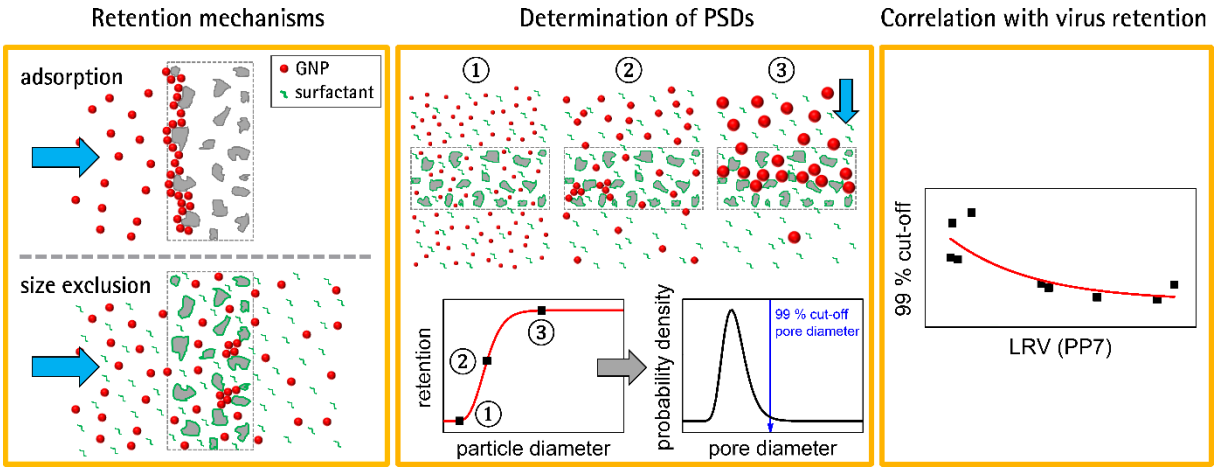

Journal of Membrane Science 533 (2017) 289–301

Contents lists available at ScienceDirect

Journal of Membrane Science

journal homepage: www.elsevier.com/locate/memsci

Determination of pore size distributions of virus filtration membranes using gold nanoparticles and their correlation with virus retention

Peter Kosiol[a,b], Björn Hansmann[a], Mathias Ulbricht[b,*], Volkmar Thom[a]

[a] Sartorius Stedim Biotech GmbH, 37079 Göttingen, Deutschland
[b] Universität Duisburg-Essen, Lehrstuhl für Technische Chemie II, 45141 Essen, Deutschland

ARTICLE INFO

Keywords:
Gold nanoparticles
Membrane structure
Particle retention
Pore size distribution
Virus filtration
Virus retention

ABSTRACT

Virus filtration membranes contribute substantially to the virus safety of biopharmaceutical drugs due to their capability to retain viral particles mainly based on the size-exclusion mechanisms. In this work, virus filtration membranes were challenged with gold nanoparticles (GNPs) in order to determine pore size distributions (PSDs) for a wide range of different commercial and non-commercial parvovirus retentive membranes differing in structure, material and surface chemistry. The retention mechanism of GNPs was investigated and effectively shifted towards size-exclusion by using an anionic surfactant to suppress particle adsorption to the membrane surface. This allowed insights into the relevance of particle retention based on size-exclusion mechanisms of the respective membranes. Membrane PSDs investigated through GNP challenges were for some membranes compared with PSDs investigated by liquid-liquid displacement porometry (LLDP). In addition, virus retention performance using *Pseudomonas aeruginosa* bacteriophage PP7 as accepted model virus was determined for the entire set of membranes and correlated with the cut-off pore size obtained from experiments using GNPs. Exemplarily, retention was examined for one membrane type using a set of different sized viruses or phages (PCV-2, PP7, MVM, HAV) ranging from 18 to 28 nm and compared to GNP retention.

1. Introduction

Throughout the last two decades, virus filtration using porous membranes has become a mature standard unit operation for virus clearance in the purification process of biopharmaceuticals derived from human or animal origin in order to ensure pathogen safety of drugs [1,2]. While first commercial virus filters (VFs) were intended to remove larger viruses with diameters > 50 nm like retroviruses, nowadays VFs have to ensure efficient and robust virus removal also of small viruses like parvoviruses with 18–24 nm in diameter by exhibiting a virus retention of at least 99.99% ($\log_{10}$ reduction value (LRV) > 4) [3–5]. The major challenge that VFs have to overcome is the high demand regarding selectivity. Typical biopharmaceutical product molecules like IgG-type monoclonal antibodies with diameters of about 10 nm are only slightly smaller than parvoviruses and have to be transmitted on a quantitative basis (> 95%) [1,6]. VFs are typically operated in dead-end mode. Size-exclusion, which is regarded as the main separation mechanism, has proven to allow for such high selectivities and is therefore considered to be mainly dependent on the pore size distribution (PSD) in the separation-active layer of the membrane [5]. Those high selectivites are achieved by VFs having very narrow PSD within the separation-active layer in comparison to ultrafiltration membranes [7,8]. Also in contrast to ultrafiltration membranes, the separation active-layer of a VF usually consists of a multitude of pore layers which reduces the risk of few abnormally large pores causing severe loss in virus retention performance [9–12]. While the first generation of parvovirus VFs has suffered from low robustness regarding virus retention [13], occasionally exhibiting severe parvovirus breakthrough, the latest second generation of VFs has proven significantly increased retention robustness [2].

A major challenge to link membrane structure properties of very different VFs to their performance properties, namely retention, permeability and fouling, is the lack of material independent techniques to characterize membrane pores in the size range of 5–50 nm. Deeper knowledge of structural properties of VFs could be the basis for developing a better mechanistic understanding of both, retention and fouling behavior.

To determine the PSD of the separation-active layer of a VF, techniques like gas-liquid displacement porometry (GLDP) as well as mercury porosimetry both require pressures too high for polymeric VFs, altering the pore structure during the measurement. Liquid-liquid displacement porometry (LLDP) has been successfully applied to VFs to determine the PSD of the separation-active layer due to significantly lower necessary pressures [14,15]. The two studies showed a correla-

* Corresponding author.
E-mail address: mathias.ulbricht@uni-essen.de (M. Ulbricht).

http://dx.doi.org/10.1016/j.memsci.2017.03.043
Received 18 January 2017; Received in revised form 27 March 2017; Accepted 28 March 2017
Available online 30 March 2017

Nomenclature

A	Membrane area [m^2]
A_{feed}	Absorbance at 527 nm in feed [dimensionless]
A_{perm}	Absorbance at 527 nm in permeate [dimensionless]
c	Concentration [wt%]
CDF	Cumulative distribution function [dimensionless]
c_{feed}	Concentration of phages/viruses in feed [PFU/mL; $TCID_{50}$/mL; virus genome copies/mL]
c_{perm}	Concentration of phages/viruses in permeate [PFU/mL; $TCID_{50}$/mL; virus genome copies/mL]
$d_{99\%}$	99% cut-off pore diameter [nm]
$\overline{d}_{99\%}$	Corrected 99% cut-off pore diameter [nm]
d_{DLS}	Particle diameter measured with DLS [nm]
d_{mean}	Mean pore diameter [nm]
$\overline{d}_{mean}$	Corrected mean pore diameter [nm]
$d_{particle}$	Particle diameter [nm]
d_{pore}	Pore diameter [nm]
d_{TEM}	Particle diameter measured with TEM [nm]
f_L	Permeance-weighted probability density function [dimensionless]
J_1	Flux of displacement liquid during displacement of wetting liquid [g/min]
J_2	Flux of pure displacement liquid [g/min]
J_{H2O}	Pure water flux [g/min]
J_{SDS}	Flux with 0.26 wt% SDS [g/min]
LRV	Log reduction value [dimensionless]
PDF	Probability density function [dimensionless]
Q	Flux ratio between J_1 and J_2 [dimensionless]
R^2	Coefficient of determination [dimensionless]
r	Retention [dimensionless]
t	Time [min]
V	Volume [L]

Greek symbols

γ	Interfacial tension of 2-phase system [mN/m]
$\delta_{hydrodyn}$	Hydrodynamic correction term [nm]
δ_{SDS}	Correction term for pore narrowing by SDS adsorption [nm]
Δ	Coefficient of variation [dimensionless]
ΔP	Transmembrane pressure [bar]
μ	Location (fit-)parameter of log-normal distribution function [dimensionless]
σ	Scale (fit-)parameter of log-normal distribution function [dimensionless]
$\hat{\sigma}$	Standard deviation [nm]

tion between LLDP results and virus retention for homologous VFs, differing only in pore size. However, by applying the same procedure to different VFs with respect to material, surface chemistry and pore size gradient, Giglia et al. [15] observed deviations from the previously obtained correlation with respect to virus retention. Although being applicable to VFs in general, the strength of LLDP is to determine PSDs of homologous membranes differing regarding the barrier pore size. Comparative LLDP studies of VFs made from different materials, with different pore size gradients and surface properties are challenging for various reasons [16]. Typical 2-phase systems utilized for LLDP consist of water/alcohol [17] or water/polyethylene glycol/ammonium sulfate [18] mixtures. Alcohol containing systems can cause significant swelling of polyethersulfone (PES) membranes leading to erroneous results [19] or even structural damaging of the membrane [20] while other materials like poly(vinylidene fluoride) (PVDF) exhibit only negligible swelling with the same alcohols. As polyethylene glycol is known to strongly interact with PES [21], measured pore sizes might not be accurate and might be dependent on contact time of the membrane with the polymer-rich phase. In addition to the variation of membrane base materials, VFs usually are surface modified exhibiting different surface chemistries, depending on the manufacturer and the specific modification methods used [5]. This leads to additional interactions between the membranes and the 2-phase systems, making interpretations of results for a variety of VFs difficult. LLDP can also suffer from low reproducibility for identifying the maximum pore size, caused by measuring flow rates significantly above the base line flow rate already at pressures much below the expected bubble-point of the individual membrane [17]. This is especially relevant as the maximum pore size, in contrast to the mean and minimum pore size, was found to be the most predictive result from LLDP towards virus retention [14]. In a previous study, the correlation between maximum pore size determined by LLDP and virus retention using *Pseudomonas aeruginosa* bacteriophage PP7 as model virus for a variety of commercial VFs was found to be quite low (R^2=0.3) [16].

Although scanning electron microscopy (SEM) is successfully applied for the determination of pore sizes in the range of VFs, quantitative applications are mostly limited to track-etched membranes or other membranes, having the separation-active pores visible on the outermost membrane surface [17]. The separation-active layer of VFs is often located deeper within the membrane structure, necessitating the preparation of cross-sections, which on the other hand can cause artifacts (e.g. by compaction or smearing). In addition, the measurement of pore sizes by image analysis of 2-dimensional pictures is challenging, as VFs have complex pore networks.

A different approach is based on rejection of solutes of known size in course of filtration experiments to gain insights into PSDs. Typical solutes can be linear/circular polymers (e.g. dextran [22–24], polyethylene glycol (PEG)/polyethylene oxide (PEO) [11,24,25], deoxyribonucleic acid (DNA) [26]) or rigid spherical particles (e.g. inorganic nanoparticles [27–29]). While the application of linear polymers such as dextrans to determine PSDs has become a standard technique for ultrafiltration membranes, results obtained for VFs are more difficult to interpret, as the results are strongly dependent on pore size gradients and membrane orientation, which the authors contributed to internal concentration polarization [22]. Susanto et al. also observed and discussed adsorption of dextrans on PES membranes, leading to membrane fouling, i.e. flux decline and changed rejection [30]. It has been further demonstrated that circular plasmid DNA with 350 nm in hydrodynamic diameter can penetrate pores of 10 nm in size due to stretching of the molecule, an effect which is also amplified by higher transmembrane pressures, leading to further increased DNA transmission [26]. This effect could also occur to linear polymers that form spherical coil-like structures in solution, leading to inaccurate determination of the largest pore, which is most relevant for virus retention [24]. The “PDA Technical Report No. 41 - Virus Filtration”, a major guideline for virus filtration, states dextran retention not to correlate with virus/phage retention [1].

Rigid spherical particles on the other hand have proven to be highly applicable for examination of virus retentive properties of VFs. Helling et al. investigated retention properties of microfilters and VFs with a set of particles exhibiting different Young's moduli ranging from < 1.2 MPa for bacteria up to > 310 MPa for *Pseudomonas aeruginosa* bacteriophage PP7 and polystyrene latex beads [31]. They found that for soft particles like bacteria retention can decline with higher transmembrane pressure caused by deformation and squeezing through of the particles while retention of stiff particles like PP7 and latex beads was observed to be constantly high within the investigated pressure range up to 10 bar. Deformation and squeezing through of

gold nanoparticles (GNPs) with even significantly higher Young's moduli of 100 GPa [32] during filtrations using VFs is therefore unlikely. Besides their stiffness, GNPs are commercially available in a wide range of sizes from below 5 nm up to several hundreds of nanometers. The spherical shape, low size dispersity and high optical absorption in the visible spectrum of GNPs are very favorable attributes for solute rejection experiments. Depletion of GNPs in a solution in course of filtration experiments can be easily measured up to a LRV of 3 using a standard UV–Vis spectrophotometer. Thus GNPs have been applied in the development of the first commercial VFs and used as virus model for filtration experiments [28,33,34]. In biopharmaceutical manufacturing GNPs are used for physical post-use integrity testing of VFs, as the retention of GNPs correlates with virus retention [1,35]. For integrity testing, however, the retention performance for a single particle size, usually 20 nm for parvovirus retentive VFs, is determined, which gives only limited insights into the actual PSD of the membrane. Arkhangelsky et al. reported the use of GNPs and silver nanoparticles in separate filtration experiments using different sized particles with various membranes made from cellulose acetate (CA), PES, PVDF, polycarbonate (PC) or ceramics [24,27]. The authors were able to determine PSDs distributions only of some of the membranes tested by using GNPs. They observed limitations of this technique to gain information on the pore structure of membranes made of PES and CA, which was caused by high affinity of the particles towards the specific membrane materials and was related to higher membrane hydrophobicity. Adsorption of metal nanoparticles, increasing the observed retention efficiency of polymeric membranes and thereby superimposing the size-exclusion properties, has also been observed by other groups [29,36,37]. One way to overcome unwanted adsorption of GNPs is the surface functionalization of GNPs using protective ligands. Although some ligands have proven to significantly reduce adsorption of GNPs on certain membrane materials, their efficiency to suppress adsorption is highly specific towards the individual membrane material and therefore not universally applicable [29]. Another way to reduce GNP adsorption was reported by Wei and Liu for the separation of GNPs by size exclusion chromatography, where adsorption of GNPs to the stationary phase has been an issue [38,39]. By addition of an anionic surfactant, namely sodium dodecyl sulfate (SDS), to the mobile phase adsorption was significantly reduced. The authors explained this observation by an interaction between the stationary phase material (polystyrene–divinylbenzene) and SDS. The presence of SDS had no significant influence on the particle size. Furthermore a post-use integrity testing procedure for VFs made from hydrophilized synthetic polymers has been patented using metal nanoparticles in complex solvents comprising of an anionic polymer together with at least one non-ionic surfactant and/or a water-soluble polymer containing a pyrrolidone group in order to reduce interfering adsorption of the nanoparticles [40].

The aim of this work was to develop a technique that is capable of determining PSDs of highly diverse commercial parvovirus retentive VFs as well as ultrafiltration membranes. For this, an approach based on solute rejection using rigid and monodisperse GNPs was chosen. Interfering adsorptive retention of GNPs was overcome by previous equilibration of the membranes using SDS solutions and by addition of SDS to the GNP solutions. The retention mechanisms with and without SDS treatment were determined. PSDs obtained for the ultrafiltration membrane and the two generations of VFs are discussed. For two VFs, results are compared with data obtained by LLDP as a complementary characterization technique. For one VF, GNP retention data as well as the therefrom derived PSD are compared with virus retention of different sized viruses (PCV-2, PP7, MVM, HAV) having diameters ranging from 18 to 28 nm. The results for the cut-off pore diameters of all VFs determined by GNP experiments are correlated with virus retention performance using *Pseudomonas aeruginosa* bacteriophage PP7 as accepted model virus.

2. Materials and methods

2.1. Materials

2.1.1. Chemicals

Sodium dodecyl sulfate (SDS; ≥99%), 0.01% poly-L-lysine solution (150–300 kDa, sterile-filtered) and uranyl acetate (≥98%) were purchased from Sigma-Aldrich.

2.1.2. Membranes

The studies were performed on a set of commercial parvovirus retentive VFs ("VF1"–"VF7") manufactured by Asahi Kasei Medical, EMD Millipore, Pall Corp. and Sartorius-Stedim Biotech and made from polyethersulfone (PES), poly(vinylidene fluoride) (PVDF) or regenerated cellulose (RC). In addition, a non-commercial variation of VF4 with larger pore sizes labelled as VF4b has been studied. For comparative reasons experiments included also a 100 kDa PES ultrafiltration membrane ("100k PES") from Sartorius-Stedim Biotech. All experiments were conducted with a single layer of membrane, while commercial devices can also contain multiple layers of the same membrane.

2.1.3. Gold nanoparticles

Aqueous solutions of citrate-stabilized gold colloids in deionized water with nominal diameters ranging from 5 to 50 nm were purchased from Nanopartz Inc. Gold concentrations were 0.050 mg/mL corresponding to optical densities of unity (SPR peak). All solutions had pH 7. Zeta potentials of the GNPs were between −30 and −40 mV.

2.1.4. Phages/viruses

Pseudomonas aeruginosa bacteriophage PP7 (ATCC 15692-B2) was used as accepted standard model virus for investigation of retention properties of parvovirus retentive VFs [1,41]. PP7 was propagated using *Pseudomonas aeruginosa* (ATCC 15692) as host. Phage titers were obtained by a plaque assay using *P. aeruginosa* as indicator cell. Propagation and titrations were carried out according to recommendations by the PDA Technical Report No. 41 - Virus Filtration [1].

Suspensions of porcine circovirus type 2 (PCV-2, Strain Stoon-1010, University of Ghent, Belgium), minute virus of mice (MVM, Strain Crawford, ATCC VR-1346) and hepatitis A virus (HAV, Strain HM175/18f, Robert Koch Institute, Berlin, Germany) were obtained and handled by an external virology laboratory ("SOP P04-029 Version 02: virological testing", "SOP LV 101 Version 06: propagation and titration of viruses", Labor Dr. Merk & Kollegen GmbH, Germany). PCV-2 was propagated in PK15 cells (University of Ghent, Belgium) and quantified by the count of genome copies using qPCR (ViroReal Kit PCV2, Ingentix, Vienna, Austria) due to absence of a visible cytopathogenic effect. MVM was propagated and titrated in A9 cells (Paul Ehrlich Institute, Langen, Germany). HAV was propagated and titrated in Rh/K cells (Robert Koch-Institute, Berlin, Germany). Infectivity titer for MVM and HAV was determined by $TCID_{50}$ assay using large volume plating techniques.

2.2. Size characterization of GNPs

2.2.1. TEM

GNPs were characterized by transmission electron microscopy (TEM) using a CM12 instrument (Philips, Netherlands) at 120 kV. Carbon-coated copper grids (200-mesh) were used as sample carriers. Immobilization of GNPs on TEM grids was achieved by dripping particle containing solutions on the grid and air drying for 1 h. TEM images were analyzed using the image processing software ImageJ 1.48v (http://rsbweb.nih.gov/ij/) to obtain size distributions of the particles. Images were binarized and the areas of the single particles determined. From the areas, the equivalent

circle diameters were calculated. Mean diameters and standard deviations were determined. Overlapping particles, which were most probably the result from sample preparation, were excluded from analysis.

2.2.2. DLS

Size measurements of GNPs utilizing dynamic light scattering (DLS) were conducted using a StabiSizer PMX 200C (Particle Metrix GmbH, Germany). At least six measurement runs with run times of 90 s have been performed for each batch of GNPs. For the calculation of number-based distributions, in order to improve comparability towards TEM measurements, a refractive index of 1.333 was assumed for water as dispersant and the refractive index/transparency setting for GNPs was set to "absorbing" in the Microtrac FLEX software program accompanied to the DLS device. Presented results are averages of the mean number diameters. Additional information on the width of the particle size distribution is provided by the measured standard deviation, which has been averaged for all replicates and is represented by errors bars, although it is not a measure of statistical error.

The additional GNP size analyses using differential centrifugal sedimentation (DCS) and UV–Vis spectroscopy are described in Supporting Information.

2.3. Size characterization of phage/virus particles

TEM was used to determine the size of phage/virus particles. Phage particles were immobilized on carbon-coated copper grids (200-mesh) previously treated with poly-L-lysine. Uranyl acetate was used for negative staining. TEM images of the phages were obtained by using a Leo 912 AB microscope (Zeiss, Germany) at 80 kV.

Sample preparation and microscopy of phage/virus particles was performed by an external virology laboratory (Labor Dr. Merk & Kollegen GmbH, Germany) using a negative staining protocol. Particle sizes were determined by manual image analysis using ImageJ 1.48v.

2.4. Filtration experiments

All filtration experiments were conducted in dead-end mode at constant pressure of 2 bar. In case of mechanically sensitive membrane types, pressure was reduced to 1 bar according to manufacturer specifications. The membranes were always oriented with the separation-active layer facing downstream.

2.4.1. Gold nanoparticles (GNPs)

Prior to the filtration of GNPs, membranes were wetted and flushed with reverse osmosis (RO) water in order to ensure complete wetting. Afterwards all membranes were equilibrated with 0.26 wt% SDS solution by flushing with at least three hold-up volumes of the membrane device. SDS occupies possible binding sites for the GNPs on the membrane surface and hence supresses adsorption of the GNPs [38,39]. The stationary water flux after possible SDS adsorption was determined for each membrane type in order to quantify pore constrictions used for corrections of the PSDs obtained by GNP retention. Flux measurements were performed gravimetrically using a Quintix balance (QUINTIX2102-1 S, Sartorius, Germany).

All GNP solutions were used at concentrations of 0.05 mg/mL (cf. Section 2.1.) and 0.26 wt% SDS added. Filtration experiments were carried out using different sized GNPs in the size range from 5 to 50 nm. At least six filtrations using different particle sizes were run in parallel for each membrane type. The amount of feed used per filtration added up to three hold-up volumes of the VF device. The last 0.5 mL of each permeate were collected as grab sample for retention determination. Finally, the membranes were again flushed with two hold-up volumes of 0.26 wt% SDS. The membranes were then removed out of their housings and dried at room temperature on a cellulose cloth for 1 h.

2.4.1.1. Pore size distributions. First, the GNP retention values were determined photometrically at 527 nm using an Infinite 200 Pro spectrophotometer (Tecan, Switzerland). By measurement of the absorbance in the feed A_{feed} and in the permeate A_{perm} the retention r can be calculated as follows

$$r = 1 - \frac{A_{perm}}{A_{feed}} \tag{1}$$

The retention is then plotted against the particle size measured by TEM (d_{TEM}).

As most commonly log-normal distributions are used to describe membrane PSDs [42], the retention data is fitted to a log-normal cumulative distribution function (CDF) using a simple nonlinear least-squares data fitting procedure [43]. The applied CDF fit function has the following notation

$$\mathrm{CDF}(d_{TEM} \mid \mu, \sigma) = \frac{1}{2}\left[1 + \mathrm{erf}\left(\frac{\ln(d_{TEM}) - \mu}{\sigma\sqrt{2}}\right)\right] \tag{2}$$

with μ and σ as fit parameters. Under a first assumption of the two-pore model, the particle size equates with the pore size [44]. The two-pore model implies that particles are transmitted if their size is smaller than the pore size while particles larger than the pore size are completely retained. The subsequent sizes were further determined from the fit parameters μ and σ

$$d_{mean} = \exp\left(\mu + \frac{(\sigma^2)}{2}\right) \tag{3}$$

$$\hat{\sigma} = \sqrt{(\exp(\sigma^2) - 1)(d_{mean})^2} \tag{4}$$

with d_{mean} being the arithmetic mean pore diameter and $\hat{\sigma}$ the standard deviation. Furthermore, the 99% cut-off pore diameter $d_{99\%}$ was obtained from numerical approximation of Eq. (2) for $\mathrm{CDF}(d_{99\%})=0.99$. Due to the simplicity of the assumption of the two-pore model, further contributions of membrane and particle properties have to be taken into account in order to obtain a more realistic picture of the PSDs. Although making size exclusion properties accessible for a wide range of membrane materials and surfaces by using SDS, its adsorption to the membrane surface perturbs the determination of the real PSD. Under consideration of the Hagen–Poiseuille equation and the fluxes measured with RO water J_{H2O} and with SDS solution J_{SDS} for each membrane type, the narrowing of the pore sizes by SDS δ_{SDS} can be determined

$$\delta_{SDS} = d_{mean}\left(\frac{1}{\sqrt{\frac{J_{SDS}}{J_{H2O}}}} - 1\right) \tag{5}$$

Additionally the larger hydrodynamic size of the GNPs in contrast to the size of the gold core determined by TEM was considered by the average deviation between TEM and DLS results (cf. Section 3.1.)

$$\delta_{hydrodyn} = \frac{1}{12}\sum_{i=1}^{12}(d_{DLS,i} - d_{TEM,i}) = 2.3\ \mathrm{nm} \tag{6}$$

Hence, the following relation between the pore size d_{pore} and the particle size d_{TEM} has been defined

$$d_{pore} = d_{TEM} + \delta_{SDS} + \delta_{hydrodyn} \tag{7}$$

Application of the expression (7) to the corresponding log-normal probability density function (PDF) of Eq. (2)

$$\mathrm{PDF}(d_{TEM} \mid \mu, \sigma) = \frac{1}{(d_{TEM})\sigma\sqrt{2\pi}}\exp\left(-\frac{[\ln(d_{TEM}) - \mu]^2}{2\sigma^2}\right) \tag{8}$$

will result in the final PDF describing the PSD

$$\mathrm{PDF}(d_{\mathrm{pore}} \mid \mu, \sigma) = \frac{1}{(d_{\mathrm{pore}} - \delta_{\mathrm{SDS}} - \delta_{\mathrm{hydrodyn}})\sigma\sqrt{2\pi}} \cdot \exp\left(-\frac{[\ln(d_{\mathrm{pore}} - \delta_{\mathrm{SDS}} - \delta_{\mathrm{hydrodyn}}) - \mu]^2}{2\sigma^2}\right) \quad (9)$$

The most relevant parameters determined are given below

$$\bar{d}_{\mathrm{mean}} = d_{\mathrm{mean}} + \delta_{\mathrm{SDS}} + \delta_{\mathrm{hydrodyn}} \quad (10)$$

$$\bar{d}_{99\%} = d_{99\%} + \delta_{\mathrm{SDS}} + \delta_{\mathrm{hydrodyn}} \quad (11)$$

$$\Delta = \frac{\hat{\sigma}}{\bar{d}_{\mathrm{mean}}} \quad (12)$$

with $\bar{d}_{\mathrm{mean}}$ and $\bar{d}_{99\%}$ being the mean and 99% cut-off pore diameters, respectively, considering the SDS adsorption and the hydrodynamic size of the GNPs, and Δ as coefficient of variation describing the dispersion of the PSDs.

2.4.2. Filtration of phages/viruses

Phage filtrations using PP7 were conducted using phage concentrations of 10^7–10^8 PFU/mL according to the recommendations for parvovirus retentive VFs by the PDA Virus Filter Task Force [41]. Pool samples of the permeates were taken after total challenges of about 10^{13} PFU/m^2 corresponding to volumetric throughputs in the range 100–1000 L/m^2.

Filtration experiments with PCV-2, MVM and HAV were conducted by an external virology laboratory (Labor Dr. Merk & Kollegen GmbH, Germany) using virus titers of 10^7 virus genome copies/mL (PCV-2) and 10^7 $TCID_{50}$/mL (MVM, HAV). Pool samples of the permeates were taken after total challenges of about 10^{12} virus genome copies/m^2 or $TCID_{50}$/m^2 corresponding to volumetric throughputs of 100 L/m^2.

In order to avoid fouling related impacts on phage/virus retention, all filtrations were conducted with protein-free buffered solutions (20 mM KPi, pH 7.2). All phage filtration experiments were carried out in quadruplicate and all virus filtration experiments in duplicate. Calculation of the $\log_{10}$ reduction value (LRV) proceeded according to the following equation

$$\mathrm{LRV} = \log_{10}\left(\frac{c_{\mathrm{feed}}}{c_{\mathrm{perm}}}\right) \quad (13)$$

with c_{feed} and c_{perm} the phage concentrations in feed and permeate respectively.

2.5. Liquid-liquid displacement porometry (LLDP)

LLDP was used as a complementary technique to determine PSDs. The basic principle of LLDP is analogous to conventional gas-liquid displacement porometry (GLDP) and described elsewhere in more detail [45]. The membrane is first wetted by a liquid phase. Then the wetting liquid is displaced by a second liquid phase. Proprietary wetting and displacing liquids have been prepared by mixing water, an alcohol and a salt in a specific proportion resulting in two liquid phases after reaching equilibrium. The interfacial tension between both liquids has been determined by a SVT 20N spinning drop tensiometer (Dataphysics, Germany) and resulted in 1.16 mN/m at 22 °C. Membrane discs (diameter 25 mm) with an effective membrane area of 3.8 cm^2 were immersed into the wetting liquid for 1 h and then introduced into the self-built porometer. The displacement liquid was filled into a pressurizable stainless steel vessel and the vessel connected to the porometer. A pressure of 0.1 bar was adjusted in the vessel using helium. Helium was used due to its low solubility in aqueous solutions in order to reduce degassing effects on the permeate side of the membrane that would otherwise interfere with gravimetric flux measurements. The system was filled and flushed with the displacing liquid on both sides of the membrane by bypassing the membrane in order to remove air from the system. Afterwards measurement was conducted automatically in constant pressure mode by stepwise increasing the transmembrane pressure in 0.1 bar intervals while monitoring the flux through the membrane gravimetrically for 60 s at each pressure step by using a Cubis MSE balance (MSE3203S-100, Sartorius, Germany). The measurement was stopped typically at 4 bar after reaching a linear flux regime indicating a complete displacement of the wetting liquid.

Analysis of measurement data was carried out using the "interfacial pore flow model" which is the most common model applied to LLDP analysis [46]. This model utilizes the Cantor equation which describes the necessary pressure difference ΔP on both sides of the pore to displace a wetting liquid inside a single pore of a defined pore diameter

$$d_{\mathrm{pore}} = \frac{4\gamma}{\Delta P} \quad (14)$$

with γ being the interfacial tension. The pore geometry is assumed to be cylindrical and the flux laminar so that the Hagen-Poiseuille law can be applied to describe the flux through an individual pore. The further approach to obtain PSDs is based on calculation of flux ratios Q between the flux during the displacement of the wetting liquid J_1 and the flux through the membrane of only one liquid J_2 without any displacement involved.

$$Q(\Delta P) = \frac{J_1(\Delta P)}{J_2(\Delta P)} \quad (15)$$

This approach is based on the work of Zeman & Zydney [45] and was successfully applied for VFs by Giglia et al. [15] resulting in a permeance-weighted probability density function for the PSD

$$f_{1,}(d_{\mathrm{pore}}) = \frac{\mathrm{d}Q}{\mathrm{d}\Delta P}\left(\frac{\Delta P^2}{4\gamma}\right) \quad (16)$$

An advantage of this approach is that besides the interfacial tension no further constants need to be determined. Deviating from previous works J_2 was not determined by an additional experiment, but extrapolated from the linear increase of J_1 at higher pressure (see Fig. 1).

For comparability reasons with PSDs obtained from GNP filtrations LLDP data was fitted using a log-normal CDF having the form of Eq. (2) and the mean pore size was calculated according to Eq. (3).

3. Results and discussion

3.1. Size characterization of GNPs

Size is the most important property of particles used in solute

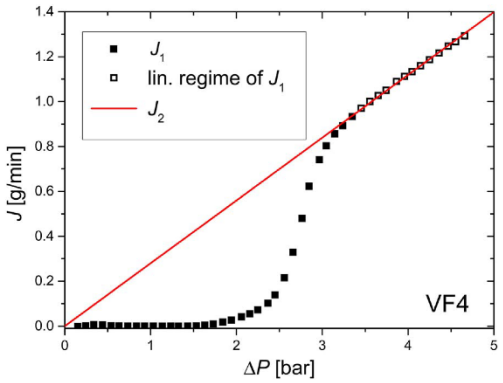

Fig. 1. Example of experimental flux-pressure data (filled and empty squares) obtained by a single LLDP run for VF4. Linear extrapolation of the linear regime from J_1 (empty squares) allowed to approximate the flux of the pure displacement liquid without prior wetting of the membrane with the wetting liquid.

rejection experiments in order to determine structural membrane properties. VFs have narrow PSDs and as a result high selectivities. Thus in the range of the barrier pore size, a very large increase of retention by increase of particle size by a few nanometer is possible (cf. Section 3.4.). Therefore, sizes of all particle batches have been measured, in addition to the manufacturer's specifications, to ensure proper knowledge of the actual sizes close to the execution of the filtration experiments.

Four complementary techniques were evaluated for size determination of GNPs, namely TEM, DLS, differential centrifugal sedimentation (DCS) and UV–Vis spectrophotometry.

Results from TEM in combination with image analysis were assumed to be most reliable and therefore used as reference for the remaining methods (Fig. 2, for more details see Fig. S1, Supporting information). Fig. 3 shows the outlines of three differently sized batches of GNPs (batches 2, 4, 11) identified by the image processing software ImageJ from TEM images. This imaging technique allows high-resolution single particle measurements over the size range of interest from 5 to 50 nm on the one hand. On the other hand, the susceptibility of size measurements towards impurities is low due to the high material contrast of gold. Additionally, direct insights into the number distribution of the particle sizes can be obtained without further conversions or assumptions. As a disadvantage only the size of the gold core is measured, while the particle shell consisting of organic ligands and the hydration shell is collapsed during the measurement in a non-native, dry environment.

In contrast, DLS provides the hydrodynamic particle diameter in a native aqueous environment. Due to the high dependency of the light scattering intensity with the 6th power of the particle size, very few large particles have a high influence on the results. As a consequence, DLS measurements are very susceptible towards larger species like dust particles and require proper sample preparation e.g. by filtration. For comparability with other techniques, results need to be transformed for instance into a number-weighed distribution, necessitating additional knowledge of the material properties of the particles namely the refractive index and the absorptivity.

DCS is based on sedimentation properties of the analyte. Particles are separated by their size and density. Thus different species are detected separately so that size measurements of gold nanoparticles are robust against impurities (e.g. dust particles). As particles sizes are determined against a standard, usually latex beads, with narrow size distribution, DCS is a relative method. For precise size measurements proper knowledge of the particle density is mandatory, which was assumed to be equal with the density of the pure element in case for the GNPs.

Size measurements according to the method of Haiss et al. [47] using UV–Vis spectroscopy require only a simple UV–Vis spectrometer that is available in a standard chemical laboratory. Due to the ease and low costs of this technique, it was also evaluated in this study although it is considered to be less robust than the other techniques applied in this study. Optical properties of the gold nanoparticles are not only dependent on the particle diameter but also on the shape, dispersity and coating thickness/chemistry. Haiss et al. also observed limitations of their technique for particles < 10 nm, further restricting its applications with regard to characterization of parvovirus retentive VFs [47].

Excellent correlations were found between results obtained using TEM/DCS and TEM/DLS as indicated by very high adjusted R^2-values of 0.993 and 0.982, respectively (Fig. S1, Supporting information). These results using three complementary methods verify TEM as being a valid and precise technique for determination of the mean particle diameters used in this study. Hence, for pore size evaluation TEM-based particle diameters will be used. In case of limited access to a transmission electron microscope, DCS and DLS are also suitable alternatives, which can properly differentiate between the single particle batches. DLS was also used to verify that addition of SDS to the GNP solutions did not significantly alter size distributions of the GNPs (Fig. S2, Supporting information). Although systematic deviations exist between TEM, DCS and DLS, which also have been observed for citrate-stabilized silver nanoparticles by Cascio et al. [48], such deviations have to be considered especially, when PSDs obtained by particle rejection are compared with other techniques. DLS results are systematically larger than TEM and DCS results as DLS measures the hydrodynamic diameter. By using TEM, only the size of the GNP core is measured, underestimating the hydrodynamic diameter by about 2.3 nm when compared to DLS results as calculated by Eq. (6). Size measurements by DCS further underestimate the particle sizes when compared to TEM. This can be related to the assumed density of pure gold for the GNPs. The real density should be lower than the one of pure gold, as the particles also consist of organic ligands that decrease the effective density, leading to slower sedimentation that is interpreted as a smaller particle size. Also a non-sphericity of the particles will result in lower sedimentation velocity, leading to smaller particle diameters [48].

Although diameters provided by the manufacturer and UV–Vis spectroscopy correlate quite well with TEM diameters (adj. R^2=0.941 and 0.911, respectively), the capability to differentiate between the individual GNP batches compared to TEM, DCS or DLS is significantly lower. Using particle diameters determined by UV–Vis spectroscopy is not favorable for applications as the pore size determination of membranes with narrow PSDs to which VFs belong (Fig. S1, Supporting information).

Besides the knowledge of mean particle sizes, an adequate low dispersity of the particles is a prerequisite to obtain sharp retention curves that display the high selectivity of a VF. High particle dispersity would lead to broader retention curves masking the real selectivity of the membrane. In such cases additional measurements of the particle size distributions in the permeates would be required in order to determine more realistic PSDs as it is common practice for solute rejection experiments using highly disperse linear polymers [22]. All dispersity indices were < 0.1 indicating very narrow particle size distributions that can be assumed as monodisperse (Fig. S3, Supporting information).

3.2. Influence of anionic surfactant SDS on GNP retention mechanism

A variation in pre-treatment and filtration conditions regarding the SDS concentration used in the equilibration (water and SDS) and in the GNP solution (water, GNPs and SDS) was conducted for VF4 (PES). As depicted in Table 1, SDS very efficiently reduces the dominant adsorptive retention

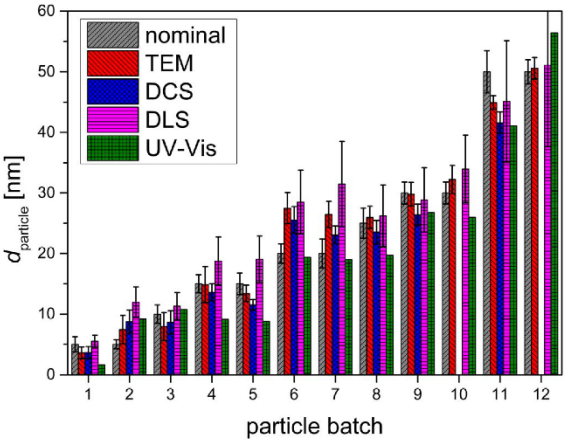

Fig. 2. Overview of nominal GNP diameters provided by the manufacturer and measured mean diameters by TEM, DCS, DLS and UV–Vis spectrophotometry for all GNP batches used for further studies. Error bars represent the standard deviations of the particle size distributions.

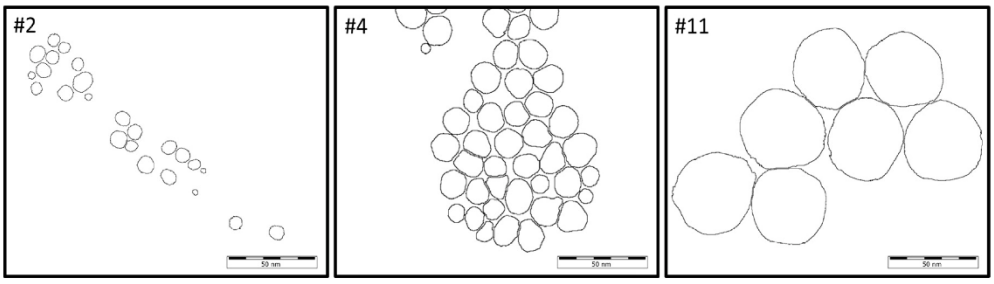

Fig. 3. Processed TEM images for GNP batches 2, 4 and 11 using ImageJ for elaboration of particle shape and size.

of citrate-stabilized GNPs in a surface modified PES membrane, shifting the overall mechanism towards a size exclusion based retention mechanism. Depending on the SDS concentration, the ratio of adsorptive to size-exclusive retention can be adjusted.

In case of filtration without SDS present (Table 1a)), GNPs were quantitatively retained on the feed facing side of the membrane which is visible by the dark purple discolouration, while the permeate facing side kept the white colour of the pristine membrane. The membrane cross section image clearly shows that the particles are retained on the outermost surface of the feed facing side. Penetration of the particles deeper into the membrane structure is minimal. Increasing the SDS concentration to 0.10 wt% in both equilibration and GNP solution allowed most of the GNPs to penetrate deeper into the membrane structure (Table 1b)). The feed facing side is slightly discoloured, while the permeate facing side shows a more intense discolouration. This indicates that the particles are retained deeper in the membrane structure, more closely to the permeate facing side. The cross section image confirms this observation. A well-defined coloured band is visible in the lower part of the cross section some micrometers above the separation-active layer with the narrowest pore sizes. The whole area above the band is also discoloured uniformly, but with much lower intensity, indicating that coverage of the membrane pore surface by SDS is incomplete, therefore allowing GNP adsorption to some extent. Further increase of the SDS concentration to 0.26 wt% results in a quantitative retention of GNPs deep within the membrane structure at a narrow location without any visible retention of particles towards the feed facing side (Table 1c)). The feed facing side shows no discolouration, while the permeate facing side shows the most intense discoloration compared. In the cross section image only a clear and intense purple coloured band closely above the retentive layer is visible.

High propensity for GNP adsorption on PES membranes can be explained by the high affinity of gold towards sulphur-containing moieties on the PES itself and towards nitrogen-containing moieties. Although all commercial VFs made from PES or PVDF are surface modified to increase hydrophilicity, it is probable that surface coverage of the hydrophilizing agent is not complete, so that still some patches with the base material are exposed. Due to the intrinsic hydrophobicity of PES (and also of PVDF) anionic surfactants like SDS adsorb on the hydrophobic surface with the hydrophobic tail while negatively charged head groups are facing away, in case of membranes into the pore void. A thus resulting high negative charge on the membrane surface causes repulsion with the negatively charged GNPs, shielding the aurophilic moieties of the membrane and reducing adsorption. Nitrogen-containing moieties can also be incorporated into PES membranes as part of frequently used hydrophilizing agents like poly(*N*-vinyl-2-pyrrolidone) (PVP) that are preferentially localized at the membrane surface [49]. PVP is also often used for surface-functionalization of GNPs as it readily undergoes a ligand exchange with weaker bound citrate ligands [50]. Therefore, besides adsorption to the base polymer another cause for GNP adsorption on PES membranes is probably based on the ligand exchange between GNP bound citrate and PVP anchored to the membrane surface. Since SDS is known to strongly interact with PVP, also forming large aggregates when both species are present free in solution [51], this interaction most probably suppresses further

Table 1
Overview of photos of VF4 showing cross sections, feed and permeate facing sides after filtration experiments with GNP (20 nm nominal diameter) utilizing different SDS concentrations in equilibration and GNP solutions. Membrane cross sections (light microscopy) oriented with feed facing side to the top. Black arrows show the position of GNPs in the membrane cross sections. The white arrow symbolizes the approximate position of the separation-active layer with the narrowest pores within the membrane structure.

	c(SDS) [wt%]	cross section	side facing feed	side facing permeate
a)	0			
b)	0.10			
c)	0.26			

ligand exchange reactions of PVP with the GNPs and thereby also reduces adsorption to the membrane surface.

In additional filtration experiments with smaller GNPs of 4 and 8 nm diameter (TEM) using VF5 (PES), the LRVs were determined throughout the course of filtration (Fig. 4).

A high initial decline in LRV was observed for all filtrations. It is contributed to the hold-up volume of the membrane device, which was corresponding to 3.5 L/m^2. Before the filtration of GNPs, the membranes were flushed with equilibration solution or RO water. When the filtration of GNPs was started the permeate side of the module was still filled with liquid. This leads to a dilution of the permeate and apparently high LRVs at the beginning of the GNP filtration. To verify the extent of this dilution effect due to the hold-up volume, a filtration was conducted with an aqueous solution of methylene blue. This small molecular dye is supposed to pass the membrane unhindered. After about two to three hold-up volumes, the LRV of methylene blue drops to approximately zero explaining the initial LRV decline for the GNPs.

GNPs of 4 nm (TEM) in diameter, the smallest particles used in this study, were filtered with a prior SDS treatment. Due to their small size compared to the pore sizes of a parvovirus retentive VF, the loading dependent LRV shows a similar progression to what was observed for methylene blue. Deviations from the experiment with methylene blue are a slightly less distinct initial LRV decline, probably caused by a lower mass transport velocity of GNPs compared to the solvent. As the particle size and the pore diameter are in same order of magnitude, effects like steric rejection and solute velocity lag [52] decrease the mass transport of the solutes. Also the lower boundary value of the LRV is slightly higher compared to the experiment with methylene blue, which can possibly be contributed to a small fraction of larger GNP species present in the feed that are retained.

Increasing the particle size to 8 nm (w/ SDS treatment) further enhances the trend already observed for the 4 nm GNPs. The initial LRV decline progresses more slowly and reaches a significantly higher boundary LRV, which is directly related to the larger average particle size. In addition, LRV starts to increase after a minimum, which can be explained by a size exclusion dominated retention mechanism. A large proportion of the particles reaches the pores in the separation-active layer located deep in the membrane structure, resulting in a progressive plugging of the pores. In contrast, the overall higher and continuously decreasing LRVs for the filtration of 8 nm particles without SDS treatment indicate that under such conditions the size exclusion mechanism is superimposed by an adsorption based retention mechanism. Similar findings were reported by Ladner et al. for 0.1 µm PVDF membranes using 6 nm sized GNPs [36]. Most of the particles are retained at the outermost membrane surface by adsorption (similar to VF4, see Table 1a)), where pore sizes are significantly larger than the actual barrier pore size. Here the reduction of effective pore size, as a result of pore wall coverage with GNPs, has only little influence on the retention capability of the pore for additional particles. At the beginning of the filtration, only very few particles are transported through the membrane by convection without collision with the pore wall and subsequent adsorption. In the course of filtration, more and more adsorption sites are occupied by GNPs at greater depths of the membrane. This leads to a lower probability for particles to be retained by adsorption and thereby decreases the LRV throughout the course of filtration. Nevertheless, because particles are mostly captured before the actual barrier layer (cf. Table 1a), LRV is significantly higher than in case of SDS addition.

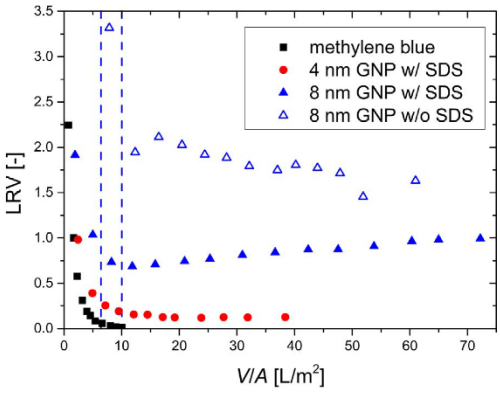

Fig. 4. LRV for 4 and 8 nm GNPs with VF5 as a function of volumetric throughput. For 8 nm GNPs both variations w/ and w/o SDS treatment were examined. In order to estimate dilution effects of the permeate caused by the hold-up volume of the device, the LRV for a low molecular weight molecule (methylene blue) was also determined as a function of the volumetric throughput. Dashed blue lines illustrate the throughput range between two and three hold-up volumes at which grab samples were taken for the rest of the experiments. (For interpretation of the references to color in this figure legend, the reader is referred to the web version of this article.)

3.3. Flux reduction with SDS solutions

High initial flux declines reaching stationary fluxes at 40–95% flux decay during the filtration of 0.26 wt% SDS solutions without GNPs were observed for most of the membranes (Fig. 5). Stationary fluxes were reached within very few hold-up volumes filtered through the membranes, indicating an adsorption of SDS rather than pore plugging by SDS micelles. Although the SDS concentration was above the critical micelle concentration (CMC) of 0.24 wt% [53] and hence SDS micelles should have been present during the filtration experiments, the micelle diameter of 4 nm [54,55] would be too small to cause significant pore plugging (cf. Section 3.4.). The interpretation is also supported by the additional results shown in Fig. S4 (Supporting information); the change of relative flux with time for different SDS concentrations reveals a systematic influence of SDS concentration and very large effects well below CMC. As a consequence of SDS adsorption, estimated pore constrictions based on the Hagen–Poiseuille equation can account for up to 50% of the pore diameter. The magnitude of flux decay and pore constriction is highly dependent on the proprietary surface chemistries the different membrane manufacturers apply. For the two selected extreme cases, VF3 and VF4, the flux progression with SDS solution is depicted in Fig. 6, showing that large flux decay is almost instantaneous for VF4 and reaching a constant value of 4% of the water flux, while flux of VF3 was barely affected by SDS. In contrast to all other membranes, VF3 did not show any adsorption of GNPs in the absence of SDS (Fig. S5, Supporting information). Therefore, consideration of the change in effective pore size by SDS adsorption is mandatory for the determination of PSDs. This diversity with respect to properties of base materials as well as surface chemistries, highly influencing other than only size exclusion characteristics, poses a major challenge for most techniques for determination of PSDs of mesoporous structures. Using a surfactant allows to equalise the membrane surfaces, while at the same time it is easily possible to quantify its impact on the pore sizes by simple flux measurements. An application of surfactants in solute rejection experiments that reduce membrane-solute interactions enables valid insights into PSDs of membranes, which exhibit very different surface characteristics.

3.4. PSDs from GNP filtration experiments

Comprehensive data depicted in Fig. 7 shows that values embracing the whole retention range from zero to unity can be obtained for all membranes, independently of the base material or the surface chemistry, by the application of SDS. It is evident that particles larger than 20 nm are retained by more than 99% for all VFs, often exceeding the detection limit of about 99.9%. In contrast for the 100k PES ultrafilter retention values for particles between 20 and 30 nm are about 97–98%. This observation confirms the expectations for parvovirus retentive VFs

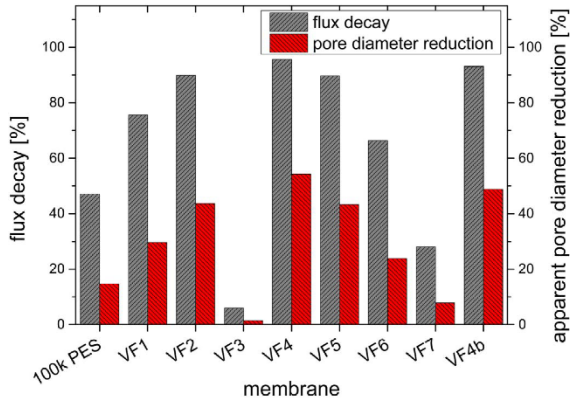

Fig. 5. Flux decays and resulting apparent pore diameter reductions as consequence of SDS adsorption for all membranes tested.

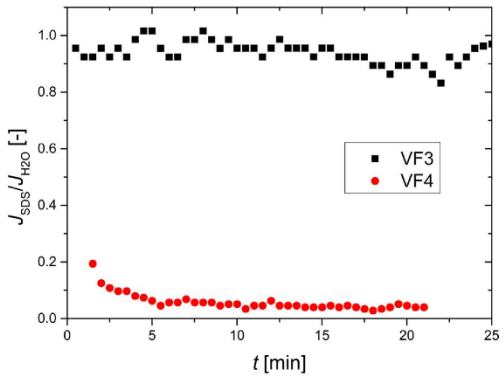

Fig. 6. Relative flux with 0.26 wt% SDS solution versus time for VF3 and VF4.

to efficiently remove particles > 20 nm mostly on basis of size exclusion.

While all membranes tested exhibit quite similar mean pore diameters of 12–16 nm, except for VF4b, variations of 99% cut-off pore diameters are much more distinct ranging from 20 to 36 nm (Fig. 8A,B). More interestingly, the coefficient of variation for the 100k PES ultrafilter membrane is significantly larger than those of all VFs, indicating a relative broad PSD (Fig. 8C). It is often stated that ultrafiltration membranes have broader PSDs compared to microfiltration membranes and VFs [9–12,15,56,57], probably caused by the presence of abnormally large pores in combination with the very thin separation-active layer, but direct experimental comparisons between these membrane types are rare. As can be seen for the VFs, the coefficients of variation are significantly smaller than for the 100k PES ultrafilter membrane and can be further classified into two groups by their absolute values. VF1-3 have coefficients of variation > 0.2, while the ones for VF4-7 are < 0.2. This classification is in accordance with two generations of VFs in the market. Recently, Giglia et al. also observed a significantly broader PSD using LLDP for a first generation parvovirus retentive VF in comparison to a second generation VF [15]. The first generation of parvovirus retentive VFs, developed in the late 1980s and 1990s, suffered from virus retention issues, exhibiting overall low virus retention and susceptibility to breakthrough due to fouling or process interruptions [13,58–61]. VFs which belong to the second generation show robust virus retention performance, although the virus retention mechanisms are not fully understood yet [2]. The low coefficients of variation for the second generation of parvovirus retentive VFs, signifying narrow PSDs, suggest that the width of the PSD is a key membrane parameter with regard to robust virus retention performance.

3.5. Comparison of PSDs from GNP filtration with LLDP

PSDs were also determined by LLDP as complementary technique to verify the validity of the results obtained from GNP filtration experiments. Due to different interactions of the 2-phase system used for LLDP with the various membrane base materials and surface chemistries results from LLDP are much more complex to interpret. Therefore, only LLDP results for the homologous membranes VF4 and VF4b are discussed; these membranes differ just by the barrier pore size but not by chemistry or the pore size gradients. Both methods used for determination of PSDs are capable of differentiation between VF4 and VF4b (Fig. 9), both show a significant difference in mean pore size of about 3 nm for the two filters (Fig. 10). Results obtained from GNP experiments are systematically smaller by 5 nm compared to LLDP. This can be contributed to more complex transport phenomena of particles inside porous structures, as discussed in Section 3.2., leading to increased observed retention values for particles only slightly smaller than the actual pore size.

3.6. Virus retention performance for different sized virus particles

Exemplarily, using VF7, retention performance for a set of different sized virus particles was determined (Fig. 11) in order to further confirm the size exclusion mechanism of VFs as already observed with GNPs (cf. Section 3.2.). Three mammalian viruses (PCV-2, MVM, HAV) and one bacteriophage (PP7) were used, having different particle diameters ranging from 18 to 28 nm as determined by TEM measurements. Virus solutions did not contain SDS as it could denaturate their capsids resulting in a decrease in infectivity and thereby detectability.

Filtration experiments with the largest virus HAV (27.9 ± 1.9 nm) showed no virus breakthroughs, resulting in LRVs above the upper detection limit of LRV 7.5. Retention of the mid-sized MVM (22.9 ± 1.2 nm) and PP7 (23.3 ± 3.4 nm) was either above the upper detection limit of LRV 6.5 for MVM or reached a high value of LRV 5.2 within the detection limit for PP7. A low LRV was observed for PCV-2 (18.0 ± 0.9 nm) as it is the smallest virus in this set of experiments, achieving only LRV 1.2. In general this LRV decline with decreasing virus particle size strongly indicates that the overall retention mechanism of VFs is mainly governed by size exclusion, which is observed with different sized GNPs for different VFs as well, although contributions from adsorptive retention cannot be ruled out in case of the viruses.

Direct comparison of the size dependent retention behavior between GNPs and viruses is a challenging task. While using GNPs the whole spectrum of retention can be mapped for parvovirus retentive VFs (cf. Section 3.4.), the very limited availability of smaller viruses than the PCV-2 allows to observe retention only for the high retention regime with r > 0.9 (> 1 LRV).

3.7. Correlation of 99% cut-off pore diameter $\bar{d}_{99\%}$ with bacteriophage PP7 retention

The 99% cut-off pore diameter determined from GNP filtration experiments using SDS as detergent shows some predictive potential towards PP7 retention for a variety of very different VFs (Fig. 12). In addition to the findings using one VF with different sized virus particles (cf. Section 3.6.), this result further supports a virus retention mechanism that is dominated by size exclusion. Virus retention performance is mostly determined by the largest pores of a membrane [14]. As $\bar{d}_{99\%}$ is extrapolated from continuous PSDs, it can be assumed that the largest pores of VFs are part of such continuous distributions, rather than being abnormal pores that are not included. Urase et al. found no correlation between PEG and phage retention for a variety of membranes involving microfiltration, ultrafiltration and desalination membranes [10]. The authors explained their observation by the

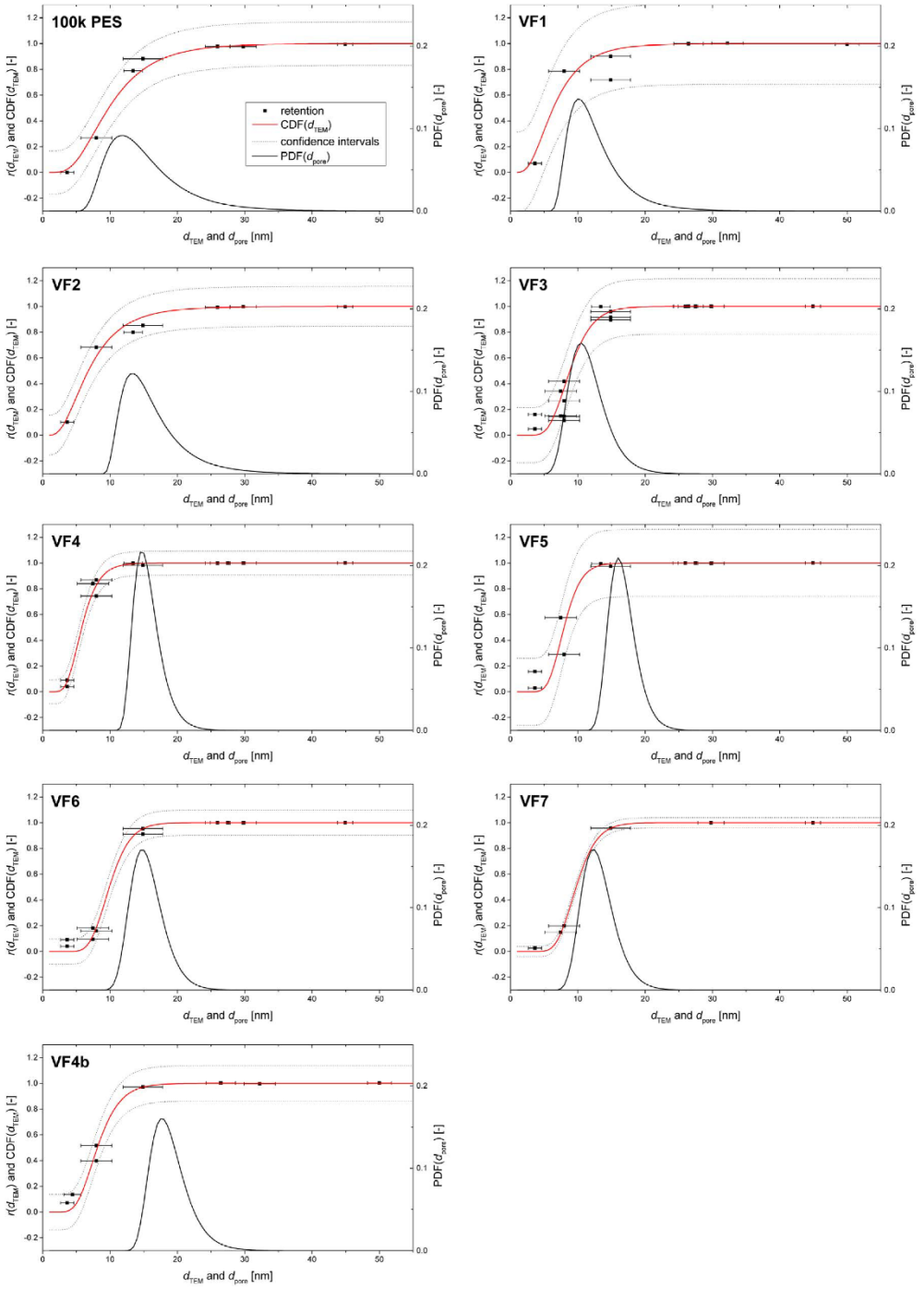

Fig. 7. Experimental data (filled squares) for the observed GNP retention versus particle diameters (TEM) and resulting probability density functions (solid black lines) describing the PSDs for all membranes tested. Calculated retention values (red solid curves) and 95% confidence intervals (black dotted curves) were obtained from nonlinear least-squares fitting of the retention data using log-normal CDFs. The error bars represent the standard deviations of the particle size distributions of the individual particle batches. (For interpretation of the references to color in this figure legend, the reader is referred to the web version of this article.)

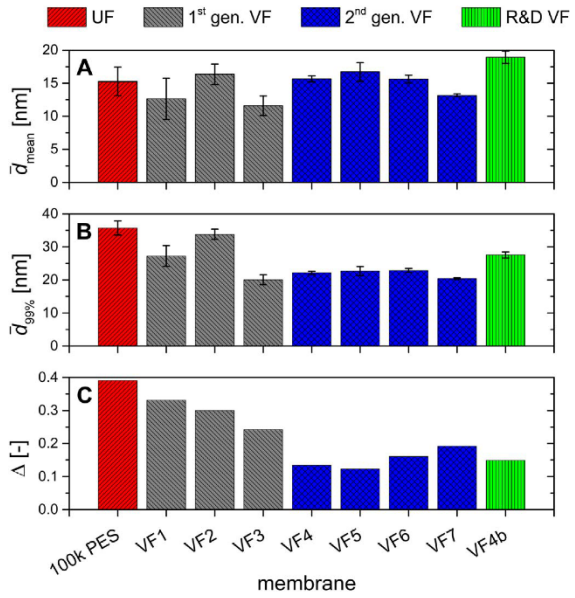

Fig. 8. Summarized results for $\bar{d}_{mean}$ (A), $\bar{d}_{99\%}$ (B) and Δ (C) for all membranes tested. Error bars represent the uncertainty estimated from the confidence intervals of the log-normal CDF fit of the retention data.

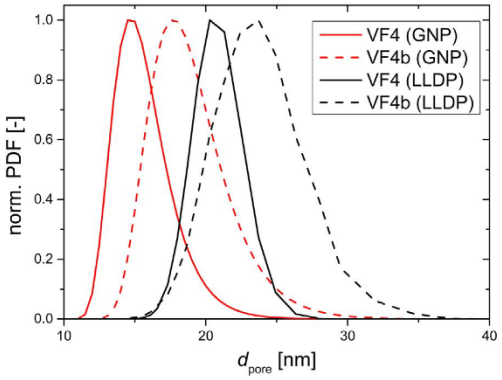

Fig. 9. Normalized log-normal probability density function versus pore diameters for homologous membranes VF4 (solid curves) and VF4b (dashed curves) differing only in pore size determined by complementary techniques using GNPs (red curves) and LLDP (black curves). (For interpretation of the references to color in this figure legend, the reader is referred to the web version of this article.)

presence of abnormally large pores being not included in a continuous PSD, although a more complex retention mechanism of flexible molecules like PEG, in contrast to rigid virus or GNPs, is also conceivable.

4. Conclusions

The presented technique of GNP filtration using SDS, an anionic detergent, allows to determine PSDs of VFs as well as of ultrafiltration membranes that are challenging to access by other techniques. It was shown that application of SDS can shift the mechanism of retention from an adsorption to a size exclusion dominated mechanism. Thereby, usage of SDS facilitates membrane characterization in an aqueous environment close to application conditions and is more independent of the individual membrane material and surface chemistry. The results

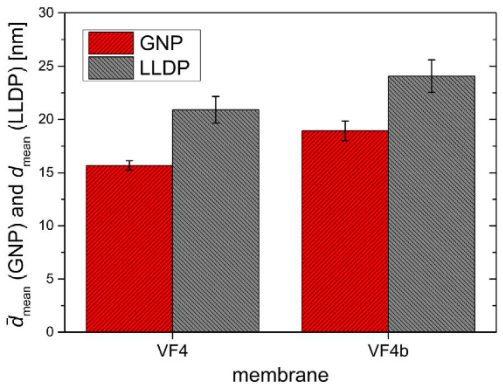

Fig. 10. Comparison of mean pore sizes of VF4 and VF4b determined using GNPs (red bars) and LLDP (grey bars). (For interpretation of the references to color in this figure legend, the reader is referred to the web version of this article.)

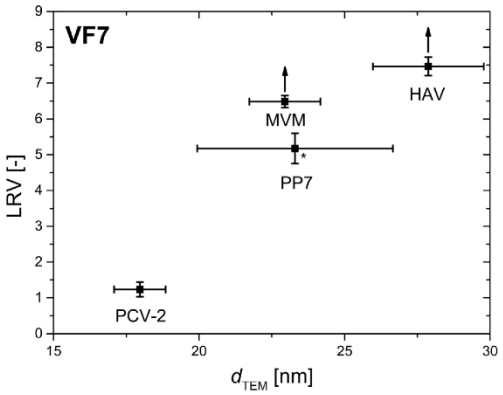

Fig. 11. LRV for a set of different viruses as a function of virus diameters determined by TEM. The horizontal error bars represent the standard deviations of the particle size distributions for the virus strains. Vertical error bars represent the standard deviations calculated from duplicate runs. For PP7, as denoted by the asterisk, particle size measurement using TEM was conducted independently at different sites and instruments resulting in a higher standard deviation.

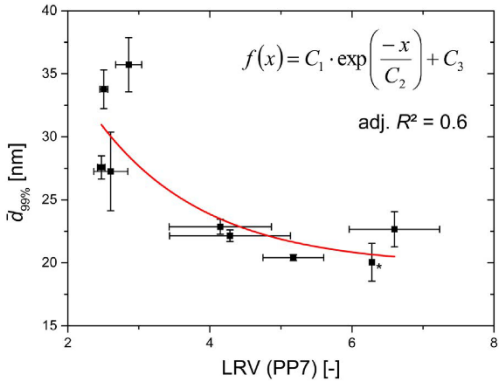

Fig. 12. Correlation of 99% cut-off pore diameters determined from GNP experiments with LRVs determined using bacteriophage PP7 as accepted model virus for the set of membranes tested. The asterisk denotes filtration runs without any phages detected in the permeates. Data was additionally fitted empirically to an exponential decay function.

show that state-of-the-art second generation VFs exhibit narrower PSDs than the first generation VFs and ultrafiltration membranes. Comparison of PSDs with virus retention data corroborates size exclusion as main retention mechanism for viruses using VFs. However, additional contributions with respect to the influence of surface chemistry on solute/particle adsorption and the role of virus, product or matrix component adsorption onto the VF pore surface may also have some impact to the overall virus removal under process relevant conditions. Ongoing work is addressing such questions, for instance by studying the retention mechanisms of viruses in presence or absence of surface-active feed components such as proteins.

Acknowledgements

The authors sincerely express their thanks to Labor Dr. Merk & Kollegen GmbH for conducting the virus filtration study. We also thank Prof. Dr. Matthias Epple and his group from Duisburg-Essen University, for the permission to use the disc centrifugation system. Further, we would like to acknowledge Dr. Wiebke Möbius of the Max-Planck Institute of Experimental Medicine in Göttingen and Dr. Vladimir Roddatis from the University of Göttingen for their support with TEM measurements.

Appendix A. Supporting information

Supplementary data associated with this article can be found in the online version at doi:10.1016/j.memsci.2017.03.043.

References

[1] PDA, Technical Report No. 41 – Virus Filtration, Parenteral Drug Association, Bethesda, MD, 2008.
[2] D. Chen, Q. Chen, Virus retentive filtration in biopharmaceutical manufacturing, PDA Lett. (2016) 20–22.
[3] R. Cameron, K. Smith, Virus clearance methods applied in bioprocessing operations: an overview of selected inactivation and removal methods, Pharm. Bioprocess. 2 (2014) 75–83. http://dx.doi.org/10.4155/pbp.13.61.
[4] S. Ray, S. Dolan, Single-use virus clearance technologies in biopharmaceutical manufacturing: case studies, in: R. Eibl, D. Eibl (Eds.), Single-Use Technology in Biopharmaceutical Manufacture, John Wiley & Sons, Hoboken (New Jersey, USA), 2011, pp. 311–322.
[5] G. Miesegaes, S. Lute, H. Aranha, K. Brorson, Virus retentive filters, in: M.C. Flickinger (Ed.)Downstream Industrial Biotechnology, John Wiley & Sons, Hoboken (New Jersey, USA), 2013, pp. 641–654.
[6] W.J. Rayfield, D.J. Roush, R.A. Chmielowski, N. Tugcu, S. Barakat, J.K. Cheung, Prediction of viral filtration performance of monoclonal antibodies based on biophysical properties of feed, AIChE J. 31 (2015) 765–774. http://dx.doi.org/10.1002/btpr.2094.
[7] C. Charcosset, Membrane Processes in Biotechnology and Pharmaceutics, 1st ed, Elsevier, Oxford (UK), 2012. http://dx.doi.org/10.1016/B978-0-444-56334-7.00001-0.
[8] S.R. Wickramasinghe, E.D. Stump, D.L. Grzenia, S.M. Husson, J. Pellegrino, Understanding virus filtration membrane performance, J. Membr. Sci. 365 (2010) 160–169. http://dx.doi.org/10.1016/j.memsci.2010.09.002.
[9] T. Hongo-Hirasaki, K. Yamaguchi, K. Yanagida, K. Okuyama, Removal of small viruses (parvovirus) from IgG solution by virus removal filter Planova® 20N, J. Membr. Sci. 278 (2006) 3–9. http://dx.doi.org/10.1016/j.memsci.2005.10.057.
[10] T. Urase, K. Yamamoto, S. Ohgaki, Effect of pore structure of membranes and module configuration on virus retention, J. Membr. Sci. 115 (1996) 21–29. http://dx.doi.org/10.1016/0376-7388(95)00269-3.
[11] E. Arkhangelsky, V. Gitis, Effect of transmembrane pressure on rejection of viruses by ultrafiltration membranes, Sep. Sci. Technol. 62 (2008) 619–628. http://dx.doi.org/10.1016/j.seppur.2008.03.013.
[12] T. Urase, K. Yamamoto, S. Ohgaki, Effect of pore size distribution of ultrafiltration membranes on virus rejection in crossflow conditions, Water Sci. Technol. 30 (1994) 199–208.
[13] S. Lute, M. Bailey, J. Combs, M. Sukumar, K. Brorson, Phage passage after extended processing in small-virus-retentive filters, Biotechnol. Appl. Biochem. 47 (2007) 141–151. http://dx.doi.org/10.1042/BA20060254.
[14] R.I. Peinador, J.I. Calvo, K. ToVinh, V. Thom, P. Prádanos, A. Hernández, Liquid – liquid displacement porosimetry for the characterization of virus retentive membranes, J. Membr. Sci. 372 (2011) 366–372. http://dx.doi.org/10.1016/j.memsci.2011.02.022.
[15] S. Giglia, D. Bohonak, P. Greenhalgh, A. Leahy, Measurement of pore size distribution and prediction of membrane filter virus retention using liquid–liquid porometry, J. Membr. Sci. 476 (2015) 399–409. http://dx.doi.org/10.1016/j.memsci.2014.11.053.
[16] P. Kosiol, B. Hansmann, M. Ulbricht, V. Thom, Structure analysis of virus filter via gold nanoparticles and liquid-liquid displacement porometry. Presented at PDA Virus & TSE Safety Forum, Lisbon, Portugal, 2015.
[17] J.I. Calvo, A. Bottino, G. Capannelli, A. Hernández, Comparison of liquid – liquid displacement porosimetry and scanning electron microscopy image analysis to characterise ultrafiltration track-etched membranes, J. Membr. Sci. 239 (2004) 189–197. http://dx.doi.org/10.1016/j.memsci.2004.02.038.
[18] M.W. Phillips, A.J. DiLeo, A validatible porosimetric technique for verifying the integrity of virus-retentive membranes, Biologicals 24 (1996) 243–253. http://dx.doi.org/10.1006/biol.1996.0033.
[19] I.M. Wienk, B. Folkers, T. van den Boomgaard, C.A. Smolders, Critical Factors in the Determination of the Pore Size Distribution of Ultrafiltration Membrances Using the Liquid Displacement Method, Sep. Sci. Technol. 29 (1994) 1433–1440. http://dx.doi.org/10.1080/01496399408003029.
[20] R.I. Peinador, J.I. Calvo, P. Prádanos, L. Palacio, A. Hernández, Characterisation of polymeric UF membranes by liquid – liquid displacement porosimetry, J. Membr. Sci. 348 (2010) 238–244. http://dx.doi.org/10.1016/j.memsci.2009.11.008.
[21] M.L. Méndez, A.I. Romero, V.B. Rajal, E.F. Castro, J.I. Calvo, L. Palacio, A. Hernández, Properties of polyethersulfone ultrafiltration membranes modified with polyethylene glycols, Polym. Eng. Sci. 54 (2014) 1211–1221. http://dx.doi.org/10.1002/pen.23637.
[22] M. Bakhshayeshi, D.M. Kanani, A. Mehta, R. Van Reis, R. Kuriyel, N. Jackson, A.L. Zydney, Dextran sieving test for characterization of virus filtration membranes, J. Membr. Sci. 379 (2011) 239–248. http://dx.doi.org/10.1016/j.memsci.2011.05.067.
[23] S.R. Wickramasinghe, S.E. Bower, Z. Chen, A. Mukherjee, S.M. Husson, Relating the pore size distribution of ultrafiltration membranes to dextran rejection, J. Membr. Sci. 340 (2009) 1–8. http://dx.doi.org/10.1016/j.memsci.2009.04.056.
[24] A. Duek, E. Arkhangelsky, R. Krush, A. Brenner, V. Gitis, New and conventional pore size tests in virus-removing membranes, Water Res. 46 (2012) 2505–2514. http://dx.doi.org/10.1016/j.watres.2011.12.058.
[25] C. Agarwal, A.K. Pandey, S. Das, M.K. Sharma, D. Pattyn, P. Ares, A. Goswami, Neck-size distributions of through-pores in polymer membranes, J. Membr. Sci. 415–416 (2012) 608–615. http://dx.doi.org/10.1016/j.memsci.2012.05.055.
[26] E. Arkhangelsky, Y. Sefi, B. Hajaj, G. Rothenberg, V. Gitis, Kinetics and mechanism of plasmid DNA penetration through nanopores, J. Membr. Sci. 371 (2011) 45–51. http://dx.doi.org/10.1016/j.memsci.2011.01.014.
[27] E. Arkhangelsky, A. Duek, V. Gitis, Maximal pore size in UF membranes, J. Membr. Sci. 394–395 (2012) 89–97. http://dx.doi.org/10.1016/j.memsci.2011.12.031.
[28] T. Tsurumi, N. Osawa, T. Hirasaki, K. Yamaguchi, S. Manabe, T. Yamashiki, Mechanism of removing monodisperse gold particles from a suspension using cuprammonium regenerated cellulose hollow fiber, Polym. J. 22 (1990) 304–311. http://dx.doi.org/10.1295/polymj.22.304.
[29] T. Mizuno, A. Namiki, S. Tsuzuki, A novel filter rating method using less than 30-nm gold nanoparticle and protective ligand, IEEE Trans. Semicond. Manuf. 22 (2009) 452–461. http://dx.doi.org/10.1109/TSM.2009.2031762.
[30] H. Susanto, S. Franzka, M. Ulbricht, Dextran fouling of polyethersulfone ultrafiltration membranes – causes, extent and consequences, J. Membr. Sci. 296 (2007) 147–155. http://dx.doi.org/10.1016/j.memsci.2007.03.027.
[31] A. Helling, A. Kubicka, I.A.T. Schaap, M. Polakovic, B. Hansmann, H. Thiess, J. Strube, V. Thom, Passage of soft pathogens through microfiltration membranes scales with transmembrane pressure, J. Membr. Sci. 522 (2017) 292–302. http://dx.doi.org/10.1016/j.memsci.2016.08.016.
[32] M. Ramos, L. Ortiz-Jordan, A. Hurtado-Macias, S. Flores, J.T. Elizalde-Galindo, C. Rocha, B. Torres, M. Zarei-Chaleshtori, R.R. Chianelli, Hardness and elastic modulus on six-fold symmetry gold nanoparticles, Materials (Basel) 6 (2013) 198–205. http://dx.doi.org/10.3390/ma6010198.
[33] T. Hirasaki, T. Noda, H. Nakano, Y. Ishizaki, S. Manabe, N. Yamamoto, Mechanism of Removing Japanese Encephalitis virus (JEV) and gold particles using cuprammonium regenerated cellulose hollow fiber (i-BMM or BMM) from aqueous solution containing protein, Polym. J. 26 (1994) 1244–1256. http://dx.doi.org/10.1295/polymj.26.1244.
[34] K. Yamaguchi, Y. Hamamoto, S. Manabe, N. Yamamoto, Microparticle removability of the regenerated cellulose hollow fiber (BMM): an electron microscopic evaluation, J. Electron Microsc. 40 (1991) 337–345. http://dx.doi.org/10.1093/oxfordjournals.jmicro.a050906.
[35] P.L. Roberts, P. Feldman, D. Crombie, C. Walker, K. Lowery, Biologicals Virus removal from factor IX by filtration: validation of the integrity test and effect of manufacturing process conditions, Biologicals 38 (2010) 303–310. http://dx.doi.org/10.1016/j.biologicals.2009.12.006.
[36] D.A. Ladner, M. Steele, A. Weir, K. Hristovski, P. Westerhoff, Functionalized nanoparticle interactions with polymeric membranes, J. Hazard. Mater. 211–212 (2012) 288–295. http://dx.doi.org/10.1016/j.jhazmat.2011.11.051.
[37] S.-C. Chen, D. Segets, T.-Y. Ling, W. Peukert, D.Y.H. Pui, An experimental study of ultrafiltration for sub-10nm quantum dots and sub-150 nm nanoparticles through PTFE membrane and Nuclepore filters, J. Membr. Sci. 497 (2016) 153–161. http://dx.doi.org/10.1016/j.memsci.2015.09.022.
[38] G.-T. Wei, F.-K. Liu, Separation of nanometer gold particles by size exclusion chromatography, J. Chromatogr. A 836 (1999) 253–260. http://dx.doi.org/10.1016/S0021-9673(99)00069-2.
[39] F. Liu, G. Wei, Effect of mobile-phase additives on separation of gold nanoparticles by size-exclusion chromatography, Chromatographia 59 (2004) 115–119. http://dx.doi.org/10.1365/s10337-003-0135-2.
[40] N. Hamasaki, S. Ide, Method for test on integrity of microporous membrane, WO2008/111510 A1, 2008.

[41] S. Lute, W. Riordan, L.F. Pease III, D. Tsai, R. Levy, M. Haque, J. Martin, I. Moroe, T. Sato, M. Morgan, M. Krishnan, J. Campbell, P. Genest, S. Dolan, K. Tarrach, A. Meyer, M.J. Tarlov, M. Etzel, K. Brorson, A consensus rating method for small virus-retentive filters. I. method development, PDA J. Pharm. Sci. Technol. 62 (2008) 318–333.

[42] A.L. Zydney, P. Aimar, M. Meireles, J.M. Pimbley, G. Belfort, Use of the log-normal probability density function to analyze membrane pore size distributions: functional forms and discrepancies, J. Membr. Sci. 91 (1994) 293–298. http://dx.doi.org/10.1016/0376-7388(94)80090-1.

[43] A.M. Brown, A step-by-step guide to non-linear regression analysis of experimental data using a Microsoft Excel spreadsheet, Comput. Methods Prog. Biomed. 65 (2001) 191–200. http://dx.doi.org/10.1016/S0169-2607(00)00124-3.

[44] A.N. Cherkasov, A rapid analysis of ultrafiltration membrane structure, Sep. Sci. Technol. 40 (2005) 2775–2801. http://dx.doi.org/10.1080/01496390500333111.

[45] L.J. Zeman, A.L. Zydney, Microfiltration and Ultrafiltration: Principles and Applications, CRC Press, New York (USA), 1996.

[46] K.R. Morison, A comparison of liquid – liquid porosimetry equations for evaluation of pore size distribution, J. Membr. Sci. 325 (2008) 301–310. http://dx.doi.org/10.1016/j.memsci.2008.07.042.

[47] W. Haiss, N.T.K. Thanh, J. Aveyard, D.G. Fernig, Determination of size and concentration of gold nanoparticles from UV–Vis spectra, Anal. Chem. 79 (2007) 4215–4221.

[48] C. Cascio, D. Gilliland, F. Rossi, L. Calzolai, C. Contado, Critical experimental evaluation of key methods to detect, size and quantify nanoparticulate silver, Anal. Chem. 86 (2014) 12143–12151. http://dx.doi.org/10.1021/ac503307r.

[49] D. Rana, T. Matsuura, Surface modifications for antifouling membranes, Chem. Rev. 110 (2010) 2448–2471. http://dx.doi.org/10.1021/cr800208y.

[50] A. Rostek, D. Mahl, M. Epple, Chemical composition of surface-functionalized gold nanoparticles, J. Nanopart. Res. 13 (2011) 4809–4814. http://dx.doi.org/10.1007/s11051-011-0456-2.

[51] M. Prasad, R. Palepu, S.P. Moulik, Interaction between sodium dodecyl sulfate (SDS) and polyvinylpyrrolidone (PVP) investigated with forward and reverse component addition protocols employing tensiometric, conductometric, microcalorimetric, electrokinetic, and DLS techniques, Colloid Polym. Sci. 284 (2006) 871–878. http://dx.doi.org/10.1007/s00396-005-1453-8.

[52] L.J. Zeman, M. Wales, Polymer solute rejection by ultrafiltration membranes, in: A. F. Turbak (Ed.), Synth. Membr. Vol. II, ACS symposium series, Washington, D. C., USA, 1981, pp. 411–434.

[53] R. Barchini, R. Pottel, Counterion contribution to the dielectric spectrum of aqueous solutions of ionic surfactant micelles, J. Phys. Chem. 98 (1994) 7899–7905. http://dx.doi.org/10.1021/j100083a025.

[54] M. Molero, R. Andreu, D. Gonza, J. Jose, An isotropic model for micellar systems: application to sodium dodecyl sulfate solutions, Langmuir 17 (2001) 314–322. http://dx.doi.org/10.1021/la0010267.

[55] C.D. Bruce, M.L. Berkowitz, L. Perera, M.D.E. Forbes, Molecular dynamics simulations of sodium dodecyl sulfate micelle in water: micellar structural characteristics and counterion distribution, J. Phys. Chem. B 106 (2002) 3788–3793. http://dx.doi.org/10.1021/jp013616z.

[56] S.R. Bellara, Z. Cui, S.L. MacDonald, D.S. Pepper, Virus removal from bioproducts using ultrafiltration membranes modified with latex particle pretreatment, Bioseparation 7 (1998) 79–88. http://dx.doi.org/10.1023/A:1008033225254.

[57] A.J. DiLeo, A.E. Allegrezza Jr, S.E. Builder, High resolution removal of virus from protein solutions using a membrane of unique structure, Nat. Biotechnol. 10 (1992) 182–188. http://dx.doi.org/10.1038/nbt0292-182.

[58] G.R. Bolton, M. Cabatingan, M. Rubino, S. Lute, K. Brorson, M. Bailey, Normal-flow virus filtration: detection and assessment of the endpoint in bioprocessing, Biotechnol. Appl. Biochem. 42 (2005) 133–142. http://dx.doi.org/10.1042/BA20050056.

[59] S.K. Dishari, A. Venkiteshwaran, A.L. Zydney, Probing effects of pressure release on virus capture during virus filtration using confocal microscopy, Biotechnol. Bioeng. 112 (2015) 2115–2122. http://dx.doi.org/10.1002/bit.25614.

[60] M.A. Woods, A.L. Zydney, Effects of a pressure release on virus retention with the ultipor DV20 membrane, Biotechnol. Bioeng. 111 (2014) 545–551. http://dx.doi.org/10.1002/bit.25112.

[61] J. Stuckey, D. Strauss, A. Venkiteshwaran, J. Gao, W. Luo, M. Quertinmont, S. O'Donnell, D. Chen, A novel approach to achieving modular retrovirus clearance for a parvovirus filter, Biotechnol. Prog. 30 (2014) 79–85. http://dx.doi.org/10.1002/btpr.1820.

Supplementary material

A1. Size characterization of gold nanoparticles

DCS. For further characterization of particle sizes, differential centrifugal sedimentation (DCS) using a disc centrifuge DC 24000 (CPS Instruments Europe, Netherlands) was used. A density gradient was established by successive injections of 1.6 mL of 9 aqueous sucrose solutions (ranging from 24 to 8 wt%). To improve long-term stability of the density gradient, 0.5 mL dodecane was injected. After thermal equilibration of the centrifuge, measurements using 100 µL sample volumes were carried out against a calibration standard consisting of poly(vinyl chloride) particles of 476 nm at 24.000 rpm. The wavelength of the laser was 470 nm. Size calculation for the GNPs was based on assuming the density of gold (19.38 g/cm³ [1]).

UV-Vis. Additionally GNP size was estimated from optical properties measured by UV-Vis spectroscopy using an Infinite 200 Pro (Tecan, Switzerland) spectrophotometer according to the method of Haiss et al. [2]. The absorbancies at 450 nm A_{450} and at the particle size dependent maxima of the surface plasmon resonance A_{SPR} are measured. The particle size is calculated by the following equation using empirically determined parameters B_1 = 3.00 and B_2 = 2.20 [2].

$$d_{\text{UV-Vis}} = \exp\left(B_1 \frac{A_{\mathrm{SPR}}}{A_{450}} - B_2\right)$$

Dispersity. Besides determination of the mean particle diameter d_{particle}, the dispersity index $Đ$ was calculated using the standard deviation $\hat{\sigma}_{\mathrm{particle}}$ of the particle size distributions

$$Đ = \left(\frac{\hat{\sigma}_{\mathrm{particle}}}{d_{\mathrm{particle}}}\right)^2$$

[1] W.M. Haynes, D.R. Lide, T.J. Bruno, CRC Handbook of Chemistry and Physics, 93rd ed., CRC Press, Boca Raton (FL, USA), 2012.

[2] W. Haiss, N.T.K. Thanh, J. Aveyard, D.G. Fernig, Determination of Size and Concentration of Gold Nanoparticles from UV-Vis Spectra, Anal. Chem. 79 (2007) 4215–4221.

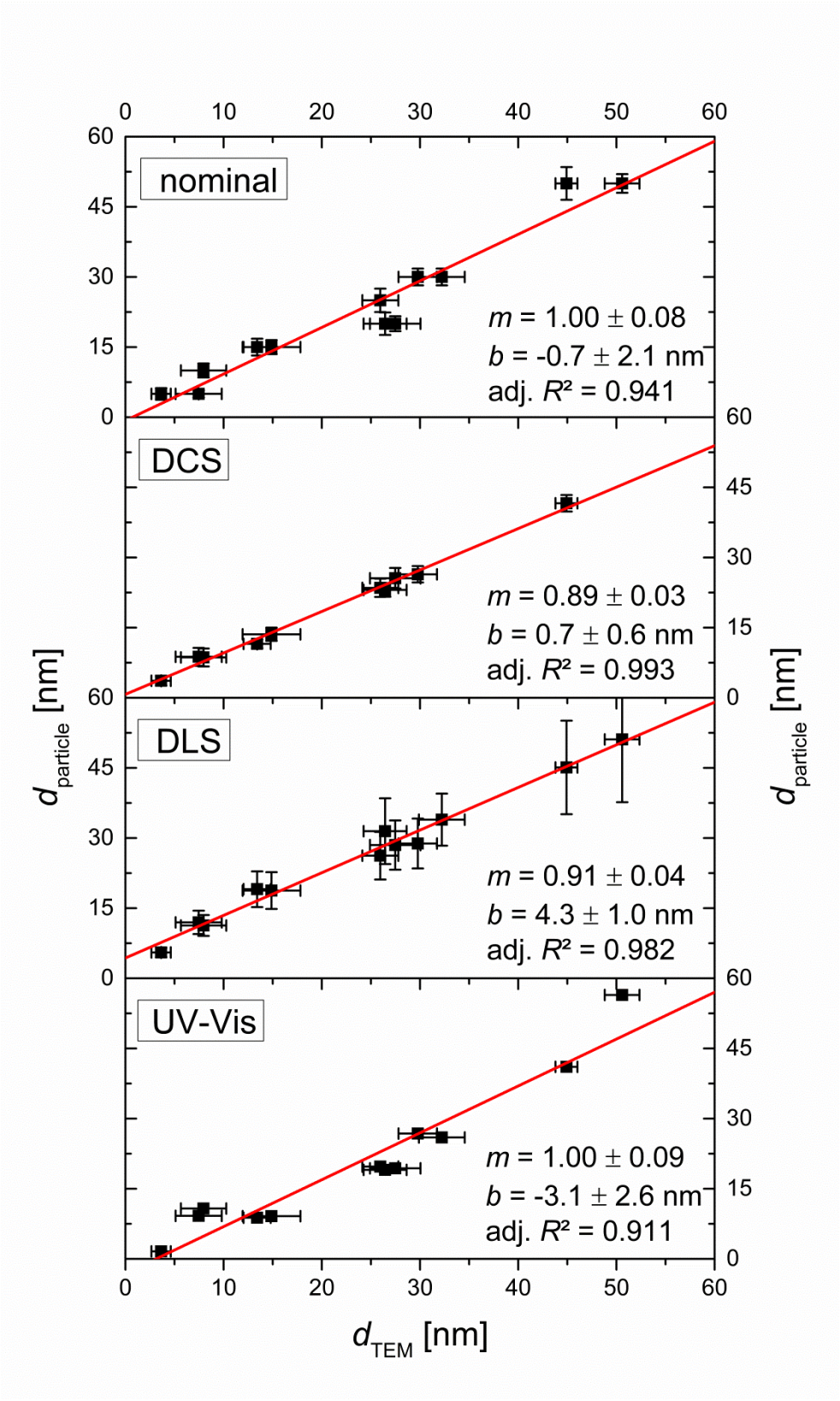

Fig. S1. Mean particle diameters provided by the manufacturer (nominal) and measured by DCS, DLS and UV-Vis plotted versus mean particle diameters measured by TEM as reference method. Red lines represent linear fits with the slope *m* and the intercept *b*.

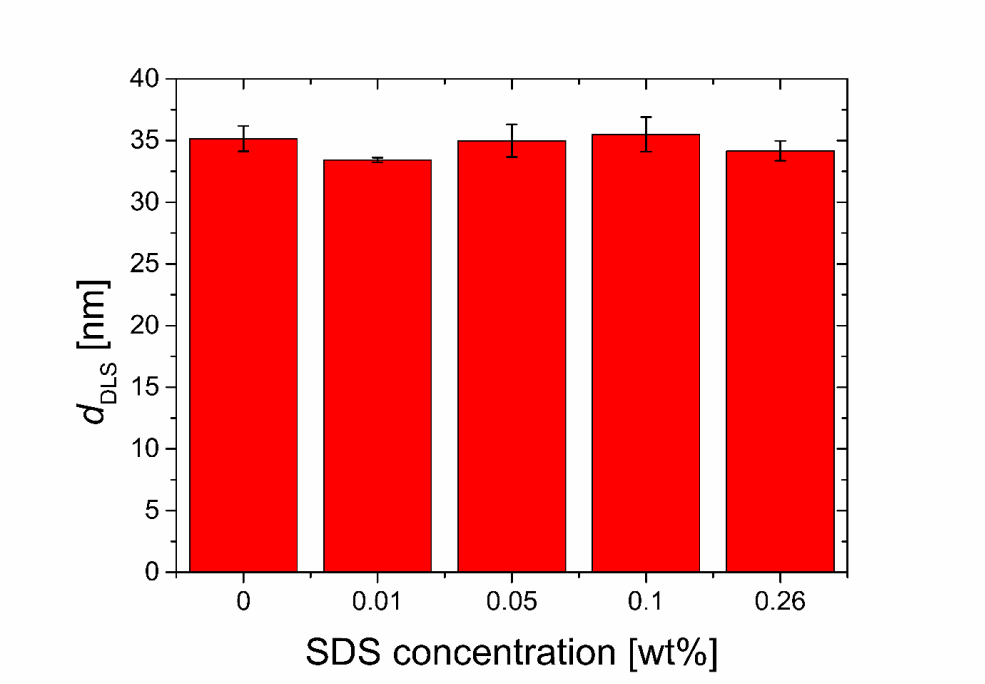

Fig. S2. Hydrodynamic diameters of GNP batch 10 with different SDS concentrations obtained by DLS. Error bars represent standard deviations from triplicate measurements.

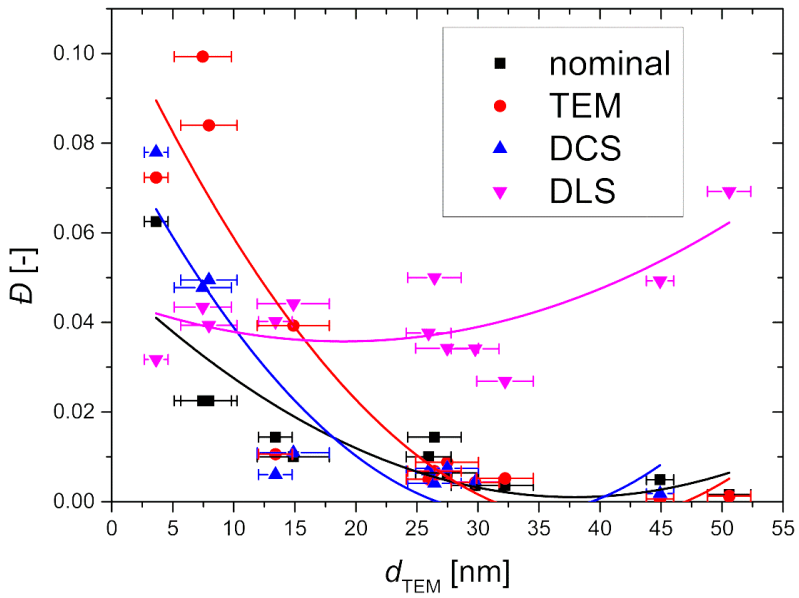

Fig. S3. Dispersity indices calculated from manufacturer's specifications (nominal) and from TEM, DCS and DLS plotted against mean particle sizes measured by TEM. Data sets were additionally fitted to cubic functions (solid lines) as eye guiding lines.

A2. SDS concentration dependence of flux profiles with VF4

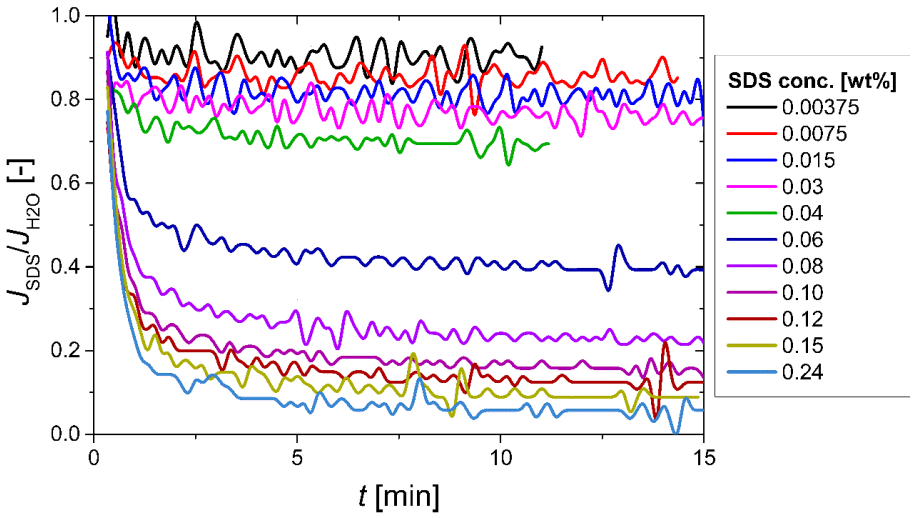

Fig. S4. Flux profiles of filtrations with SDS solutions having different concentrations using VF4.

A3. Cross-section of GNP challenged VF3

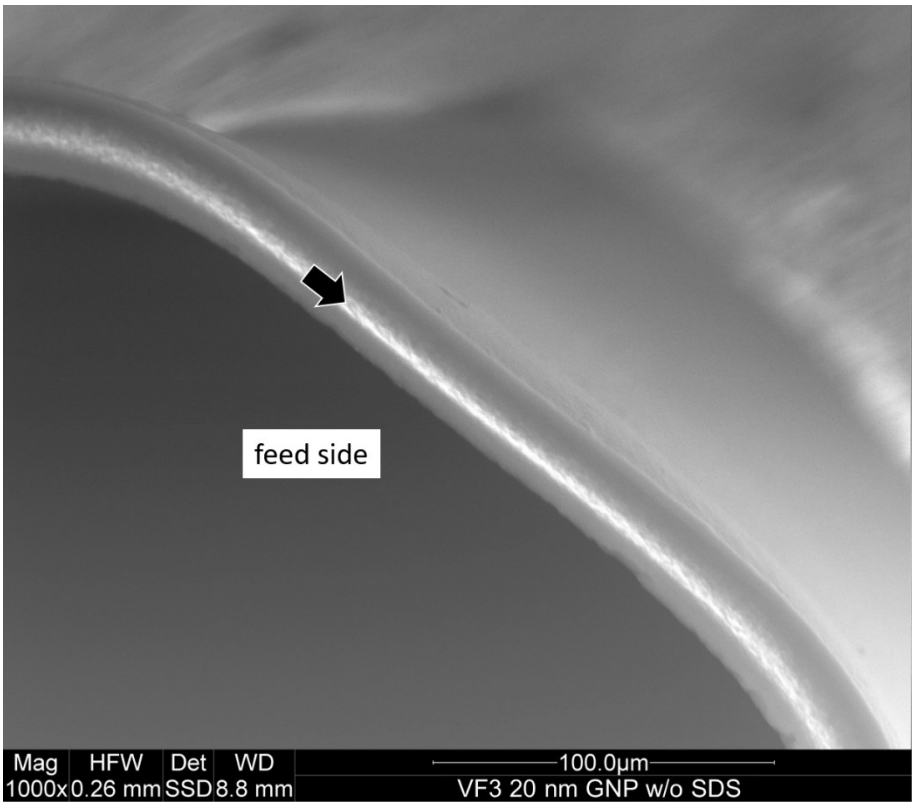

Fig. S5. SEM image (back-scattering detector) of VF3 showing the cross section after filtration with GNP (20 nm nominal diameter) in the absence of SDS. Side facing feed = bottom left. Black arrow shows the position of GNPs (white band) being located mainly in the interior of the membrane cross section.

3.2 Determination of pore size gradients of virus filtration membranes using gold nanoparticles and their relation to fouling with protein containing feed streams (paper 2)

P. Kosiol, M.T. Müller, B. Schneider, B. Hansmann, V. Thom, M. Ulbricht,

Determination of pore size gradients of virus filtration membranes using gold nanoparticles and their relation to fouling with protein containing feed streams,

J. Memb. Sci. 548 (2018) 598–608.

doi: 10.1016/j.memsci.2017.11.048.

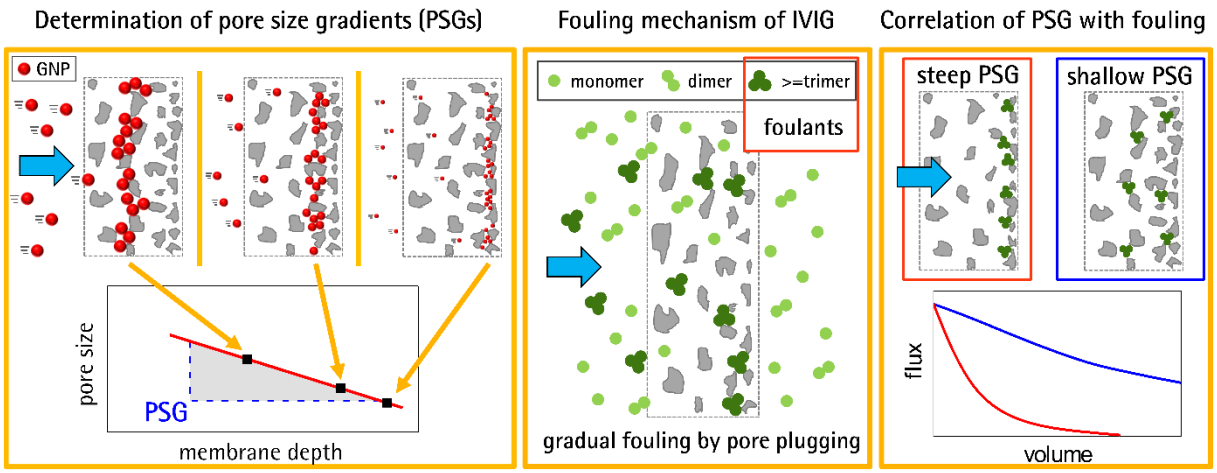

Journal of Membrane Science 548 (2018) 598–608

Contents lists available at ScienceDirect

Journal of Membrane Science

journal homepage: www.elsevier.com/locate/memsci

Determination of pore size gradients of virus filtration membranes using gold nanoparticles and their relation to fouling with protein containing feed streams

Peter Kosiol[a,b], Marie Theres Müller[a], Benjamin Schneider[a], Björn Hansmann[a,*], Volkmar Thom[a], Mathias Ulbricht[b]

[a] Sartorius Stedim Biotech GmbH, August-Spindler-Str. 11, 37079 Göttingen, Germany
[b] Lehrstuhl für Technische Chemie II, Universität Duisburg-Essen, Universitätsstr. 7, 45141 Essen, Germany

ARTICLE INFO

Keywords:
Fouling mechanism
Protein aggregates
Gold nanoparticles
Membrane structure
Pore size gradient
Virus filtration

ABSTRACT

Virus filtration membranes contribute to the virus safety of biopharmaceutical drugs due to their capability to retain virus particles mainly based on size-exclusion mechanisms. Typical product molecules like monoclonal antibodies with 9–12 nm in hydrodynamic diameter have to be transmitted by > 95% while small viruses, e.g. *parvoviridae* (B19, MVM, PPV) with a diameter of 18–26 nm, have to be retained by at least 99.99%. Therefore, membrane fouling caused by product aggregates, which are similar in size compared to the viruses that have to be retained, is a common observation. Minimal membrane fouling is a requirement for economical processes and is influenced by both the membrane surface chemistry and the membrane structure, particularly with regard to the pore size gradient (PSG). In this work, virus filtration membranes were challenged with gold nanoparticles (GNPs) in order to determine PSGs for a wide range of different commercial and non-commercial parvovirus retentive membranes differing in structure, material and surface chemistry. GNP adsorption to the membrane material was suppressed by the use of an anionic surfactant, allowing to gain insights into size-exclusion properties of the membranes. Membrane performance with regard to fouling was further investigated by determination of protein mass throughputs up-to a defined membrane flux decay using solutions containing intravenous immunoglobulin (IVIG) as model protein. Additionally, the fouling mechanism of IVIG was investigated and confirmed to be caused by trace amounts of species larger than IVIG monomers and dimers, which were already present in the feed. The fouling results are discussed in relationship to the determined PSGs, since the porous support structure of virus filtration membranes can act as a depth pre-filter protecting the separation-active layer from particulate foulants.

1. Introduction

Parvovirus retentive virus filters (VFs), designed to remove even small viruses like parvoviruses with 18–24 nm in diameter, have become a widely applied and mature industry standard [1,2]. These filters are expected to provide robust parvovirus reduction of ≥99.99% by size-exclusion and thereby significantly contribute to pathogen safety of biopharmaceutical drugs derived from mammalian cell culture or from human blood plasma. IgG-type antibodies, a major class of biopharmaceutical molecules to which most of the commercial monoclonal antibodies belong and which are the main component of intravenous immunoglobulin (IVIG) [3], exhibit hydrodynamic diameters of 9–12 nm for aggregate free solutions [4]. VFs, which are expected to transmit such product molecules by > 95%, are reported to have only slightly larger mean pore diameters of 12–17 nm [5,6]. By having narrow pore size distributions, VFs achieve high selectivities which enable the mandatory high virus retention while allowing quantitative product transmission.

Typical product related membrane foulants, e.g. protein aggregates, often are in the size range of parvoviruses and effectively foul the membrane due to pore blocking [7,8]. Such membrane fouling was also found to reduce virus retention performance of VFs [9]. Studies of Barnard et al. using monoclonal antibodies revealed that trace amounts of protein aggregates (1×10^{-4}% of the total mass of protein in solution) in the size range of 20–40 nm are sufficient to cause significant flux decay during virus filtration [7]. Furthermore, Brown et al. determined the size range of dimers up to pentamers of IgG-type monoclonal antibodies to be 16–23 nm with respect to their hydrodynamic diameter, which is very similar to the reported size range for parvoviruses [8]. Other smaller impurities like product fragments, host cell

* Corresponding author.

https://doi.org/10.1016/j.memsci.2017.11.048
Received 7 May 2017; Received in revised form 27 October 2017; Accepted 19 November 2017
Available online 21 November 2017

List of symbols

A	Membrane area [m^2]
$A_{220\ nm}$	Absorbance at 220 nm [a.u.]
$A_{280\ nm}$	Absorbance at 280 nm [a.u.]
$d_{particle}$	Particle diameter [nm]
d_{pore}	Effective pore diameter [nm]
d_{TEM}	Particle diameter measured with TEM [nm]
J_{IVIG}/J_{H2O}	Flux ratio of IVIG solution to pure water [dimensionless]
m/A	Protein mass throughput per membrane area [kg/m^2]
x	Membrane depth [μm]
x_{max}	Membrane depth at intensity maximum of GNP band [μm]
$\delta_{hydrodyn}$	Hydrodynamic correction term [nm]
δ_{SDS}	Correction term for pore narrowing by SDS adsorption [nm]
∇d_{pore}	Pore size gradient [nm/μm]

proteins and DNA can also cause fouling due to adsorption to the membrane. One strategy to maximize the throughput of the virus filtration step is to locate the unit operation of virus filtration close to the end of the downstream purification process, where the feed typically has already a high purity [10]. Another strategy involves the specific optimization of the unit operations upstream of the virus filtration to further reduce impurities [11].

Fouling resistance can also be achieved by developing membranes with low interacting surfaces. Therefore, membrane manufacturers use low interacting base materials like regenerated cellulose (RC) or render high interacting base materials like polyethersulfone (PES) or polyvinylidene fluoride (PVDF) low interacting by a separate surface modification step.

Besides a low interacting membrane surface, the pore size gradient (PSG) of a VF can have a considerable impact on its fouling resistance, especially with feeds containing impurities larger than the monomeric protein product. In contrast to ultrafilters (UFs), which have thin separation-active layers (SALs) of single digit microns thickness and support structures having pore sizes that are magnitudes larger compared to the ones within the SALs, VFs can have thick SALs with up to 30 μm thickness, consisting of a multitude of pore layers, contributing to the high selectivity [12–14]. While UFs have very steep PSGs, commercially available VFs exhibit a wide range of PSGs from UF-like steep to very shallow [15]. Some early VFs on the market were derived from UFs exhibiting similar membrane structures. For UFs and UF-like VFs operated in cross-flow mode with the SAL facing towards the feed, the support structure acts mainly as mechanical support for the thin SAL and does not contribute to the fouling resistance. Some studies using these early commercial, UF-like structured VFs, intended for application in cross-flow mode, investigated the impact of membrane orientation on fouling behavior [16–18]. The authors of these studies found significantly increased performance with respect to fouling resistance when the membranes were oriented with the SAL facing away from the feed. In such orientation the mode of operation, either dead-end or cross-flow, had no impact on anti-fouling performance. The performance increase was attributed to the porous membrane support structure, acting as a depth pre-filter. This pre-filtration effect protects the SAL from fouling by "trace levels of submicron-sized particles" [17]. Nowadays all commercially available VFs are used in the orientation with the SAL facing away from the feed. Those VFs are also designed for dead-end use. Wide application in dead-end mode is also due to higher simplicity of use and lower capital requirements for filtration equipment.

The effectivity of the support structure acting as a pre-filter is highly dependent on the actual PSG. Commercial VFs with an UF-like steep PSG offer high water permeability. Their thin SAL is the main contributor to the overall hydraulic resistance of the membrane. Due to the steep PSG only a small section of the membrane in close proximity to the SAL has pore sizes in the range of protein aggregates, which are probably < 40 nm [7], resulting in low depth pre-filter capacities and higher susceptibility towards fouling. Accumulation of foulants being retained by size exclusion closely to the SAL of microfiltration membranes having steep PSGs was visualized by other groups using confocal scanning laser microscopy [19,20]. VFs with shallow PSGs have typically lower water permeability as a larger part of the membrane structure contributes to the hydraulic resistance. This can increase processing times which negatively impacts the productivity of such VF. On the other hand, such membranes often show higher robustness against fouling due to the fact, that a larger part of the membrane structure is capable of retaining the fouling species. However, membranes having very shallow PSGs with constant mean pore diameters across the membrane cross-section, in the typical range for parvovirus retentive VFs, could be very susceptible to fouling. As larger foulants would be mostly retained close to or directly on the outer membrane surface facing towards the feed, such a membrane would exhibit low depth pre-filter capacities and low fouling robustness similar to a membrane with a very steep PSG. Track-etched membranes typically have cylindrical pores and therefore no PSG. Such membranes are very rarely used in biopharmaceutical processes due to their high susceptibility towards fouling with aggregate containing protein feed streams [21]. An overview of commercial VFs including a very qualitative classification regarding their PSGs was given by Miesegaes et al. [22].

PSGs that exhibit pore sizes reflecting the particle size of foulants could help to utilize a large extent of the total membrane structure to retain fouling species in order to maximize the depth pre-filter capacity while keeping the hydraulic resistance as low as possible achieving highest possible permeability. However, we are not aware of a technique that is capable to quantitatively determine the PSG in normal direction to the outer surface of a parvovirus retentive membrane. Determining the PSG is an especially challenging task with view on method's applicability towards the high diversity of membrane materials and surface chemistries that commercial VFs exhibit [22].

Utilizing high resolution imaging techniques such as scanning or transmission electron microscopy (SEM/TEM) to investigate membrane cross-sections already provides good qualitative impressions of membrane structures and related PSG. Quantitative analysis using SEM/TEM is significantly more challenging [23] and often limited to determination of pore sizes on the outermost membrane surface [24] rather than within the inner membrane structure. Samples of membrane cross-sections need to be prepared carefully by freeze fracturing or microtomy avoiding artifacts that alter the pore structure (e.g. by compaction or smearing). In contrast to track-etched membranes with cylindrical pores, VFs have a complex sponge-like pore structure with highly interconnected pores. Quantitative image analysis of such structures requires binarization of grayscale images which is a very subjective procedure with resulting pore sizes highly dependent on the individual operator [23]. For the evaluation of two-dimensional images, also simplifications with respect to the definition of the term "pore size" are required. Ziel et al. proposed a computer-aided method to determine PSGs of 0.2 μm rated microfilters measuring the distances of the pore voids using "equidistant lines parallel to the (outer) membrane surface and perpendicular to the flow direction in the membrane" (= mean free path length) [25]. While the PSG throughout the whole cross-section was determined quite well, the magnitude of the mean free path lengths was significantly larger than 0.2 μm, even in the SAL. This is related to the simplified definition of the mean free path length, which can be determined from a single two-dimensional image of a membrane cross-section. For a proper quantitative description of the

porous structure, additional information on the third dimension is required. This information can be obtained by more sophisticated techniques such as X-ray computed tomography [26,27] or serial slicing and imaging of cross-sections using electron microscopy in combination with 3D reconstruction of the membrane structure [28,29].

Another more application-related way to gain quantitative insights into the membrane structure is based on retention of particles mainly by size exclusion in course of filtration experiments. Filtration of gold nanoparticles (GNPs) can provide information regarding the PSG of a VF [30–32] as they are spherical, well defined in size and monodisperse (dispersion index < 0.1 [5]). An often observed drawback of using GNPs can be unwanted adsorption [33–36] of the GNPs to the VFs masking the size exclusion properties of the membrane. We recently proposed a technique to determine barrier pore size distributions (PSDs) of the SAL of VFs and UFs by filtration experiments using different sized gold nanoparticles (GNPs) together with an anionic detergent to suppress GNP adsorption [5]. While the PSDs were determined from retention measurements of the GNPs, we analyze the same GNPs challenged VFs in the present paper in order to determine the PSGs of these VFs. As the pore size narrows towards the permeate-side of a typical VF, rejected particles are retained at a distinct depth of the VF depending on the particle size, causing a local change of membrane colour and membrane composition. A similar retention behavior was also observed by confocal laser scanning microscopy of VFs challenged with fluorescently labelled virus particles [37–39]. In case of the GNPs, the position of this colouration in the membrane cross-section can be easily determined by light microscopy or scanning electron microscopy using backscatter electron detection without the necessity of additional labelling of the GNPs. Relating the size of the GNPs retained to their position in the membrane provides insights into the PSG.

The aim of this work was to develop a technique that is capable to determine PSGs of highly diverse commercial parvovirus retentive VFs as well as UFs. An approach based on solute/particle rejection using rigid and monodisperse GNPs in the size range of 5–50 nm was chosen. Interfering adsorptive retention of GNPs was overcome by previous equilibration of the membranes using sodium dodecyl sulfate (SDS) solutions and by addition of SDS to the GNP solutions/dispersions [5]. Fouling susceptibility of all membranes was determined by filtration of solutions containing intravenous immunoglobulin (IVIG) as model protein. The fouling mechanism for IVIG was determined. Protein mass throughputs determined with IVIG are discussed in relationship to the PSGs obtained from GNP filtration experiments.

2. Materials and methods

2.1. Materials

2.1.1. Chemicals

Sodium dodecyl sulfate (SDS; ≥99%) was purchased from Sigma-Aldrich. A 5 wt% human intravenous immunoglobulin (IVIG) solution, which consists of pooled human immunoglobulin G, was purchased from SeraCare Life Sciences and used as accepted standard model protein for fouling studies using parvovirus retentive VFs [2].

2.1.2. Membranes

The studies were performed on a set of commercial parvovirus retentive VFs (“VF1″–“VF9″) manufactured by Asahi Kasei Medical, EMD Millipore, Pall Corp. and Sartorius-Stedim Biotech and made from polyethersulfone (PES), poly(vinylidene fluoride) (PVDF) or regenerated cellulose (RC). In addition, a non-commercial variation of VF6, labelled as VF6b, has been studied which had a less hydrophilic membrane surface rendering the membrane more interacting with proteins. For comparative reasons experiments included also a 100 kDa PES ultrafiltration membrane (“100k PES”) from Sartorius-Stedim Biotech. All experiments were conducted with a single layer of membrane, while commercial devices can also contain multiple layers of the same membrane.

2.1.3. Gold nanoparticles

Aqueous solutions of citrate-stabilized gold colloids in deionized water with nominal diameters ranging from 5 to 50 nm were purchased from Nanopartz Inc. Gold concentrations were 0.050 mg/mL corresponding to optical densities of unity (SPR peak). All solutions had pH 7. Zeta potentials of the GNPs were between −30 and −40 mV.

2.2. Size characterization of GNPs

2.2.1. TEM

GNPs were characterized by transmission electron microscopy (TEM) using a CM12 instrument (Philips, Netherlands) in combination with image analysis as described before [5].

2.2.2. DLS

Size measurements of GNPs utilizing dynamic light scattering (DLS) were conducted using a StabiSizer PMX 200C (Particle Metrix GmbH, Germany) as described before [5].

2.3. Characterization of IVIG

2.3.1. DLS

DLS studies of IVIG solutions were conducted using a Zetasizer Nano ZSP (Malvern Instruments Ltd., UK). In order to remove potentially present large particle contaminants that are not relevant for virus filter fouling but highly influence DLS measurements, the samples were filtered through a Minisart RC4 0.2 µm syringe filter (Sartorius-Stedim Biotech) made from RC. All samples were measured in single-use micro UV-cuvettes (Brand, Germany) after a thermal equilibration at 20 °C for 3 min. For each sample at least three measurement runs have been performed with an angle of detection of 173° (backscattering). The measurement duration for each run was set to “automatic”. Data acquisition and analysis was conducted using the Zetasizer Software v7.11 accompanied to the DLS device. For data analysis both distribution analysis using the “protein analysis” algorithm as well as the method of cumulants for determination of the z-average hydrodynamic diameter have been applied.

2.3.2. SEC

Size exclusion chromatography (SEC) was performed to quantify fractions of IVIG aggregates. For this purpose a YARRA 3 µm Section 3000, 7.8 × 300 mm column (Phenomenex, USA) in combination with an Agilent 1100 HPLC system (Agilent Technologies, USA) was used at room temperature (25 °C). The mobile phase consisted of 100 mM sodium phosphate and 100 mM sodium sulfate at pH 6.6. Sample volumes of 5 µL having protein concentrations of 1 g/L were injected. The chromatography was performed at a flow rate of 1 mL/min while UV absorbance was recorded at 220 nm.

2.3.3. HIC

A solution of IVIG was fractionated by hydrophobic interaction chromatography (HIC) using an ÄKTA Prime Plus system (GE Healthcare, UK). The protein solution was diluted to 5 g/L using a 1 M $(NH_4)_2SO_4$ plus 50 mM potassium phosphate buffer (“equilibration buffer”) at pH 7 and filtered through a 0.22 µm bottle top filtration unit (Sartorius-Stedim Biotech). The solution was loaded to a HiLoad 16/10 Phenyl Sepharose High Performance column (GE Healthcare, USA) which was previously equilibrated with the equilibration buffer. After loading the column was washed with the equilibration buffer. Stepwise elution obtaining three fractions was achieved by adjusting three different $(NH_4)_2SO_4$ concentrations using a 50 mM potassium phosphate buffer (elution buffer) at pH 7 and a flow rate of 3 mL/min (Fig. S1, Supporting Information). For further analysis all fractions were desalted by using a 2 kDa RC dialysis membrane (Spectrum Labs, USA) in combination with a 20 mM TRIS buffer at pH 7.2. The dialyzed solutions were diluted to 1 g/L for further experiments, using the same

buffer as used for dialysis.

2.4. Filtration experiments

All filtration experiments were conducted in dead-end mode at constant pressure of 2 bar. In case of mechanically sensitive membrane types pressure was reduced to 1 bar according to manufacturer specifications. The membranes were oriented with the SAL facing away from the feed if not stated otherwise.

2.4.1. Gold nanoparticles (GNPs)

The filtration procedure using GNPs was conducted as reported before [5]. Prior to the filtration of GNPs flat sheet membranes were mounted into 25 mm syringe filter holders (3.1 cm^2, order no. 16517————————E, Sartorius). Hollow fiber membranes were received pre-built in proprietary devices (1 or 5 cm^2). All membranes were wetted and flushed with reverse osmosis (RO) water in order to ensure complete wetting. Afterwards, all membranes were equilibrated with 0.26 wt% SDS solution by flushing with at least three hold-up volumes of the membrane device. SDS occupies possible binding sites for the GNPs on the membrane surface and hence supresses adsorption of the GNPs [5,40,41]. The stationary water flux after possible SDS adsorption is highly dependent on the individual surface chemistry of the membranes and therefore was determined for each membrane type in order to quantify the pore diameter reduction caused by the SDS. Values for the pore diameter reduction can be used as correction to calculate more realistic pore diameters. Flux measurements were performed gravimetrically using a Quintix balance (QUINTIX2102-1S, Sartorius) with an accuracy of 0.01 g.

All GNP solutions were used at concentrations of 0.05 mg/mL (cf. Section 2.1.) and 0.26 wt% SDS added. Filtration experiments were carried out using different sized GNPs in the range from 5 to 50 nm. Usually six or more filtrations using different particle sizes were conducted for each membrane type. The amount of feed used per filtration added up to three hold-up volumes of the VF device. Finally, the membranes were again flushed with two hold-up volumes of 0.26 wt% SDS. The membranes were then removed out of their housings and dried at room temperature on a cellulose cloth for 1 h.

2.4.1.1. Pore size gradients. Cross-sections of the membranes loaded with GNPs ranging from 5 to 50 nm have been prepared by freeze-fracturing using liquid nitrogen. Due to the size of the GNPs and the asymmetric funnel-like structure of the membrane, the particles are retained at a certain depth of the membrane causing a local dark colouration. This colouration can be observed by light microscopy (Fig. 1A) or by scanning electron microscopy (SEM) with back-scattered electron detection (Fig. 1 B,C) based on the high material contrast between gold and the light atoms of the polymers. Images of the cross-sections were obtained by using a Stemi 2000C light microscope (Zeiss, Germany) or a Quanta 200F SEM (FEI, USA) equipped with a back-scattered electron detector without sputtering of the samples. SEM was

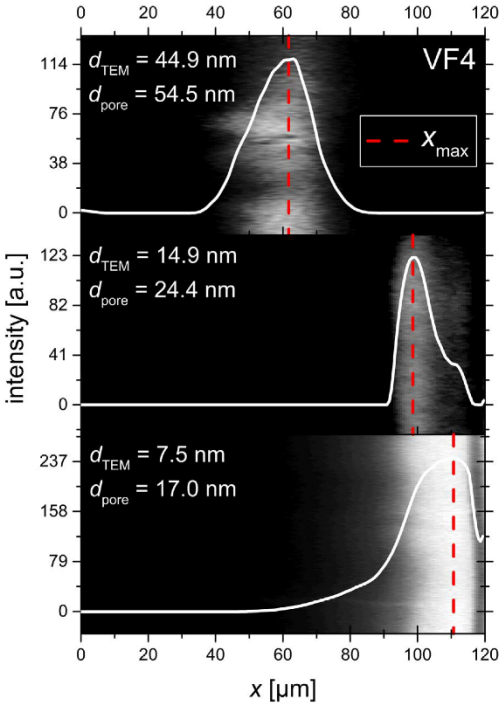

Fig. 2. Exemplary determination of x_{max} (dashed red lines) for VF4 separately challenged with three different sized GNPs. The SAL is facing to the right. Light microscopy images were converted into grayscale and inverted so that membrane areas with GNPs are represented by bright colours. Brightness intensities (white solid lines) were obtained from image analysis. (For interpretation of the references to color in this figure legend, the reader is referred to the web version of this article.)

chosen especially for UF-like membranes with steep PSGs. For such samples a higher resolution than possible with light microscopy was required because the GNPs of the whole size range used were all retained in close proximity to the SAL. A very high resolution, as required for direct measurements of pore sizes by resolving single pores using SEM (Fig. 1 D, cf. Section 2.5.), however, is not necessary.

For quantification of the position of the deposited GNPs within the membrane structure all images were converted in grayscale and analysed using the image processing software ImageJ 1.48 v (http://rsbweb.nih.gov/ij/). The membrane depth x at which the colouration intensity was maximal x_{max} has been determined in triplicate for all GNP sizes using different areas of each membrane sample. An example for the determination of x_{max} for three different GNP diameters with VF4 is given in Fig. 2.

The effective pore diameter d_{pore} at x_{max} was assumed to be equal to the mean particle diameter d_{TEM} determined using TEM with additional

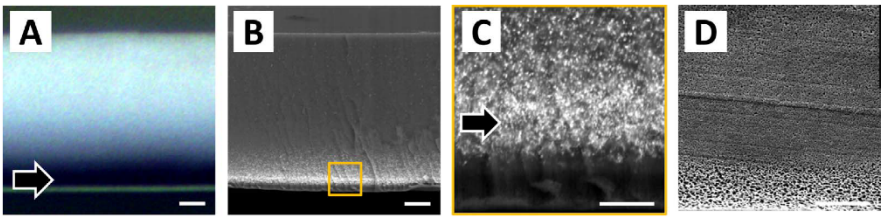

Fig. 1. Microscopy images of cross-sections of VF4 challenged with 7.5 nm (TEM) GNPs (A)-C)) and a pristine VF4 (D)). The approximate position of the SAL is indicated by the black arrows. During filtration, the SAL was facing away from the feed. A) Light microscopic image showing the captured GNPs within the membrane structure as dark colouration close to the lower edge of the membrane. The scale bar represents 20 µm. B) SEM image of the same sample as shown in A) using the same magnification. GNPs are visible as a bright colouration and form a narrow band within the membrane cross-section of the VF at a defined position. Almost no GNPs were observed in the cross-section above the bright band. C) Higher magnification of a section (orange frame) from B) showing that single GNPs are identifiable and that no GNPs were retained in the lower structure of the VF. The scale bar represents 5 µm. D) High resolution SEM image using a secondary electron detector to visualize the VF structure of a pristine membrane of the same section as in C) showing larger pore sizes below the SAL. (For interpretation of the references to color in this figure legend, the reader is referred to the web version of this article.)

contributions from SDS adsorption δ_{SDS} and the particle's surface bound ligands and hydration shell $\delta_{hydrodyn}$

$$d_{pore} = d_{TEM} + \delta_{SDS} + \delta_{hydrodyn} \quad (1)$$

δ_{SDS} was calculated for each membrane under consideration of the Hagen–Poiseuille equation, the mean pore diameter in the SAL, as determined from GNP retention data, and the fluxes measured with RO water J_{H2O} and with SDS solution J_{SDS}. Data regarding the flux decline caused by SDS and the calculation of the resulting pore diameter reduction on the set of membranes investigated here is presented and discussed in [5]. The values for δ_{SDS} are ranging between 0.1 and 7.3 nm for the given set of membranes. $\delta_{hydrodyn}$, the difference between the diameter of the gold core of the GNP, as measured by TEM, and the hydrodynamic diameter, as measured by DLS, also including the particle's ligands and hydration shell, was determined to be 2.3 nm as average for all GNPs used in this study [5]. Using GNP diameters solely based on DLS measurements would be possible as well, but due to the higher sensitivity towards larger impurities, DLS was regarded as less robust than TEM.

The PSG ∇d_{pore} as measure for membrane symmetry, valid for the effective pore diameter range from 10 to 55 nm, is obtained as the slope from a linear fit having the following notation

$$d_{pore} = \nabla d_{pore} x_{max} + b \quad (2)$$

2.4.2. IVIG

In order to determine fouling susceptibility of the membranes, filtrations using IVIG (20 mM KP_i, pH 7.2) as model protein were carried out. For most experiments an IVIG concentration of 5 g/L was chosen. Filtrations using HIC fractions were conducted with 1 g/L IVIG. Protein mass throughputs have been determined for all membranes. Flux measurements were performed gravimetrically using a Quintix balance (QUINTIX2102-1S, Sartorius, Germany) with an accuracy of 0.01 g. For throughput comparison of the complete set of membranes the protein mass throughputs at 37% flux decay have been determined.

2.5. Characterization of the pore size profile by electron microscopy and image analysis

In addition to the structural analysis based on GNPs, the pore size profile of a pristine VF4 was exemplarily determined by image analysis from high-resolution SEM images of the membrane cross-section. The measurement of the pore sizes was conducted manually at six different locations of the cross-section along the normal of the membrane. At least seventy individual pore sizes were measured at each location by determining the mean free path length of the individual pore voids as described in [25].

3. Results and discussion

Using a set of different sized GNPs ranging from 5 to 50 nm in combination with filtration experiments with these particles was used here to determine PSGs. We previously investigated the retention mechanisms of citrate-stabilized GNPs with VFs und UFs [5]. It was shown that the use of SDS, an anionic detergent, significantly shifted the retention mechanism from adsorption towards size exclusion, which allowed the use of GNPs in order to determine the pore size distributions (PSDs) in the SALs including the same membranes also investigated here. For analysis of the PSDs, the retention of the GNPs in presence of SDS was measured as a function of the GNP diameter using the feed and permeate solutions. For the determination of the GNP diameter, which is the most import characteristic of the GNPs with respect to their application towards quantification of membrane structures, a set of different methods had been used. Among those methods, a combination of TEM (robust batch-to-batch size differentiation) and DLS (determination of more relevant hydrodynamic diameters instead of the smaller

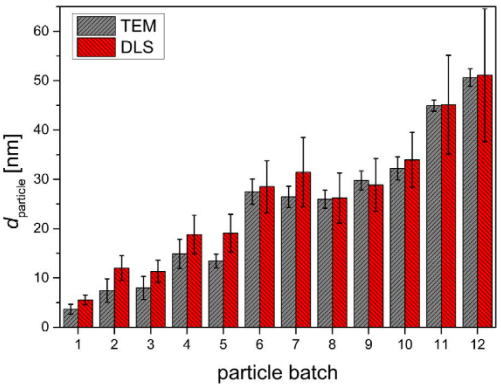

Fig. 3. Overview of mean GNP diameters by TEM and DLS for all GNP batches used for further studies, reproduced from [5]. Error bars represent the standard deviations of the particle size distributions.

GNP core diameters) was found to be very well suitable to relate GNP sizes with PSDs of porous membranes (also see Eq. (1)). As a major basis for the investigations on the PSGs, the TEM and DLS results for the GNP diameters from our previous study [5] are reproduced here (Fig. 3).

3.1. PSGs from GNP filtration experiments

In this present study, we use the GNP challenged membrane samples, generated in course of our previous study, and investigate the position of the GNPs located within the membrane structure, also as a function of the GNP diameter, for determination of the PSGs. The application of SDS as additive significantly reduced adsorption of the GNPs within the membranes and allowed the GNPs to penetrate deep into the membrane structure until, at a certain depth, reaching pores small enough to be capable of size exclusion for the specific size of the GNPs [5]. As a consequence, for each GNP diameter a distinct coloured band in the membrane cross-sections can be observed (Fig. 1, Fig. 2) and the position of its intensity maximum, having the highest local GNP concentration, can be quantified.

The effective pore diameter at this position is estimated using Eq. (1). This estimation includes the GNP diameters measured by TEM, corresponding to the diameter of the gold core, and the contribution from the ligand and hydration shell as estimated from using both TEM and DLS. Measuring the fluxes with both pure water and 0.26 wt% SDS showed flux declines caused by SDS adsorption that were highly dependent on the membrane material and surface chemistry reducing the flux by up to 95%. The resulting pore diameter reduction by the SDS adsorption was calculated by the Hagen-Poiseuille equation [5] and also used for the estimation of the effective pore diameters of the membranes that they would exhibit in absence of SDS.

The effective pore diameters were plotted as a function of the corresponding positions of the GNPs in the membranes (Fig. 4). Since for most of the membranes linear relationships were observed, for sake of simplicity, the PSGs were defined as the slopes from linear fits to these data sets. For some membranes (100k PES, VF2, VF4, VF6, VF9) the PSGs are valid for the pore size region ranging from 10 to 55 nm, as all particles within this range were able to penetrate into the membrane structure. For several other membranes (VF1, VF3, VF5, VF7) the PSGs are limited to pore sizes from 10 to 30–40 nm. In such cases, the largest GNPs used in this study were excluded from penetration into the membrane structure and therefore not considered for the PSGs. Additionally the PSG of VF5 displays a special case (Fig. 4, VF5). For the whole pore size region of interest the PSG cannot be described by a single value. The smaller GNPs were retained in close proximity to the SAL forming thin bands in the membrane cross-section. A linear fit to

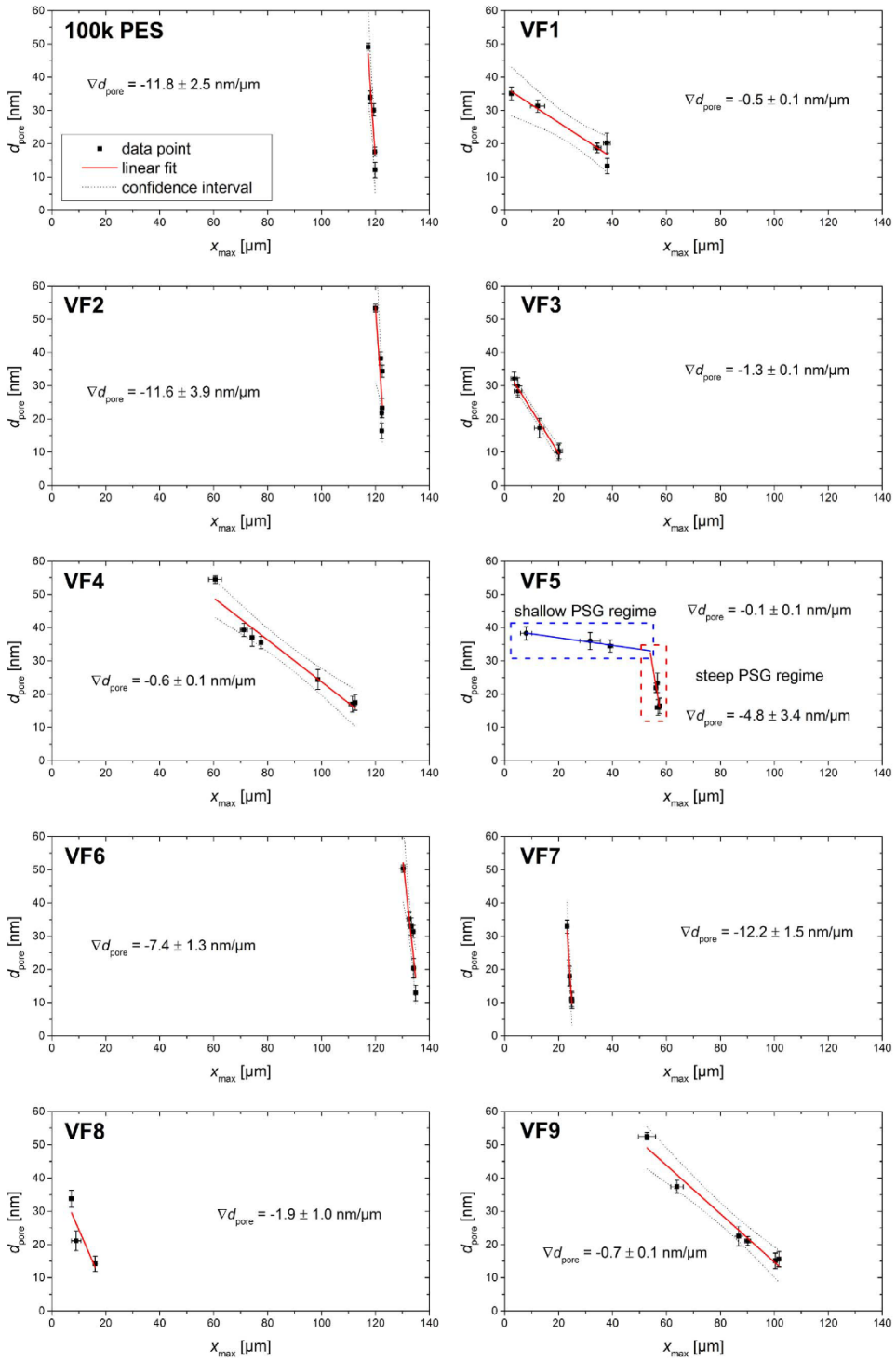

Fig. 4. Effective pore diameters at different positions in the membranes (filled squares) for the set of membranes tested. x_{max} = 0 denotes the outermost part of the membrane facing towards the feed. Additional linear least-squares fitting (solid red and blue lines) was used to determine PSGs including 95% confidence intervals (black dotted curves). VF5 displays a special case as the PSG can be divided into two different linear regimes (compare solid red and blue line). The vertical error bars represent the standard deviations of the particle size distributions of the individual particle batches. The horizontal error bars represent the standard deviations for x_{max} determined from triplicate measurements. (For interpretation of the references to color in this figure legend, the reader is referred to the web version of this article.)

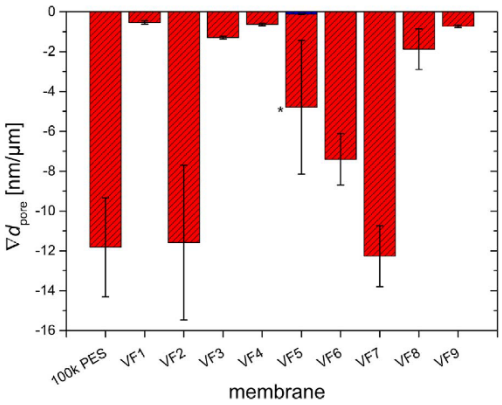

Fig. 5. Overview on PSGs for the set of membranes. The asterisk denotes VF5 as a special case exhibiting a steep PSG regime close to the SAL and a shallow PSG regime (small blue bar) for the rest of the membrane structure. The error bars represent the standard errors for the slopes of the linear fits depicted in Fig. 4. (For interpretation of the references to color in this figure legend, the reader is referred to the web version of this article.)

this part of the dataset indicated a steep PSG so that this section of the membrane ranging from effective pore sizes from 15 to 25–30 nm was labelled as "steep PSG regime". The larger GNPs were retained throughout larger parts of the whole membrane structure showing higher size dependence and also forming broader bands. Both observations indicate a shallow PSG for this part of the membrane, so that this section ranging from effective pore sizes from 30 to 35–40 nm was labelled as "shallow PSG regime". PSGs for all membranes were determined and are summarized in Fig. 5.

In order to verify the validity of the PSGs obtained by the GNP method, exemplarily the results obtained for VF4 are compared to a pore size profile determined by image analysis of a SEM image of the cross-section of a pristine VF4 (Fig. 6). As most obvious difference, the pore sizes determined by SEM image analysis are significantly larger than those determined by the GNP method. For this image analysis, the pore sizes were manually measured as mean free path lengths of the individual pore voids. These mean free path lengths were not

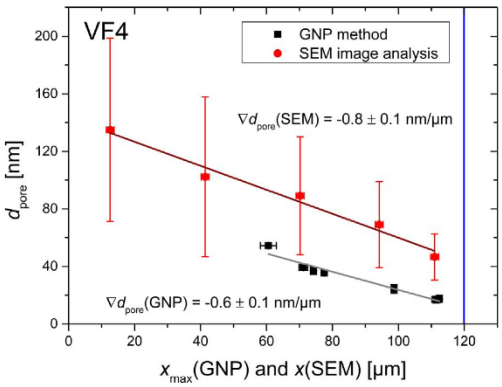

Fig. 6. Pore diameters at different positions of VF4 determined by the GNP method (black squares, fit = grey line) and by image analysis of SEM images (red circles, fit = dark red line). x_{max} or $x = 0$ denote the outermost part of the membrane facing towards the feed. The vertical error bars represent the standard deviations of the particle size distributions of the individual particle batches (GNP method) respectively the standard deviations of the pore size distributions (SEM image analysis). The horizontal error bars represent the standard deviations for x_{max} determined from triplicate measurements (GNP method) or the membrane section considered for analysis (SEM image analysis). (For interpretation of the references to color in this figure legend, the reader is referred to the web version of this article.)

specifically determined at the individual bottlenecks of the pore voids, which account for only a small part of the whole pore void, but for a random position within the pore void. This results in the fact that the pore sizes determined by this technique significantly overestimate the effective pore sizes that particles encounter and which were determined by the GNP method. Measurement of pore sizes of a dry and not swollen membrane additionally also results in larger pores compared to a wetted and swollen membrane similar to application conditions. It can be therefore assumed that the pore sizes obtained from the GNP method are more representative to describe retention and fouling by virus particles, protein aggregates or other larger foulants. Besides the difference regarding the absolute magnitude of the pore sizes between both techniques, the PSGs of −0.6 nm/µm (GNP) and −0.8 nm/µm (SEM) are similar supporting the validity of the GNP method.

3.2. Fouling mechanism of IVIG

In order to understand the relevance of the PSG with respect to fouling, the specific fouling mechanism of the model protein needs to be understood and the fouling species identified. In this study, IVIG is used as accepted model protein for virus filtration. IVIG consists mainly of monomeric IgG-type antibodies of about 150 kDa molecular weight, which represent a very relevant class of biopharmaceutical molecules also including monoclonal antibodies.

Using a freshly prepared IVIG solution, exemplarily for filtration with VF4 (Fig. 7), shows that flux declines gradually with increasing protein mass throughput. Filtration of an IVIG solution that has been already filtered using VF4 shows a significantly lower gradual flux decline compared to a non-pre-filtered solution allowing to achieve higher protein mass throughputs. This observation indicates a depletion of fouling species, originally present in the feed, by the pre-filtration using VF4.

Therefore, a fouling mechanism caused by internal concentration polarization is unlikely. Also a continuous formation of fouling species inside the membrane structure, which could be potentially caused by an increased level of shear stress that protein molecules have to undergo during the their transport through the porous structure, can be ruled out as main fouling mechanism.

Using a 0.1 µm microfiltration membrane with a low-interacting surface as pre-filter did not reduce subsequent fouling of VF4 (data not shown). Hence, the fouling species should be smaller than 0.1 µm. In addition pre-filtration was also conducted using a 0.1 µm hydrophobic interaction (HI) membrane, specifically developed for pre-filtration of

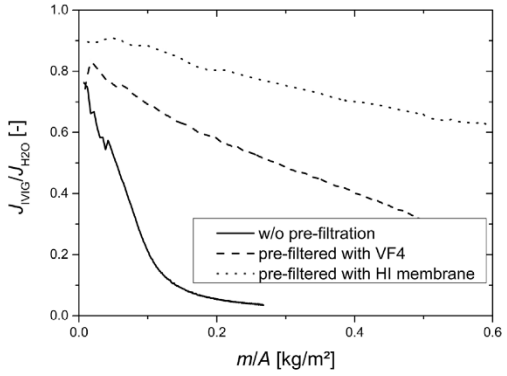

Fig. 7. Flux profiles of IVIG (5 g/L) filtrations using VF4 with different pre-treatments of the feed solutions. The solid black line denotes a filtration of a feed without pre-filtration, while the dashed black line shows a filtration of a pre-filtered solution using VF4 for pre-filtration. Additionally the dotted black line displays a flux profile for a pre-filtered solution using an adsorptive 0.1 µm rated pre-filter working on basis of hydrophobic interaction.

feeds prior to virus filtration, significantly reducing the fouling of VF4 (Fig. 7). This HI pre-filter is capable of retaining fouling species, which are typically more adsorptive towards hydrophobic surfaces. Such fouling species, in case of the polyclonal IVIG, can possibly be small hydrophobic fragments, a more hydrophobic subset of monomeric IVIG as well as aggregates, which have been found to be more prone to irreversible adsorption on hydrophobic surfaces [42]. Similar observations that pre-filtration using VFs or hydrophobic pre-filters can reduce fouling were also reported by Bolton et al. for IVIG as well as monoclonal antibodies and antibody fragments [43,44].

SEC analysis of the feed shows the IVIG monomer to be the main species besides low amounts of dimers and fragments (Fig. 8). Similar results have been found using analytical ultracentrifugation (data not shown). A comparison of feed and permeate with respect to species larger or smaller than the monomer shows no significant differences. As no significant depletion of dimers can be observed, dimeric IgG-type antibodies in general, which were determined by Brown et al. to be 16.4 nm in hydrodynamic diameter [8], cannot be the primary cause for fouling. The fouling species could be below the lower detection limit of the SEC method applied and comprised of trace amounts of aggregates larger than dimers as already reported by Barnard et al. for monoclonal antibodies [7].

Due to the high sensitivity of DLS towards the largest species present in the sample, DLS is capable to determine trace amounts of larger species. Particle size distributions for the same samples as used for SEC were determined by DLS (Fig. 9). For both feed and permeate solution no particles > 30 nm were detected. This finding is in agreement with the ineffectiveness of using low-interacting 0.1 µm microfiltration membranes for pre-filtration, capable of removing species > 100 nm. Due to the inherent lack of resolution of DLS, the particle size distributions cannot be resolved into individual n-mer species but relative comparisons between feed and permeate can be made. The particle size distribution of the feed sample shows the presence of species in the size range from about 19–30 nm. Such species were not found in the permeate and are therefore assumed to be fully retained by the VF mainly contributing to fouling. DLS measurements strongly support the hypothesis of larger species than the monomer being the main fouling species for the IVIG solutions used in this study. The hydrodynamic diameter of IgG-type antibody monomers is reported to be 9–12 nm [4].

Besides from aggregates, fouling can be also caused by more hydrophobic species which can be a subset of IVIG monomers as well as IVIG fragments. To further narrow down the possible origin of the fouling species, IVIG was fractionated by HIC. The fractions containing differently hydrophobic subsets of the original IVIG feed were

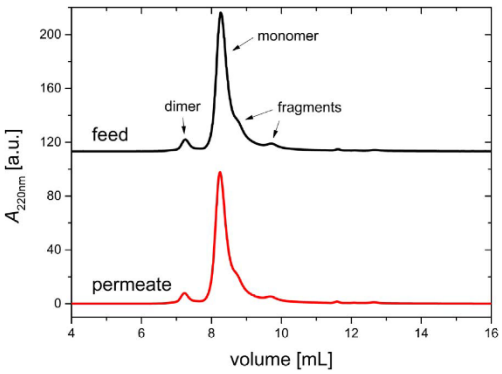

Fig. 8. SEC chromatograms of an IVIG feed solution (black line) and an IVIG permeate solution (red line) obtained by using VF4. (For interpretation of the references to color in this figure legend, the reader is referred to the web version of this article.)

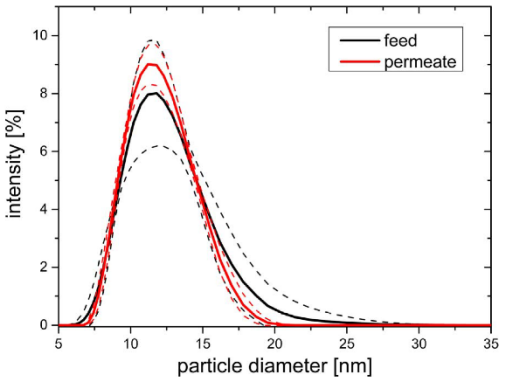

Fig. 9. Particle size distributions (intensity weighted) of a 5 g/L IVIG feed solution (black line) and an IVIG permeate solution (red line) obtained by using VF4 determined by DLS. Solid lines represent the average values of six measurements while the dashed lines represent 68% confidence intervals. (For interpretation of the references to color in this figure legend, the reader is referred to the web version of this article.)

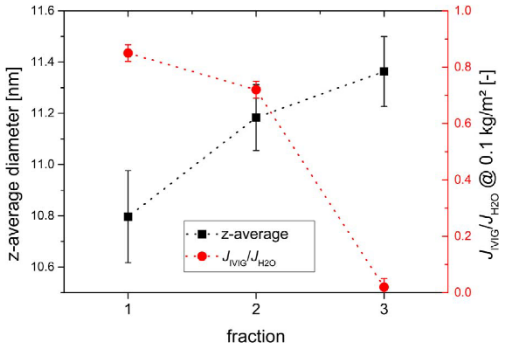

Fig. 10. DLS measurements (black squares) determining z-average diameters and flux measurements (red circles) with VF4 for the three fractions of IVIG obtained by HIC and adjusted to 1 g/L IVIG. Fractions labelled with a higher number contain more hydrophobic IVIG sub-species as they needed to be eluted from the hydrophobic resin at harsher conditions. Relative fluxes for each fraction are given at protein mass throughputs of 0.1 kg/m^2. The error bars represent the standard deviations determined from triplicate measurements. (For interpretation of the references to color in this figure legend, the reader is referred to the web version of this article.)

examined by DLS and utilized for filtration experiments using VF4 (Fig. 10). It can be observed that fractions containing more hydrophobic IVIG subsets exhibit larger z-average diameters. Since the z-average diameter is a single value, which describes a mean diameter for the whole ensemble of different particles in the sample, larger values can be indicative for the presence of aggregates. Fractions with larger z-average diameters also resulted in higher fouling. This further supports the hypothesis that larger (and more hydrophobic) species than the monomer are responsible for fouling, rather than a just more hydrophobic and therefore more adsorptive subset of IVIG monomers or fragments.

It can be concluded that fouling by the IVIG solution used in this study is most probably caused by trace amounts of small IVIG aggregates < 30 nm. Such fouling aggregates are probably larger than dimers which were determined by Brown et al. to be 16.4 nm in hydrodynamic diameter [8]. It is highly likely for species > 16 and < 30 nm to block the pores of a parvovirus retentive VF as those particles are efficiently retained by the SAL by size exclusion.

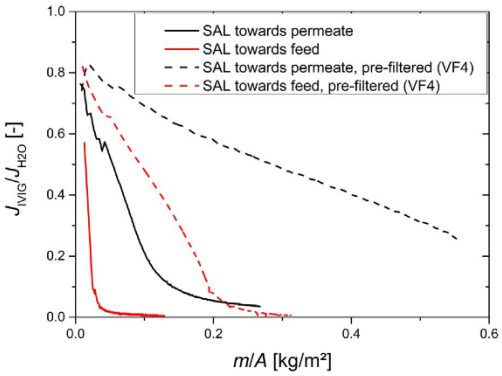

Fig. 11. Flux profiles of IVIG (5 g/L) filtrations using VF4 with different membrane orientations. Black lines denote the typical application relevant membrane orientation with the SAL facing towards the permeate, while red lines label the unusual orientation with the SAL facing towards the feed. Data was obtained using previously unfiltered solutions (solid lines) and solutions that were pre-filtered by using VF4. (For interpretation of the references to color in this figure legend, the reader is referred to the web version of this article.)

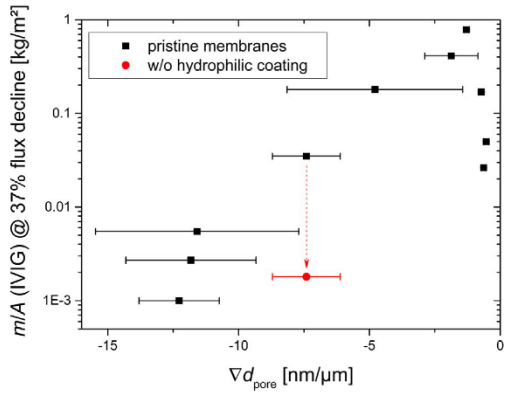

Fig. 12. Plot of protein mass throughputs with IVIG (5 g/L) as model protein at 37% flux decline as a function of the individual PSGs determined by the GNP method for the complete set of membranes in this study. Additionally to the commercial membranes in their original state (black squares), exemplarily for VF6 its hydrophilic surface coating has been removed resulting in VF6b (red circle). The importance of low interacting membrane surfaces, as part of the fouling mitigation strategy, is illustrated by the data points connected by the red arrow. The error bars represent the standard errors for the slopes of the linear fits depicted in Fig. 4. (For interpretation of the references to color in this figure legend, the reader is referred to the web version of this article.)

3.3. Correlation of PSGs with IVIG throughputs

A first indication of the relevance of the PSG with respect to fouling can be observed by changing the membrane orientation for filtration experiments with aggregate containing feed streams. Typically, the VFs are operated with SAL facing towards the permeate in order to maximize protein throughputs. VF4 has a shallow PSG which results in larger section of the membrane being capable to retain larger fouling species and thereby protecting the SAL from fouling. Using VF4 for filtration of IVIG solutions with the SAL facing towards the permeate utilizes these structural properties of the membrane and allows to achieve 4–5 times higher protein mass throughputs than with the opposite membrane orientation (Fig. 11). For the orientation of the membrane with the SAL facing towards the feed this SAL-protecting structure does not contribute to fouling resistance since the foulants are directly retained by the SAL causing early fouling. This observation is also true for IVIG feed solutions that have been pre-filtered by VF4. The concentration of foulants is only reduced by pre-filtration using a VF, as shown by using DLS (cf. Section 3.2.), allowing to achieve about ten times higher throughputs in general but still exhibiting the same effect of the membrane orientation.

Protein mass throughputs, at a flux decline of 37% with respect to the buffer flow rate, were determined for the whole set of membranes used in this study and related to the individual PSGs of the different membranes (Fig. 12). The results span a wide range from 0.001 to about 1 kg/m^2 with respect to the protein mass throughput. Membranes with steep PSGs (< -10 nm/µm) exhibit the lowest protein throughputs in the range of 0.001–0.006 kg/m^2, membranes with intermediate PSGs (-10 to -2.5 nm/µm) exhibit protein throughputs of 0.03–0.2 kg/m^2 and membranes with shallow PSGs (> -2.5 nm/µm) achieve the highest protein throughputs of 0.03–0.8 kg/m^2. A connection between PSG and protein mass throughput can clearly be shown, as membranes with shallow PSGs tend to be less susceptible towards fouling than those having steep PSGs. Within the group of membranes having shallow PSGs, this trend cannot be observed. This can be ascribed to the fact that all membranes in this study have proprietary surface chemistries developed in order to further reduce fouling. Not all surface chemistries have the same effectivity to improve fouling resistance, which can cause significant deviations from the trend between PSG and protein mass throughput.

Therefore, it is important to state, that susceptibility towards fouling is not only dependent on structural properties, such as the PSG or the PSD of the SAL, but also on the individual surface chemistry of the membrane. Low interacting surface chemistries can be very effective in order to decrease adhesion forces for foulants and thereby reduce fouling susceptibility [45,46]. To illustrate this effectivity, the protein mass throughput was determined for VF6b, a non-commercial variation of VF6 with a more interacting surface due to the lack of a hydrophilic coating (Fig. 12, red circle). Structurally, VF6 and VF6b can be assumed to be very similar. However, without the hydrophilic coating the protein mass throughput is reduced by more than an order of magnitude from 0.03 down to 0.002 kg/m^2.

Hence, a successful strategy to develop VFs that are less susceptible towards fouling by protein aggregates requires surface chemistries that are as low interacting as possible while having PSGs that allow to utilize a large extent of the membrane structure to act as a depth pre-filter protecting the SAL. Fig. 13 shall illustrate the available sections of two membranes with very different PSGs that are capable of retaining foulants in the size range of 16–30 nm. VF4 has a shallow PSG (> -2.5 nm/µm) and 100k PES has a steep PSG (< -10 nm/µm), as determined by the GNP method. Both membranes have a similar thickness of 120 µm. About 18% of the structure of VF4 (Fig. 13 B) and only 1% of the structure of 100k PES (Fig. 13C) have effective pore diameters in the size range of 16–30 nm. This significant structural difference can help to explain the ten times higher protein mass throughput that has been achieved with VF4 rather than the absolute depth pre-filter volume upstream of the SAL (Fig. S2, Supporting Information).

4. Conclusions

The application of monodisperse GNPs of defined size during filtration experiments under conditions where particle adsorption to the membrane surface is minimized enables to estimate an effective pore diameter within the membrane structure at the position where the particles were mainly captured by size exclusion. Furthermore, utilizing a set of differently sized GNPs ranging from 5 to 50 nm allowed the determination of the PSGs close to the SAL for a variety of highly diverse commercial parvovirus retentive VFs as well as UFs with respect to different membrane materials and surface chemistries. SEM image analysis was exemplarily used to verify the validity of the results obtained by the GNP method. The relevance of the PSG towards fouling

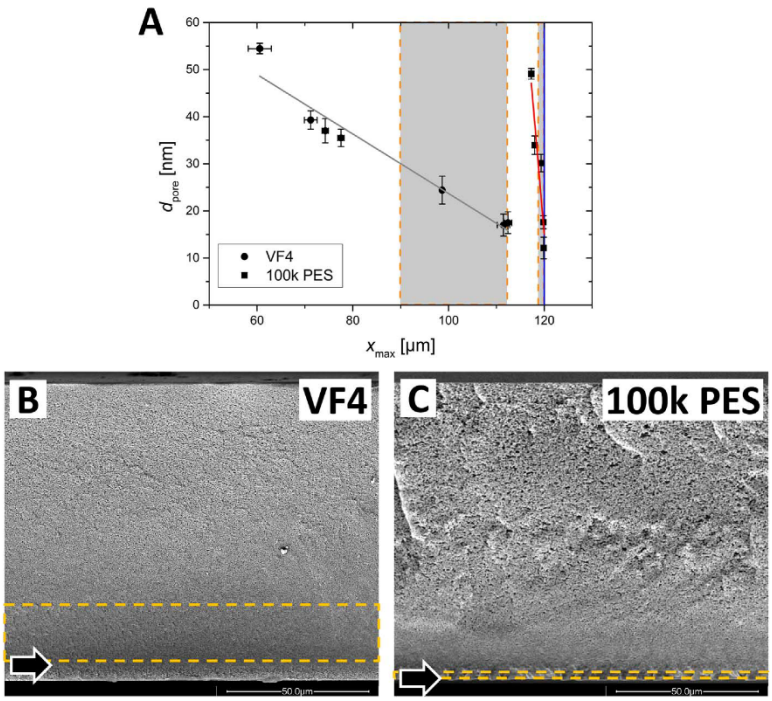

Fig. 13. A) Comparison of effective pore diameters at different positions in the membranes for VF4 (black circles, fit = grey line) and 100k PES (black squares, fit = red line) based on data from Fig. 4. Grey areas surrounded by dashed oranges lines highlight the sections of both membranes capable of retaining particles of 16–30 nm. Both membranes are 120 µm thick as indicated by the blue line. B) SEM image of cross-sections of VF4. C) SEM image of cross-sections of 100k PES. The approximate position of the SAL is indicated by the black arrows. Sections capable of retaining particles having 16–30 nm in hydrodynamic diameter, as determined under A), are highlighted by dashed orange lines. (For interpretation of the references to color in this figure legend, the reader is referred to the web version of this article.)

using IVIG as an accepted model protein was shown throughout the complete set of membranes used in this study. Fouling by the IVIG used was mechanistically investigated and determined to be mainly caused by trace amounts of small aggregates, probably in the size range of 16–30 nm. Membranes having more shallow PSGs were less susceptible to fouling than those having steeper PSGs. This can be explained by the fact that membranes with more shallow PSGs utilize a larger section of their structure to act as a depth pre-filter protecting the SAL from foulants. In addition to the PSG, a low interacting surface chemistry of the membrane also significantly contributes to fouling resistance. Therefore, for the development of robust VFs that are intended for the application with highly fouling feed streams both the PSG and the surface chemistry need to be optimized.

Acknowledgements

We would like to acknowledge Dr. Vladimir Roddatis and Matthias Hahn from the University of Göttingen for their support with TEM analyses.

Appendix A. Supplementary material

Supplementary data associated with this article can be found in the online version at http://dx.doi.org/10.1016/j.memsci.2017.11.048.

References

[1] D. Chen, Q. Chen, Virus retentive filtration in biopharmaceutical manufacturing, PDA Lett. (2016) 20–22.
[2] P.D.A. Technical, Report No. 41 - Virus Filtration, Parenteral Drug Association, Bethesda, MD, 2008.
[3] A. Buchacher, W. Kaar, Intravenous immunoglobulin G from human plasma—Purification concepts and important quality criteria, in: J. Bertolini, N. Goss, J. Curling (Eds.), Production of Plasma Proteins for Therapeutic Use, 1st ed, WILEY, Hoboken (New Jersey, USA), 2013.
[4] R. Esfandiary, D.B. Hayes, A. Parupudi, J. Casas-Finet, S. Bai, H.S. Samra, A.U. Shah, H.A. Sathish, A systematic multitechnique approach for detection and characterization of reversible self-association during formulation development of therapeutic antibodies, J. Pharm. Sci. 102 (2013) 3089–3099, http://dx.doi.org/10.1002/jps.23654.
[5] P. Kosiol, B. Hansmann, M. Ulbricht, V. Thom, Determination of pore size distributions of virus filtration membranes using gold nanoparticles and their correlation with virus retention, J. Memb. Sci. 533 (2017) 289–301, http://dx.doi.org/10.1016/j.memsci.2017.03.043.
[6] S. Giglia, D. Bohonak, P. Greenhalgh, A. Leahy, Measurement of pore size distribution and prediction of membrane filter virus retention using liquid–liquid porometry, J. Memb. Sci. 476 (2015) 399–409, http://dx.doi.org/10.1016/j.memsci.2014.11.053.
[7] J.G. Barnard, D. Kahn, D. Cetlin, T.W. Randolph, J.F. Carpenter, Investigations into the fouling mechanism of parvovirus filters during filtration of freeze-thawed mAb drug substance solutions, J. Pharm. Sci. 103 (2014) 890–899, http://dx.doi.org/10.1002/jps.23881.
[8] A. Brown, C. Bechtel, J. Bill, H. Liu, J. Liu, D. Mcdonald, S. Pai, A. Radhamohan, R. Renslow, B. Thayer, S. Yohe, C. Dowd, Increasing parvovirus filter throughput of monoclonal antibodies using ion exchange membrane adsorptive pre-filtration, Biotechnol. Bioeng. 106 (2010) 627–637, http://dx.doi.org/10.1002/bit.22729.
[9] G.R. Bolton, M. Cabatingan, M. Rubino, S. Lute, K. Brorson, M. Bailey, Normal-flow virus filtration: detection and assessment of the endpoint in bioprocessing, Biotechnol. Appl. Biochem. 42 (2005) 133–142, http://dx.doi.org/10.1042/BA20050056.
[10] R. Cameron, K. Smith, Virus clearance methods applied in bioprocessing operations: an overview of selected inactivation and removal methods, Pharm. Bioprocess. 2 (2014) 75–83, http://dx.doi.org/10.4155/pbp.13.61.
[11] R. Falkenstein, S. Hepbildikler, W. Kuhne, T. Lemm, H. Rogl, E. Rosenberg, G. Winter, F. Zettl, R. Zippelius, Protein purification and its relation to protein aggregation, in: H.-C. Mahler, W. Jiskoot (Eds.), Analysis of Aggregates and Particles in Protein, 1st ed, WILEY, Hoboken (New Jersey, USA), 2012, pp. 350–354.
[12] B. Hansmann, A. Meyer, H. Henning, V. Thom, Retentive properties of virus filter membranes in challenging experiments – Understanding virus retention by porous membranes, Parenter. Drug Assoc. Virus TSE Saf. Forum (2013).
[13] T. Burnouf, M. Radosevich, Nanofiltration of plasma-derived biopharmaceutical products, Haemophilia 9 (2003) 24–37.
[14] T. Hongo-Hirasaki, K. Yamaguchi, K. Yanagida, K. Okuyama, Removal of small viruses (parvovirus) from IgG solution by virus removal filter Planova* 20 N, J. Memb. Sci. 278 (2006) 3–9, http://dx.doi.org/10.1016/j.memsci.2005.10.057.
[15] R. van Reis, A. Zydney, Bioprocess membrane technology, J. Memb. Sci. 297 (2007) 16–50, http://dx.doi.org/10.1016/j.memsci.2007.02.045.
[16] Z.H. Syedain, D.M. Bohonak, A.L. Zydney, Protein fouling of virus filtration membranes: effects of membrane orientation and operating conditions, Biotechnol. Prog. 22 (2006) 1163–1169, http://dx.doi.org/10.1021/bp050350v.
[17] D.M. Bohonak, A.L. Zydney, Compaction and permeability effects with virus filtration membranes, J. Memb. Sci. 254 (2005) 71–79, http://dx.doi.org/10.1016/j.

memsci.2004.12.035.
[18] M. Bakhshayeshi, A.L. Zydney, Effect of solution pH on protein transmission and membrane capacity during virus filtration, Biotechnol. Bioeng. 100 (2008) 108–117, http://dx.doi.org/10.1002/bit.21735.
[19] M. Marroquin, A. Vu, T. Bruce, R. Powell, S.R. Wickramasinghe, S.M. Husson, Location and quantification of biological foulants in a wet membrane structure by cross-sectional confocal laser scanning microscopy, J. Memb. Sci. 453 (2014) 282–291, http://dx.doi.org/10.1016/j.memsci.2013.11.011.
[20] D.M. Kanani, X. Sun, R. Ghosh, Reversible and irreversible membrane fouling during in-line microfiltration of concentrated protein solutions, J. Memb. Sci. 315 (2008) 1–10, http://dx.doi.org/10.1016/j.memsci.2008.01.053.
[21] C. Ho, A.L. Zydney, Effect of membrane morphology on the initial rate of protein fouling during microfiltration, J. Memb. Sci. 155 (1999) 261–275.
[22] G. Miesegaes, S. Lute, H. Aranha, K. Brorson, Virus retentive filters, in: M.C. Flickinger (Ed.), Downstream Industrial Biotechnology, John Wiley & Sons, Hoboken (New Jersey, USA), 2013, pp. 641–654.
[23] S. Nakao, Determination of pore size and pore size distribution, J. Memb. Sci. 96 (1994) 131–165, http://dx.doi.org/10.1016/0376-7388(94)00128-6.
[24] I. Masselin, L. Durand-Bourlier, J.-M. Laine, P.-Y. Sizaret, X. Chasseray, D. Lemordant, Membrane characterization using microscopic image analysis, J. Memb. Sci. 186 (2001) 85–96, http://dx.doi.org/10.1016/S0376-7388(00)00657-8.
[25] R. Ziel, A. Haus, A. Tulke, Quantification of the pore size distribution (porosity profiles) in microfiltration membranes by SEM, TEM and computer image analysis, J. Memb. Sci. 323 (2008) 241–246, http://dx.doi.org/10.1016/j.memsci.2008.05.057.
[26] T. Li, X. Lu, B. Wang, Z. Wu, K. Li, D.J.L. Brett, P.R. Shearing, X-ray tomography-assisted study of a phase inversion process in ceramic hollow fiber systems – Towards practical structural design, J. Memb. Sci. 528 (2017) 24–33, http://dx.doi.org/10.1016/j.memsci.2017.01.004.
[27] J. Viguié, T. Savart, P. Duru, J.-C. Rouch, J.-C. Remigy, Characterisation of 3D porous macrostructure of hollow fibre membranes using X-ray tomography — Effects of some spinning process conditions, J. Memb. Sci. 435 (2013) 11–20, http://dx.doi.org/10.1016/j.memsci.2013.01.062.
[28] H. Reingruber, A. Zankel, C. Mayrhofer, P. Poelt, Quantitative characterization of microfiltration membranes by 3D reconstruction, J. Memb. Sci. 372 (2011) 66–74, http://dx.doi.org/10.1016/j.memsci.2011.01.037.
[29] G. Sundaramoorthi, M. Hadwiger, M. Ben-Romdhane, A.R. Behzad, P. Madhavan, S.P. Nunes, 3D membrane imaging and porosity visualization, Ind. Eng. Chem. Res. 55 (2016) 3689–3695, http://dx.doi.org/10.1021/acs.iecr.6b00387.
[30] K. Yamaguchi, Y. Hamamoto, S. Manabe, N. Yamamoto, Microparticle removability of the regenerated cellulose hollow fiber (BMM): an electron microscopic evaluation, J. Electron Microsc. 40 (1991) 337–345, http://dx.doi.org/10.1093/oxfordjournals.jmicro.a050906.
[31] T. Hirasaki, T. Noda, H. Nakano, Y. Ishizaki, S. Manabe, N. Yamamoto, Mechanism of removing Japanese Encephalitis virus (JEV) and gold particles using cuprammonium regenerated cellulose hollow fiber (i-BMM or BMM) from aqueous solution containing protein, Polym. J. 26 (1994) 1244–1256, http://dx.doi.org/10.1295/polymj.26.1244.
[32] M. Bakhshayeshirad, Performance characteristics of virus filtration membranes: protein fouling and virus retention, Ph.D. Thesis, The Pennsylvania State University, PA, USA, 2011.
[33] E. Arkhangelsky, A. Duek, V. Gitis, Maximal pore size in UF membranes, J. Memb. Sci. 394–395 (2012) 89–97, http://dx.doi.org/10.1016/j.memsci.2011.12.031.
[34] A. Duek, E. Arkhangelsky, R. Krush, A. Brenner, V. Gitis, New and conventional pore size tests in virus-removing membranes, Water Res. 46 (2012) 2505–2514, http://dx.doi.org/10.1016/j.watres.2011.12.058.
[35] D.A. Ladner, M. Steele, A. Weir, K. Hristovski, P. Westerhoff, Functionalized nanoparticle interactions with polymeric membranes, J. Hazard. Mater. 211–212 (2012) 288–295, http://dx.doi.org/10.1016/j.jhazmat.2011.11.051.
[36] T. Mizuno, A. Namiki, S. Tsuzuki, A novel filter rating method using less than 30-nm gold nanoparticle and protective ligand, IEEE Trans. Semicond. Manuf. 22 (2009) 452–461, http://dx.doi.org/10.1109/TSM.2009.2031762.
[37] M. Bakhshayeshi, N. Jackson, R. Kuriyel, A. Mehta, R. Van Reis, A.L. Zydney, Use of confocal scanning laser microscopy to study virus retention during virus filtration, J. Memb. Sci. 379 (2011) 260–267, http://dx.doi.org/10.1016/j.memsci.2011.05.069.
[38] S.K. Dishari, A. Venkiteshwaran, A.L. Zydney, Probing effects of pressure release on virus capture during virus filtration using confocal microscopy, Biotechnol. Bioeng. 112 (2015) 2115–2122, http://dx.doi.org/10.1002/bit.25614.
[39] S.K. Dishari, M.R. Micklin, K.-J. Sung, A.L. Zydney, A. Venkiteshwaran, J.N. Earley, Effects of solution conditions on virus retention by the Viresolve(®) NFP filter, Biotechnol. Prog. 31 (2015) 1280–1286, http://dx.doi.org/10.1002/btpr.2125.
[40] G.-T. Wei, F.-K. Liu, Separation of nanometer gold particles by size exclusion chromatography, J. Chromatogr. A 836 (1999) 253–260, http://dx.doi.org/10.1016/S0021-9673(99)00069-2.
[41] F. Liu, G. Wei, Effect of mobile-phase additives on separation of gold nanoparticles by size-exclusion chromatography, Chromatographia 59 (2004) 115–119, http://dx.doi.org/10.1365/s10337-003-0135-2.
[42] J.T. McCue, P. Engel, A. Ng, R. Macniven, J. Thömmes, Modeling of protein monomer/aggregate purification and separation using hydrophobic interaction chromatography, Bioprocess Biosyst. Eng. 31 (2008) 261–275, http://dx.doi.org/10.1007/s00449-008-0200-1.
[43] G.R. Bolton, J. Basha, D.P. Lacasse, Achieving high mass-throughput of therapeutic proteins through parvovirus retentive filters, Biotechnol. Prog. (2010) 1671–1677, http://dx.doi.org/10.1002/btpr.494.
[44] G.R. Bolton, S. Spector, D. LaCasse, Increasing the capacity of parvovirus-retentive membranes: performance of the Viresolve Prefilter, Biotechnol. Appl. Biochem. 63 (2006) 55–63, http://dx.doi.org/10.1042/BA20050108.
[45] J.A. Koehler, M. Ulbricht, G. Belfort, Intermolecular forces between proteins and polymer films with relevance to filtration, Langmuir 13 (1997) 4162–4171, http://dx.doi.org/10.1021/la970010m.
[46] J.A. Koehler, M. Ulbricht, G. Belfort, Intermolecular forces between a protein and a hydrophilic modified polysulfone film with relevance to filtration, Langmuir 16 (2000) 10419–10427, http://dx.doi.org/10.1021/la000593r.

Supplementary material

Fractionation of IVIG by HIC

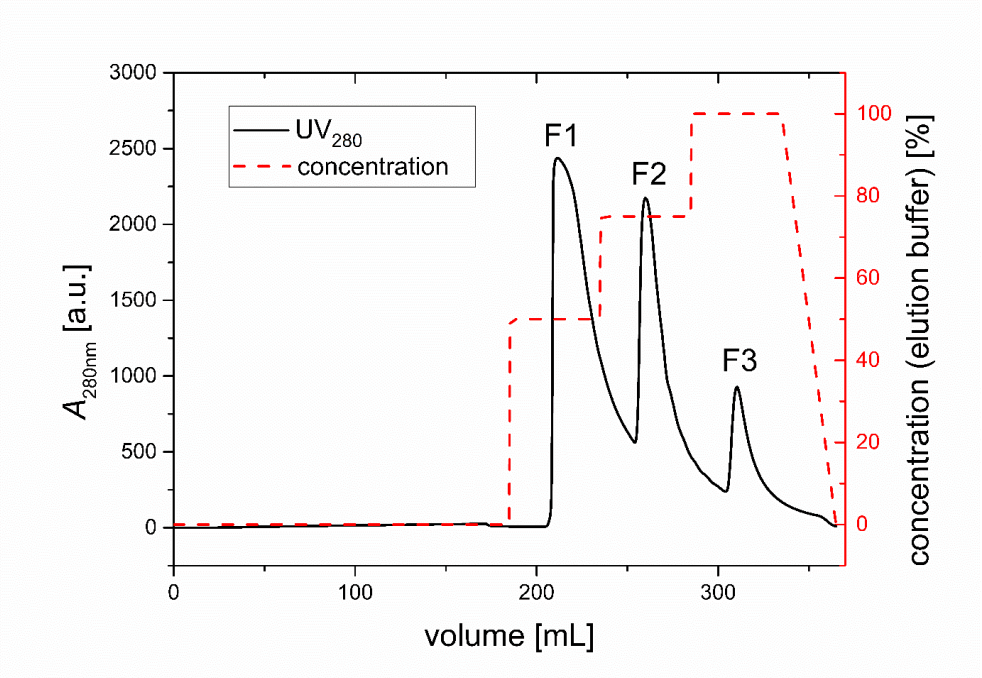

Fig. S1. Fractionation of IVIG by HIC. The elution profile (solid black line) showing three peaks (F1-F3) corresponding to fractions that were captured separately as a consequence of a stepwise increase of the concentration of the elution buffer (dashed red line).

Correlation of the depth pre-filter volume per filter area with IVIG throughputs

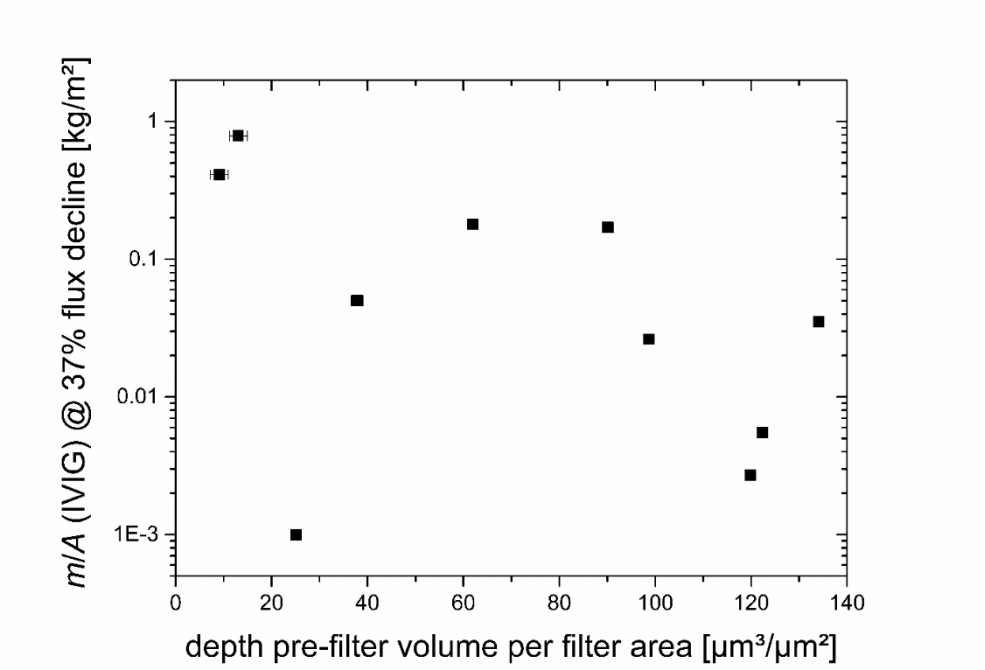

Fig. S2. Plot of protein mass throughputs with IVIG (5 g/L) as model protein at 37 % flux decline as a function of the depth pre-filter volumes per filter area for the complete set of membranes in this study. The depth pre-filter volume corresponds to the total membrane volume upstream of $x_{\max}(\sim 20\ \mathrm{nm\ GNP})$.

3.3 Investigation of virus particle retention by size exclusion membranes under different flow regimes (paper 3)

P. Kosiol, C. Kahrs, V. Thom, M. Ulbricht, B. Hansmann,

Investigation of virus particle retention by size exclusion membranes under different flow regimes,

Biotechnol. Prog. (2018) (under revision).

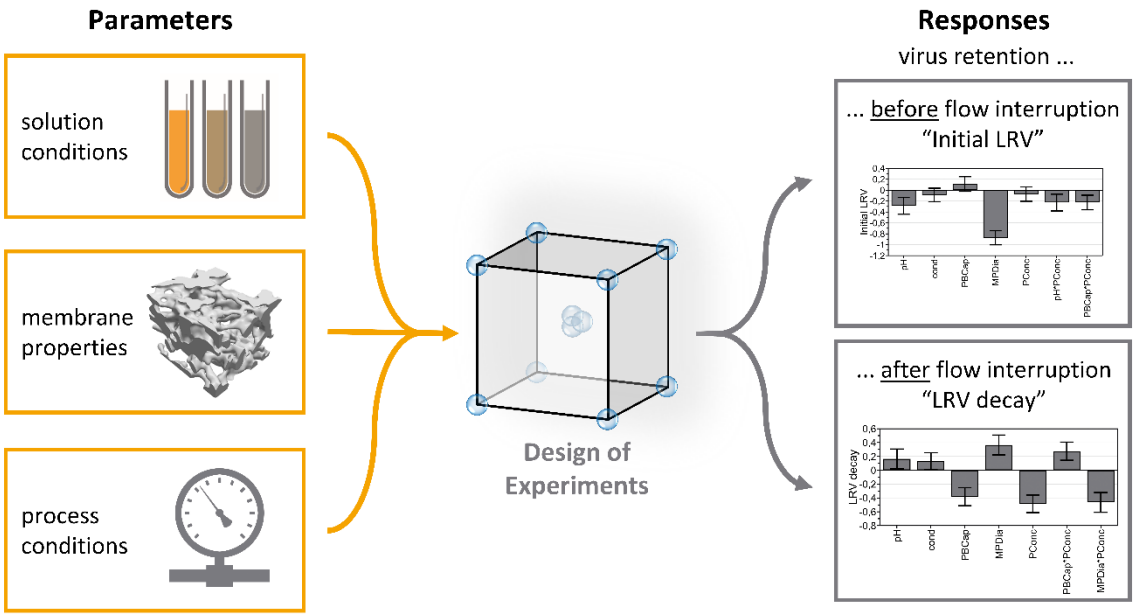

Investigation of virus particle retention by size exclusion membranes under different flow regimes

Peter Kosiol [a,b], Catharina Kahrs [a], Volkmar Thom [a], Mathias Ulbricht [b], Bjoern Hansmann [a,*]

[a] Sartorius Stedim Biotech GmbH, 37079 Göttingen, Deutschland

[b] Universität Duisburg-Essen, Technische Chemie II, 45141 Essen, Deutschland

[*]Address for Correspondence:

Email: bjoern.hansmann@sartorius.com

Phone: +495513081286

Abstract: Virus removal by filter membranes is regarded as a robust and efficient unit operation, which is frequently applied in the downstream processing of biopharmaceuticals. The retention of virus particles by virus filtration membranes is predominantly based on size exclusion. However, recent results using model membranes and bacteriophage PP7 as model virus point to the fact that virus retention can also significantly be influenced by adsorptive interactions between virus particles, product molecules and membranes. Furthermore, the impact of flow rate and flow interruptions on virus retention have been studied and responsible mechanisms discussed. The aim of this investigation was to gain a holistic understanding of the underlying mechanisms for virus particle retention in size exclusion membranes as a function of membrane structure and membrane surface properties, as well as flow and solution conditions. The results of this study contribute to the differentiation between size exclusion and adsorptive effects during virus filtration, and confirm and broaden the current understanding of mechanisms related to virus breakthroughs after temporary flow interruptions. Within the frame of a Design of Experiments approach it was found that the level of retention of virus filtration membranes was mostly influenced by the membrane structure during typical process-related flow conditions. The retention performance after a flow interruption was also significantly influenced by membrane surface properties and solution conditions. While size exclusion was confirmed as main retention mechanism, the analysis of all results suggests that especially after a flow interruption virus retention can be influenced by adsorptive effects between the virus and the membrane surface.

Keywords: virus filtration, virus retention, pressure release, flow interruption, diffusive movement

1. Introduction

The inactivation or removal of potential viral contaminants is an obligatory step in downstream processing of biologically or biotechnologically derived drugs such as monoclonal antibodies, recombinant proteins or plasma-derived products (PDA, 2008; Shukla and Aranha, 2015). Regulatory authorities like the FDA require for a downstream process at least two orthogonal methods to remove or inactivate viruses in order to increase the biological product safety (Marichal-Gallardo and Álvarez, 2012; Wieser et al., 2015). Unit operations such as virus inactivation by low pH treatment have limited efficacy against non-enveloped viruses (Marichal-Gallardo and Álvarez, 2012; World Health Organization, 2004). Chromatography based unit operations such as ion-exchange chromatography lack robustness with respect to process conditions and efficacy can be highly dependent on the virus species (Marichal-Gallardo and Álvarez, 2012; World Health Organization, 2004). In contrast, virus filtration using size exclusion based filters is known as an effective and robust unit operation for virus clearance (Marichal-Gallardo and Álvarez, 2012).

Size exclusion based virus filtration membranes (VFM) have a complex internal pore network, which is capable of transmitting product molecules that are smaller than 15 nm on a quantitative basis. Small virus particles in the size range of *Parvoviridae* (18-24 nm) and all larger viruses, a range which covers the majority of relevant virus species, are retained by at least 99.99 % ($\log_{10}$ reduction value (LRV) > 4), mainly by size exclusion (Miesegaes et al., 2013; Ray and Dolan, 2011). This selectivity is achieved by a defined pore size distribution, which can typically be well described by a log-normal distribution function (Giglia et al., 2015; Kosiol et al., 2017; Zydney et al., 1994). Peinador et al. observed that virus retention correlates with the maximum pore diameter, which they determined by using liquid-liquid displacement porometry (LLDP) (Peinador et al., 2011). Furthermore, Giglia et al. predicted LRVs of commercial and non-commercial VFM for different sized viruses based on LLDP data taking account of the entire pore size distribution (Giglia et al., 2015). Good correlation between predicted and measured virus retention was found for convection-dominated flow conditions. In contrast to retention mechanisms of soft pathogens such as mycoplasma or common bacteria using microfiltration membranes, where deformation of the pathogen at high transmembrane pressure was found to be a cause for pathogen breakthrough, viruses such as

bacteriophage PP7 exhibit a magnitudes higher stiffness preventing virus breakthrough at elevated transmembrane pressures (Helling et al., 2017).

However, it has been shown that virus retention can additionally be influenced by other mechanisms, which are dependent on flow and solution conditions. Flux decay as a result of fouling, caused by either product-related foulants or by the virus spike, was shown to have a very significant negative impact on the virus retention of the first-generation VFM (Bolton et al., 2005; Lute et al., 2007). This observation was explained by selective pore plugging of the small retentive pores deviating the convective flux into larger non-retentive pores (Bolton et al., 2005). More recently, a study was published investigating the pore size distributions of a broad set of commercial VFM (Kosiol et al., 2017). In this study it was shown that first-generation VFM typically exhibit broad pore size distributions, where the maximum pore size is significantly larger than observed in the second-generation VFM, which are generally more robust with respect to retention in general as well to retention at higher flux decays (Chen and Chen, 2016).

Kreil et al. investigated the impact of antibody-virus interaction on the virus retention of 35 nm VFM (Kreil et al., 2006). The authors observed a significant virus reduction for a 20 nm B19V parvovirus by 5 $\log_{10}$ during a pre-filtration step using a 0.1 µm rated filter, when virus specific antibodies were present that could aggregate with the virus. Others observed pH and ionic strength to have an impact on virus retention, which they attributed to non-specific electrostatic interactions between membrane and virus as well as between product molecule and virus (Dishari et al., 2015a; Strauss et al., 2017).

Furthermore, it has been first published in 2011 that flow interruptions (FI) can reduce virus retention levels of VFM (Asper, 2011). Since then, it has repeatedly been observed that the virus retention for different types of VFM decreased when the filtration was resumed after a temporary FI (Dishari et al., 2015b; Hansmann et al., 2013; Hongo-Hirasaki, 2015). Depending on the filter and the experimental conditions applied in these studies, the virus concentrations in the filtrate fraction directly after the FI were found to be 10 to 1000-fold higher after a temporary FI. However, in most cases the decreased level of retention was reversible and recovered for later fractions (Dishari et al., 2015a; Dishari et al., 2015b; Lacasse et al., 2013; LaCasse et al., 2016; Woods and Zydney, 2014). It is assumed that the decreased level of virus retention results from Brownian motion of the virus particles during the FI or under low flow conditions (Trilisky and Lenhoff, 2009; Yamamoto et al., 2014). Under normal flow conditions,

the virus particles are forced through the pore network until reaching pores small enough to be capable of size exclusion. Virus particles are constrained to these retentive pores by the convective flow, reducing their mobility based on diffusive movement. In contrast, under low or no flow conditions, the constraint of captured particles to the retentive pores is reduced or lacking completely resulting in a diffusive movement that allows previously retained virus particles to cover a certain distance within the pore network. Due to the log-normal pore size distribution of the membrane, these virus particles have a certain chance to reach larger non-retentive pores. When the filtration is then resumed and a typical convective flow reinstated, the majority of virus particles, which again reached retentive pores, will be constraint to these. The smaller share of virus particles that had reached non-retentive pores can pass through these further downstream into the VFM until either being re-captured in a deeper zone or even transmitted through the membrane, leading to a higher virus concentration in the filtrate. A diffusion-based mechanism of virus reorganization during a FI is further supported by observing impacts of solution viscosity (LaCasse et al., 2016; Yamamoto et al., 2014) and the duration of the FI (LaCasse et al., 2016) as both affect the distance that can be covered by the virus particles by diffusion. Furthermore, it has been reported that retention after a FI can be influenced by pH and ionic strength, which was attributed to electrostatic interactions between virus, membrane and product molecule (Dishari et al., 2015a). It is assumed that attractive electrostatic interactions between the virus and the inner membrane surface could cause an additional constrain for virus particles.

Commercial VFM from different brands, even different VFM types from a single brand, have shown significant differences in retention performance and robustness (Dishari et al., 2015b; Kosiol et al., 2017; Lacasse et al., 2013; LaCasse et al., 2016; Lute et al., 2007). Due to the proprietary nature of the manufacturing processes of these VFM, each membrane type is unique, differing with respect to pore size distribution (Kosiol et al., 2017), pore size gradient (Kosiol et al., 2018) and surface chemistry. This complexity makes conclusions on membrane-related impact factors concerning retention behavior difficult. Very few studies are available focusing on the membrane properties especially considering the effect of FI on virus retention. In order to gain a holistic picture of the underlying mechanisms for virus retention by size exclusion membranes, a Design of Experiments (DoE) approach was chosen. Virus filtration experiments using *Pseudomonas aeruginosa* bacteriophage PP7, an accepted size-based virus model for polio- and parvovirus retentive membranes (Aranha-Creado and Brandwein, 1999;

PDA, 2008), were conducted. In contrast to previous studies, a wider range of parameters was studied. Model VFM were prepared to investigate membrane-related parameters like the maximum pore diameter and membrane surface properties, described by the measured differences in protein binding capacity. Different feed solutions were used in order to study the impact of solution-related properties like pH, conductivity and protein concentration. From each individual filtration run the LRV was determined before and after a FI for the purpose of involving an important process-related parameter to this study. Both datasets were analyzed separately to determine the significance and the effect strength for each parameter during a typical convective flow condition and shortly after a FI. Furthermore, the presence of significant interactions between parameters was determined.

2. Materials and methods

2.1. Study design

A DoE approach was applied in order to comprehensively determine the impact of various parameters on the virus retention behavior of VFM. The investigated parameters are summarized in Table I and include the solution conditions pH, conductivity and protein concentration as well as the membrane properties protein binding capacity and maximum pore diameter.

Table I. Parameters, parameter ranges and responses evaluated for virus filtration experiments.

Parameter	**Abbreviation**	**Range**
pH	pH	5.5 – 9.0
Conductivity [mS/cm]	cond	3.5 – 16.5
Protein concentration [g/L]	PConc	0 – 0.5
Protein binding capacity [mg/cm³]	PBCap	2.9 – 6.4
Maximum pore diameter [nm]	MPDia	26.2 – 33.6

Response	**Abbreviation**	
Virus retention before a FI	Initial LRV	
Virus retention decrease after a FI	LRV decay	

The evaluated responses are the virus retention before a FI ("initial LRV") and the potential decrease in virus retention right after a FI ("LRV decay"). A 2^5 full factorial study design with additional experiment conditions for mid-range pH was selected as depicted in Table SI (supporting information) comprising a total of 44 different experimental conditions with 164 individual filtration runs.

Data were analyzed with Umetrics MODDE Pro 12 (Sartorius Stedim Data Analytics AB, Sweden) by using a multiple linear regressions (MLR) approach in order to determine effect strengths of the parameters and possible interactions. Model quality is evaluated by calculation of the coefficient of determination (R^2) and coefficient of prediction (Q^2), both measures for the goodness-of-fit. $R^2 < 0.5$ represents a mode with a rather low significance. $Q^2 > 0.1$ indicates a potentially significant model, values $Q^2 > 0.5$ are considered a good model. Confidence intervals were set to a confidence level of 95 %.

2.2. Membranes

All filtration experiments were performed using model flat sheet polyethersulfone VFM in a single layer configuration. In contrast, commercial flat sheet virus filters consist of two to three membrane layers. Commercial VFM often show a high level of retention above the upper detection limit of the plaque assay used for virus quantification. Overall, virus retention performance of the model membranes was lower compared to commercial VFM in order to assess the effects of the parameters investigated well within the detection limits of the plaque assay. 5 cm^2 membrane discs were housed into Minisart® devices (Sartorius, Germany). A major focus of the present study is the mechanistic investigation of the impact of membrane properties including their pore structure and their surface. While the membrane structure is represented by the maximum pore diameter, the membrane surface property is characterized by its protein binding capacity, which is a measure for its interaction with proteins. The exterior surface of non-enveloped viruses also consists of a protein capsid, so that the protein binding capacity is assumed to be also a measure for the interaction between the membrane surface and non-enveloped viruses. A strategy facilitating the investigation of both of these membrane properties was implemented by utilizing a proprietary membrane casting process to generate two base membranes having different maximum pore diameters, but similar low protein binding capacities (1a and 2a, Table II). The inner and outer surface of some of these

base membranes was altered by a proprietary procedure, which is able to remove a minor share of the hydrophilizing agent from the membrane surface and rendering these membranes more adsorptive (1b and 2b, Table II). This procedure allowed to obtain membranes with a significantly higher protein binding capacity, while maintaining the structural properties of the base membranes, as indicated by the maximum pore diameter and the buffer permeability, both after surface modification.

Table II. Membranes used for the DoE study and their properties.

Membrane	**Buffer permeability [$Lm^{-2}h^{-1}bar^{-1}$] @ 20 °C**	**Protein binding capacity [mg/cm^3]**	**Maximum pore diameter [nm]**	**pI**
1a	155 ± 9	2.9 ± 0.1	27.3 ± 0.1	< 4
1b	150 ± 12	6.3 ± 0.5	26.2 ± 0.7	< 4
2a	187 ± 9	3.0 ± 0.2	33.6 ± 1.5	< 4
2b	170 ± 7	6.4 ± 0.3	32.6 ± 0.1	< 4

Apart from the model VFM used in the DoE study, additional filtration experiments using commercial second-generation VFM were conducted for a variety of solution conditions adopted from the DoE study. For this purpose Virosart® CPV (545VM----------B), Virosart® HC (539VM----------B) and Virosart® HF (3VI--28-BCGMLITV) 5 cm^2 down-scale devices from Sartorius (Germany) were used.

Protein binding capacity

Protein binding capacities of all model VFM were determined by utilizing a bicinchoninic acid (BCA) assay (Pierce™ BCA reagent kit, ThermoFisher Scientific, Germany). 10 mm disc samples of the VFM were placed in a 48-well plate (Greiner Bio-One, Austria). 200 µL of 3 g/L human intravenous immunoglobulin (IVIG) from SeraCare Life Sciences (USA) in 20 mM potassium phosphate at pH 7.0 were added to each well. After static incubation overnight at room temperature, VFM samples were washed three times with 20 mM potassium phosphate at pH 7.0. The BCA assay solution was prepared by mixing BCA reagents A and B 50:1 (v/v). 300 µL BCA assay solution were added to each well and incubation was carried out for 1 h at room temperature. 200 µL solution from each well were transferred to a new 48-well-pate.

Absorbance at 562 nm was measured using a well-plate compatible Infinite M2000 spectrophotometer (Tecan, Switzerland).

Maximum pore diameter

LLDP was applied to all model VFM as described by Kosiol et al. to determine pore size distributions (data not shown) (Kosiol et al., 2017). Maximum pore diameters were determined from the pore size distributions by numerical approximation of the cumulative distribution functions. The maximum pore diameter is defined as 99 % of the pores being smaller and 1 % being larger.

Isoelectric point (pI)

Zeta potentials of all model VFM were measured using a SurPASS™ elektrokinetic analyzer (Anton Paar, Austria) in the pH range from 4 to 10 based on a protocol by Lei et al. (Lei and Ulbricht, 2014). pI values were determined from plots of zeta potential vs. pH.

2.3. Bacteriophage PP7

Pseudomonas aeruginosa bacteriophage PP7 (ATCC 15692-B2), a small non-enveloped virus (pI 4.3-4.9 (Brorson et al., 2008)), was used as accepted standard model virus for investigation of retention properties of parvovirus retentive VFM (Lute et al., 2008; PDA, 2008). PP7 was propagated using *Pseudomonas aeruginosa* (ATCC 15692) as host. Phage titers were obtained by a plaque assay using *P. aeruginosa* as indicator cell. Propagation and titrations were carried out according to recommendations by the PDA Technical Report No. 41 – Virus Filtration (PDA, 2008).

2.4. Preparation of feed solutions

A set of different buffers was used for the DoE study to determine the impact of solution conditions on virus retention. Buffers at pH 5.5 and 7.3 (20 mM potassium phosphate) and pH 9.0 (20 mM Tris-HCl) were adjusted to 3.5, 10 or 16.5 mS/cm by addition of sodium chloride. Buffer conditions were selected to represent a broad range of typical conditions while maintaining sufficient stability and infectivity of PP7. To examine the effect of proteins

that are present in biopharmaceutical feed solutions, an IVIG solution, which consists of pooled human immunoglobulin G, was purchased from SeraCare Life Sciences (USA). Feed solutions used for the DoE study contained either no or 0.5 g/L IVIG. Due to the filter fouling nature of IVIG, a low concentration of 0.5 g/L was chosen in order to exclude potentially extensive filter fouling from the investigation that could occur at certain solution conditions. PP7 stock solution was spiked to the feed solutions to obtain a phage titer of 10^7 plaque forming units (pfu) per mL. After addition of PP7 spike, the solutions were stirred for 20 min and pre-filtered through a 0.1 µm rated membrane (Sartorius, Germany) to remove aggregated phages. Subsequently, hold samples were taken and stored for the duration of the filtration experiments to assess any possible virus inactivation during that timeframe.

2.5. Virus filtration experiments

All filtration experiments were conducted in pressure-controlled mode using air-pressurized feed reservoirs as depicted in Fig. 1 A. Prior to phage filtration, all VFM were equilibrated with 10 mL pure buffer at 2 bar (29 psi). After switching to phage containing feed streams, all filtrations were conducted at 2 bar (29 psi) and three permeate fractions were collected at each filtration.

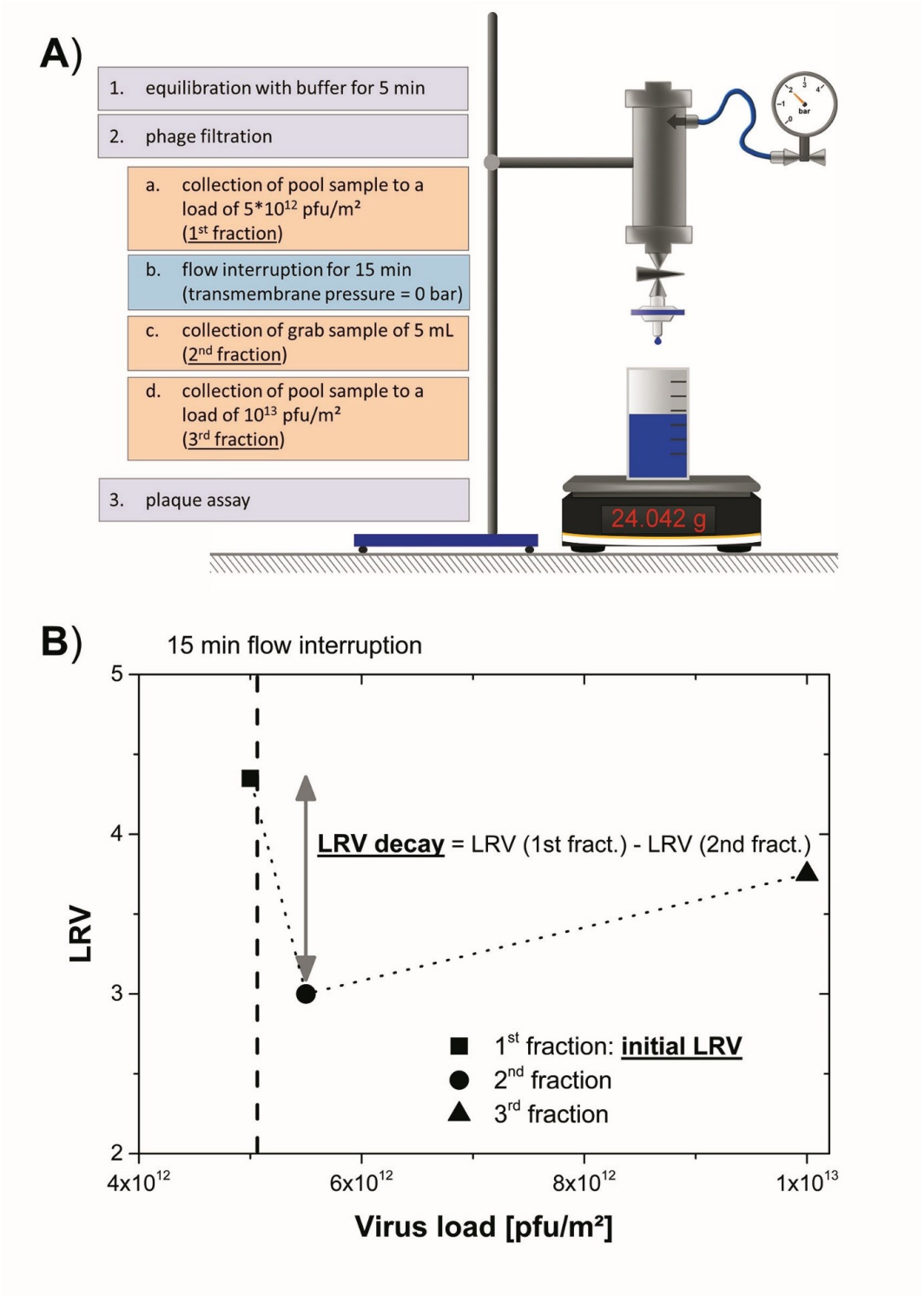

Fig. 1. Illustration of the filtration set-up including the sequence of experimental steps (A) and depiction of a typical LRV profile of a single filtration experiment (B), visualizing the permeate fractions taken and their relation towards the DoE study observables “initial LRV” and “LRV decay”.

A pool sample was taken to yield a virus load of $5*10^{12}$ pfu/m² as first fraction. After taking the first fraction, the flow was interrupted by releasing the pressure (transmembrane pressure = 0 bar) for 15 min. This duration for the FI was determined in a pre-experiment using experimental condition 21 (Table SI, supporting information) under variation of the duration between 0.5, 1, 5 and 20 min (Fig. S1, supporting information). Longer durations than 15 min did not significantly increase the LRV decline. After re-pressurization of the feed reservoir to 2 bar (29 psi), the first 5 mL were collected as second fraction. A larger third fraction was taken as pool sample to yield a virus load of 10^{13} pfu/m² to visualize the LRV recovery.

Phage titers of all samples were determined by a pfu assay as described within the PDA Technical Report No. 41 – Virus Filtration (PDA, 2008). Virus retention performance was calculated for each fraction as $\log_{10}$ reduction value (LRV), which is the logarithmic ratio of the phage titer in the feed C_{feed} to the titer in the permeate $C_{permeate}$.

$$\text{LRV} = \log_{10} \frac{C_{feed}}{C_{permeate}}$$

The LRV of the first fraction taken before the FI is defined as “initial LRV” and used as response for the DoE study (Fig. 1 B). The second response “LRV decay” is calculated as difference between the LRV of the first fraction before and the second fraction right after the FI, which is often termed as “pressure release” in virus filtration literature.

2.6. Particle size measurements of PP7/IVIG solutions using dynamic light scattering (DLS)

To obtain PP7 suspensions with suitable high titers and purities for DLS measurements, a polyethylene glycol (PEG) precipitation protocol according to Nguyen et al. (Nguyen et al., 2011) was applied. Further, remaining PEG was removed by diafiltration using 50 kDa Vivaspin® 6 centrifugal concentrators (3,400 g for 15 min at 20 °C, Sartorius, Germany) and the individual target buffers as described in section 2.4. Two additional buffers at pH 4.5 (20 mM sodium acetate), adjusted to 3.5 and 16.5 mS/cm by addition of sodium chloride, were used. In case of measurement of PP7 in presence of IVIG, the IVIG concentration was set to 1 g/L. IVIG solutions without PP7 were also measured at 1 g/L. In order to remove

potentially present large particle contaminants, the samples were filtered through a Minisart® RC4 0.2 µm syringe filter (Sartorius, Germany) prior to DLS measurements.

DLS studies were conducted using a Zetasizer Nano ZSP (Malvern Instruments Ltd., UK). All samples were measured in single-use micro UV-cuvettes (Brand, Germany) after a thermal equilibration at 20 °C for 3 min. For each sample three measurement runs have been performed with a detection angle of 173° (backscattering). The measurement duration for each run was set to "automatic". Data acquisition and analysis were conducted using the Zetasizer Software v7.11 accompanied to the DLS device. For data analysis, the method of cumulants for determination of the z-average hydrodynamic diameter has been applied.

3. Results and discussion

3.1 Virus retention without FI – initial LRV

For the MLR analysis (cf. Section 2.1) of the initial LRV a good model was obtained as indicated by $R^2 = 0.65$ and $Q^2 = 0.61$ (Fig. 2). Two parameters were found to be significant: pH and maximum pore diameter. Also, two significant interactions were found: pH and protein concentration (pH*PConc) as well as protein binding capacity and protein concentration (PBCap*PConc). Parameters or interactions between two or more parameters are considered to be significant, when their error bars do not include zero.

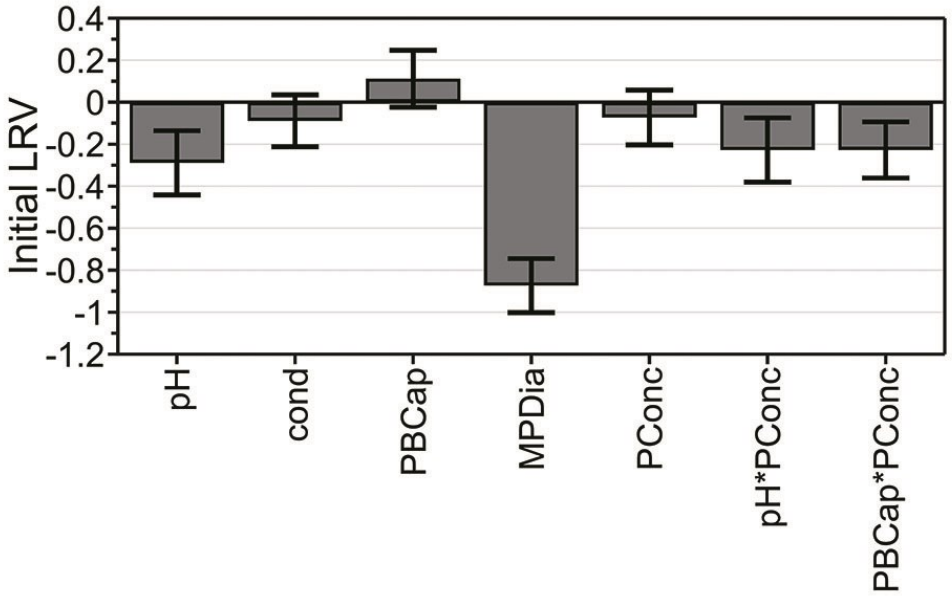

Fig. 2. MLR model coefficient plot for the initial LRV as response. The parameters are the pH, the conductivity (cond), the protein concentration (PConc), the protein binding capacity (PBCap) and the maximum pore diameter (MPDia). The interactions identified are the interaction between pH and protein concentration (pH*PConc) and the interaction between protein binding capacity and protein concentration (PBCap*PConc). Significance of the model is supported by R^2 = 0.65 and Q^2 = 0.61.

As expected for a VFM mainly working by size exclusion, the maximum pore diameter was found to have a strong negative impact on the initial LRV as already observed by a previous study (Peinador et al., 2011). Typically, log-normal distributions are used to describe pore size distributions of porous membranes (Zydney et al., 1994). For homologous membranes obtained from the same material with the same manufacturing process just by variation of manufacturing parameters, as the maximum pore diameter increases, the whole pore size distribution shifts to larger values. This results in an increased fraction of larger, non-retentive pores, reducing the initial LRV.

An increase in pH yields a lower initial LRV indicating the relevance of electrostatic interactions for the level of retention. A comprehensive discussion of the electrostatic interactions requires the consideration of all components involved, such as the phage itself, the protein present in the feed as well as the membrane.

The electrostatic charges of these components are summarized in Table III for the pH conditions of the DoE study and additionally for pH 4.5, a pH close to the pI of PP7. As can be seen, within the pH range of the DoE study the charge of the bacteriophage PP7 was always negative. In addition, the VFM applied in this study, having pIs < 4, were always negatively

charged. The model protein IVIG consists of polyclonal antibodies of different donors and therefore exhibits a broad range of pIs between 6 and 9 (data not shown), rendering the majority of antibody species positively charged at pH 5.5, mostly uncharged or positively charged at pH 7.3 and mostly negatively charged at pH 9.0.

Table III. Overview of pI values and charge states of the major components of the DoE study: the bacteriophage PP7, the membranes and the model protein IVIG.

Component	**pI**	**pH**			
		4.5*	5.5	7.3	9.0
PP7	4.3 – 4.9	0	-	-	-
Membranes	< 4	-	-	-	-
IVIG	6 – 9	+	+	+/0	-

-: negative net charge
0: neutral net charge
+: positive net charge
*: not included in DoE study

DLS experiments of PP7 suspensions in absence and in presence of IVIG were conducted to provide experimental proof for aggregation during conditions of the DoE study (Fig. 3). Typically, results provided by DLS overestimate the mean particle size compared to other techniques, e.g. based on microscopy, due to higher weighing of the larger species present in the sample rendering DLS to be very sensitive towards detection of aggregated species.

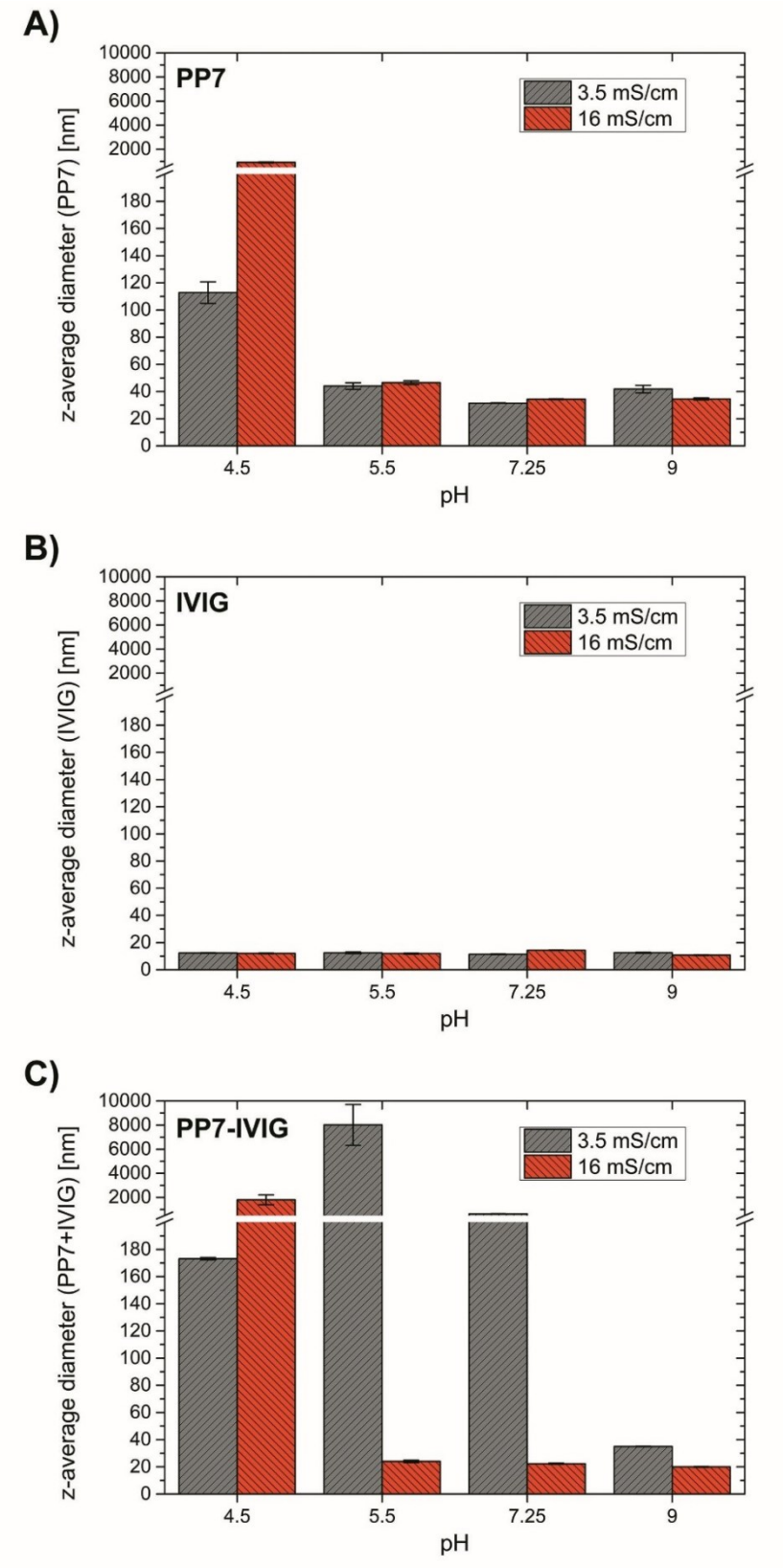

Fig. 3. Hydrodynamic (z-average) diameters determined by DLS for PP7 suspensions (A), IVIG solutions (B) and PP7 suspensions in presence of IVIG (C). Solution conditions were examined for pH 4.5, 5.5, 7.3 and 9.0 and solution conductivities of 3.5 and 16 mS/cm. Error bars represent standard deviations calculated from triplicate runs.

In the absence of IVIG, hydrodynamic diameters of PP7 were determined to be between 32 and 47 nm for pH 5.5, 7.3 and 9.0, independently of the solution conductivity, and tending to be slightly larger at pH 5.5 (Fig. 3 A). Values of 30-33 nm for PP7, measured by a similar DLS procedure, have been reported for highly purified and mostly monomeric PP7 suspensions (Lute et al., 2008). Recent results using techniques for size measurements that are less sensitive towards aggregates such as transmission electron microscopy (TEM) or that include a size-based separation step such as size exclusion chromatography-multi-angle light scattering (SEC-MALS) indicate 26 nm (TEM) and 34 nm (SEC-MALS) in diameter for PP7 (Johnson et al., 2017). In the same study PP7 results are compared with the minute virus of mice (MVM), an often used small mammalian virus for spiking studies, having 25 nm (TEM) and 35 nm (SEC-MALS) and thereby rendering PP7 to be a representative size-based model virus for small mammalian viruses. Therefore, slightly increased hydrodynamic diameters of 44-47 nm for PP7 at pH 5.5 indicate minor aggregation of PP7 at this condition; that aggregation strongly increases towards a lower pH value of 4.5, closer to the pI of the phage. In the presence of IVIG a more significant aggregation was observed at pH 5.5 and 7.3 under low solution conductivity (Fig. 3 C), supporting the hypothesis of heterogeneous aggregation due to oppositely charged PP7 and IVIG particles. This increased aggregation tendency cannot be attributed to aggregation of IVIG alone, as IVIG solutions showed no significant aggregation under all solution conditions examined (Fig. 3 B).

The observation made by DLS could be used as an explanation for the observed effect of pH in the DoE study as well as the significant negative interaction between pH and the protein concentration (pH*PConc) (Fig. 4 A). A distinct decrease of the initial LRV with increasing pH is observed for the case where IVIG was present in the feed. This can be attributed to the high amount of PP7/IVIG aggregates at low pH conditions that are more easily retained by size exclusion. This decrease of the initial LRV is less distinct in the absence of IVIG (“PConc (low)”), as could be explained by the DLS results showing overall less aggregation within the pH range of the DoE study.

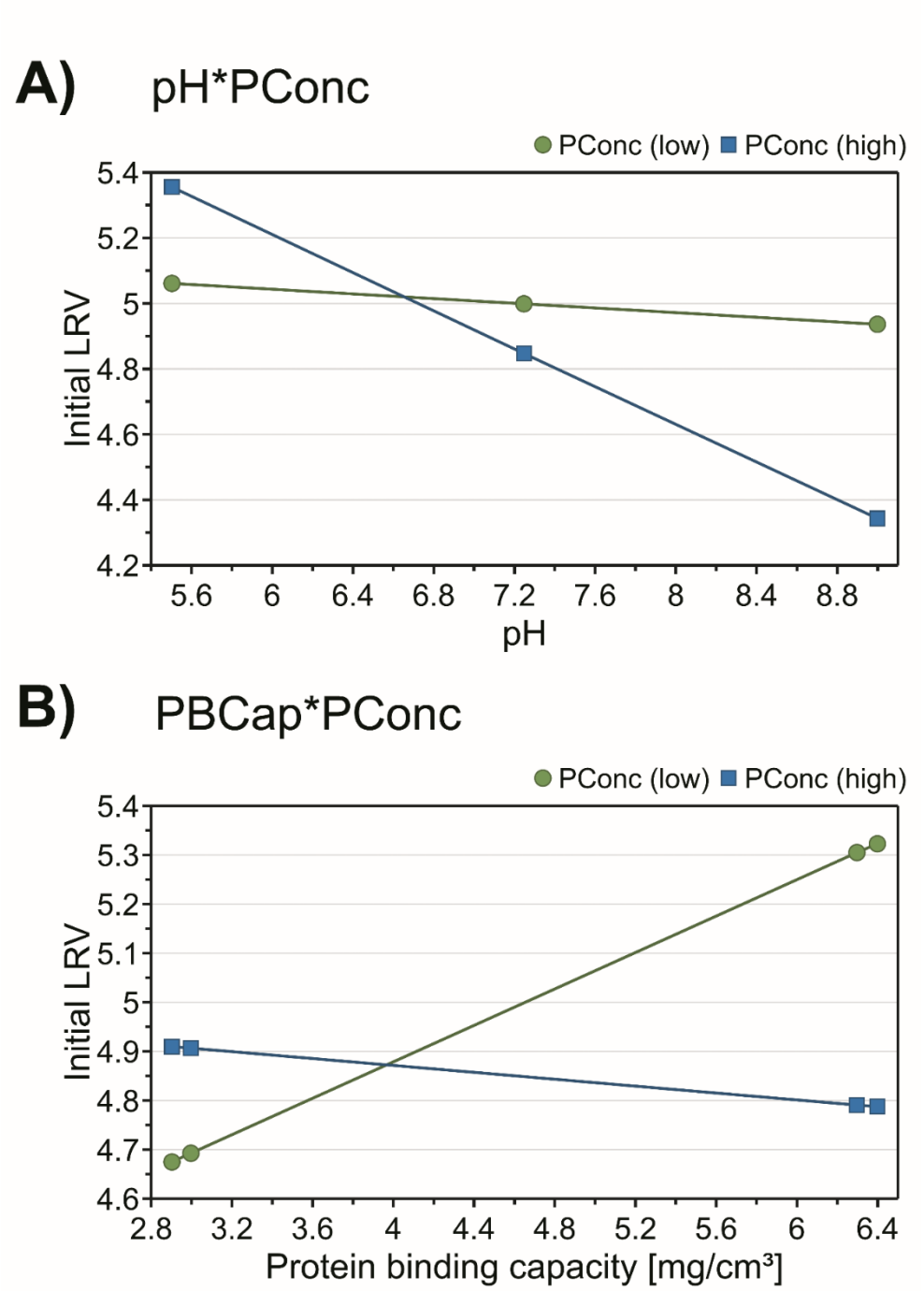

Fig. 4. Interaction plots for pH and protein concentration (pH*PConc) (A) and for protein binding capacity and protein concentration (PBCap*PConc) (B) with respect to the initial LRV.

To fully understand why the initial LRV is higher at pH 9.0 in the absence than in the presence of IVIG, also interactions involving the membrane have to be considered. All membranes used in this study had protein binding capacities between 2.9-6.4 mg/cm³. Hence, in the absence of IVIG the adsorptive capacity of the membrane potentially contributed towards retention of PP7 by adsorption. In the presence of IVIG ("PConc (high)") on the other hand, such adsorptive

spaces were mostly occupied by IVIG, which is present in solution in a much larger concentration than PP7, and therefore suppresses further adsorption of PP7.
Another support for the hypothesis that adsorption of PP7 can contribute to the initial LRV is given by the significant negative interaction between the protein binding capacity and the protein concentration (PBCap*PConc) (Fig. 4 B). Here, in the absence of IVIG, the initial LRV strongly increases with the protein binding capacity, while in the presence of IVIG the protein binding capacity merely has an impact on the initial LRV.

3.2 Virus retention after FI – LRV decay

Data analysis for the LRV decay provided a similarly good MLR model as for the initial LRV, indicated by $R^2 = 0.70$ and $Q^2 = 0.67$ (Fig. 5). All parameters were found to be significant together with the two interactions between the protein binding capacity and the protein concentration (PBCap*PConc) and between the maximum pore diameter and the protein concentration (MPDia*PConc).

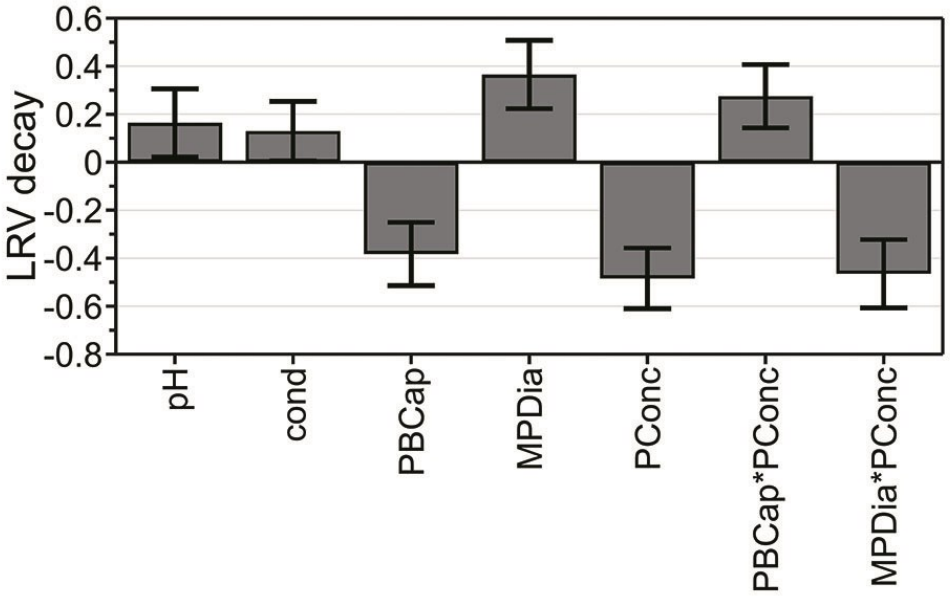

Fig. 5. MLR model coefficient plot for the LRV decay as response. The parameters are the pH, the conductivity (cond), the protein concentration (PConc), the protein binding capacity (PBCap) and the maximum pore diameter (MPDia). The interactions identified are the interaction between protein binding capacity and protein concentration (PBCap*PConc) and the interaction between maximum pore diameter and protein concentration (MPDia*PConc). Significance of the model is supported by R^2 = 0.70 and Q^2 = 0.67.

While having by far the largest impact on the initial LRV compared to all other parameters, the maximum pore diameter has a significant and large positive impact on the LRV decay as well. In contrast to the initial LRV, the protein concentration and the protein binding capacity have even larger impacts on the LRV decay.

As proposed by Yamamoto et al., under typical process conditions mass transport of viruses through the porous network of a VFM is dominated by convection, while in case of FI or low convective flow rates mass transport can be dominated by diffusion (Yamamoto et al., 2014). Within the convection-dominated regime, viruses move in downstream direction through the porous network of the membrane until they encounter a pore with a smaller diameter than the diameter of the virus. Convective forces constrain these viruses in the retentive pores, resulting in size exclusion. Within the diffusion-dominated regime, the constriction of the previously retained viruses is removed, allowing these viruses to travel a certain distance within the porous network by Brownian motion. By a certain chance, some of these viruses can reach larger non-retentive pores within the possible travel distance. After reinstating typical process conditions, these viruses can be transported through these non-retentive

pores further downstream into the membrane leading to an increased transmission of viruses into the filtrate and by this resulting in a larger LRV decay.

The positive impact of the maximum pore diameter can be explained by the increased amount of larger, non-retentive pores for membranes with a larger maximum pore diameter. The probability for viruses to reach non-retentive pores by diffusive movement during the FI increases with a higher share of non-retentive pores in the pore size distribution.

The protein binding capacity and the protein concentration on the other hand have large negative impacts on the LRV decay. The protein binding capacity is a measure for the interaction of the membrane with proteins and assumed to be also valid for the interaction with non-enveloped viruses such as the bacteriophage PP7. The results strongly suggest that adsorptive interaction can reduce the LRV decay after a FI. The adsorption/desorption equilibrium of the viruses with the membrane surface will probably be shifted towards adsorption for membranes with a higher protein binding capacity, reducing the effective travel distance during the diffusive movement. For commercial VFM, increasing the protein binding capacity poses no viable strategy in order to increase retention robustness. Such a strategy would interfere with the size exclusion as main and robust retention mechanism. Furthermore, membranes with increased protein binding capacity are more prone towards fouling with protein containing feed streams, which would reduce the productivity of such membranes and can also lead to product loss. The negative impact of the protein concentration could be explained by the interaction between IVIG and PP7 as was already observed by DLS (Fig. 3 C). Heterogeneous IVIG-PP7 aggregates undergo, due to their increased size, a reduced diffusive movement compared to monomeric PP7.

For a more comprehensive understanding, a consideration of the significant positive interaction between the protein binding capacity and the protein concentration (PBCap*PConc) is helpful (Fig. 6 A). In absence of IVIG (“PConc (low)”), only interactions between PP7 and the membrane are relevant. In that case, the LRV decay for membranes with low protein binding capacities, that are more similar to commercial VFM, is high. Increasing the protein binding capacity significantly decreases the LRV decay, as adsorptive interactions between PP7 and the membrane surface increase. In presence of IVIG (“PConc (high)”), the LRV decay is very low in general and the dependency of the protein binding capacity is low as well. This suggests that the membrane surface and/or the surface of PP7 are shielded from

each other by IVIG in a way that changes so that the protein binding capacity has only little effect on the LRV decay.

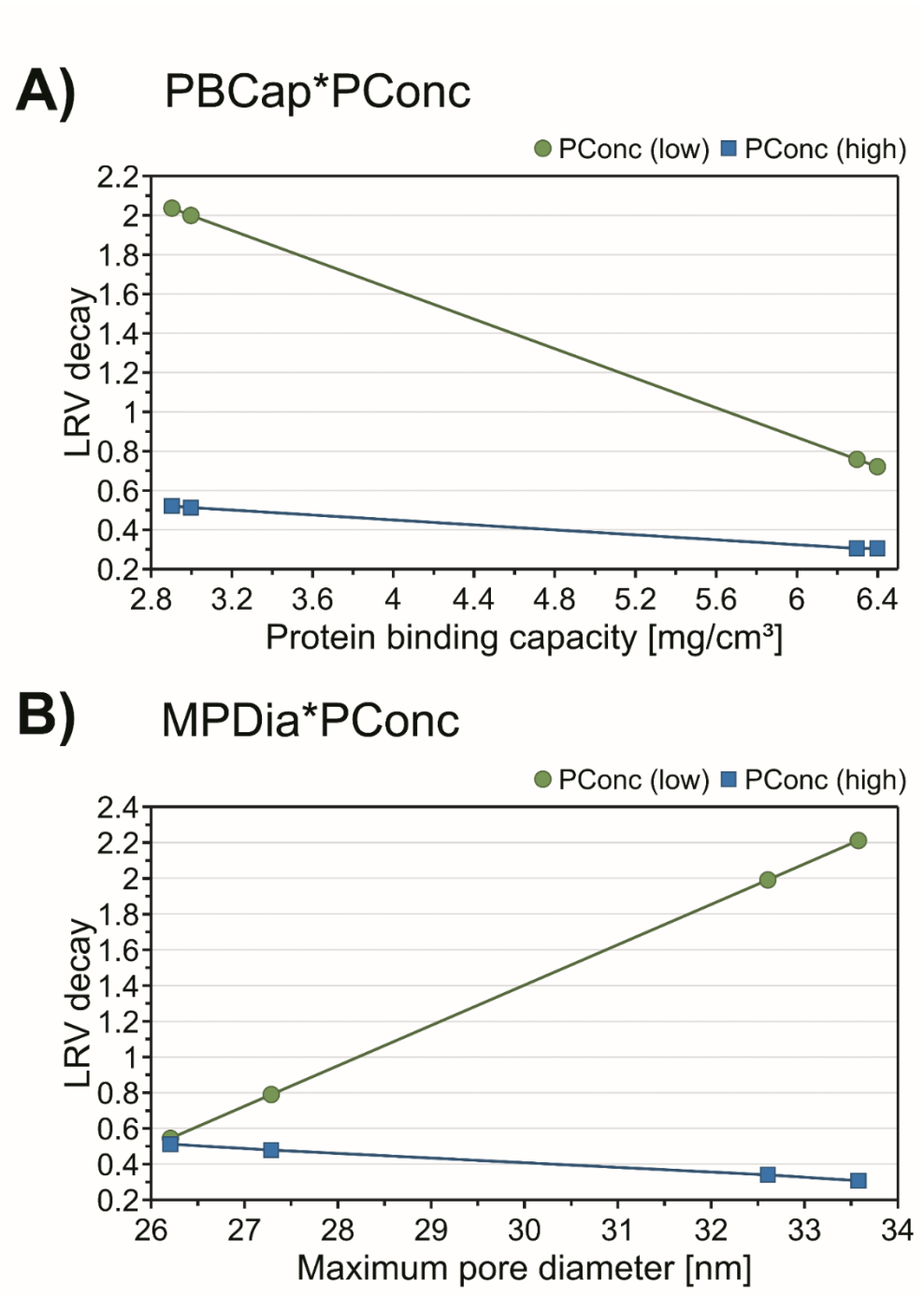

Fig. 6. Interaction plots for protein binding capacity and protein concentration (PBCap*PConc) (A) and for maximum pore diameter and protein concentration (MPDia*PConc) (B) with respect to the LRV decay.

A very interesting interaction is the significant negative interaction between the maximum pore diameter and the protein concentration (MPDia*PConc) (Fig. 6 B). In the presence of IVIG, the LRV decay is low and shows only a negligible dependence on the maximum pore diameter as discussed before. In the absence of IVIG, a strong dependence of the maximum pore diameter can be observed. Membranes with a larger maximum pore diameter exhibit a very significant LRV decay, while lowering the maximum pore diameter within the tested range drastically reduces the LRV decay. From a membrane manufacturer's perspective, these results indicate that retention robustness with respect to LRV decay as a consequence of a FI can be achieved by reducing the maximal pore diameter. These findings are in agreement with a previous study by Kosiol et al. determining pore size distributions of commercial VFM (Kosiol et al., 2017). It was found that the first-generation VFM, that are known to lack retention robustness, exhibit a higher share of larger pores compared to the second-generation VFM that typically do not show significant LRV decays.

The impacts of the pH and the conductivity were found to be significant, however, exhibit lower impacts than all other parameters studied. The impact of the pH on the LRV decay is positive, as similarly observed by other authors using bacteriophage ϕX174 (Dishari et al., 2015a). This could be related to the increasing repulsive electrostatic interaction between PP7 and the VFM as the pH increases. Thus, overall attractive interactions are reduced that could otherwise reduce diffusive movement. The solution conductivity has a similar positive impact on the LRV decay like the pH. The increased solution conductivity results from higher salt concentrations, which cause pore diameters to appear larger and PP7 smaller as consequence from electrostatic charge shielding. Both larger pores and smaller PP7 would favor diffusive movement of PP7 within the pore network.

3.3 Virus retention of commercial second-generation VFM

Besides the mechanistic study using model membranes having a lower retention level, additional filtration experiments were carried out using commercial second-generation VFM. Process and solution conditions were adopted from the DoE study, including the worst-case solution conditions high pH and high conductivity.

In contrast to the model VFM, the commercial products exhibit high levels of virus retention, having LRVs typically >= 6 (Fig. 7). With respect to the upper LRV detection limit of the assay

between 6.2 and 6.8, most results for Virosart® CPV and Virosart® HC are above the detection limit, showing no detectable virus breakthrough. Results for Virosart® HF show detectable virus breakthrough for a larger number of filtration runs but still having high LRVs, mostly 6 and higher.

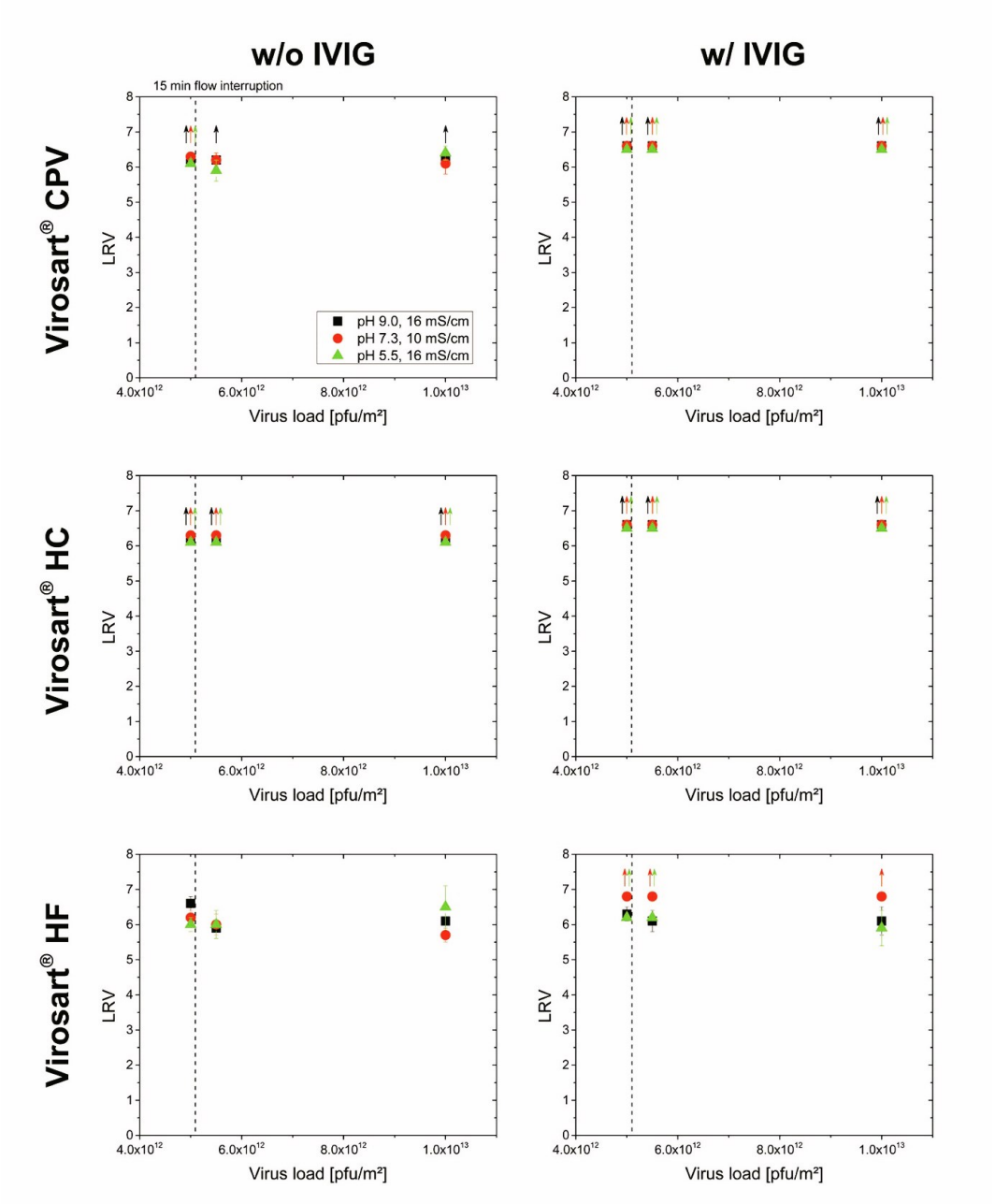

Fig. 7. PP7 retention data of commercial second-generation VFM (Virosart® CPV, Virosart® HC and Virosart® HF) at different solutions conditions adopted from the DoE study including a 15 min FI. The upper LRV detection limits are between 6.2 and 6.8. All data points represent the mean values of duplicate filtration runs, while error bars represent plus/minus one standard deviation. Arrows indicate duplicate filtration runs without any virus breakthroughs observed.

With respect to solution (pH and presence of IVIG) and process (FI) conditions no systematic differences are observed for the initial LRV and the LRV decay, indicating high retention robustness.

4. Conclusions

A holistic study using low retentive non-commercial model membranes was conducted to investigate the virus retention mechanisms during typical process-related flow conditions (initial LRV) and after a FI (LRV decay) as a function of membrane properties and solution conditions. The study supports the current understanding that the initial LRV is dominated by a size exclusion based retention mechanism and thereby is mostly influenced by the maximum pore diameter. Further, the LRV decay after a FI is reported by numerous authors to be based on a diffusive reorganization of previously constrained virus particles by retentive pores within the membrane structure with a certain chance for each virus particle to reach a non-retentive pore. The results of this study are consistent with the reported diffusion based mechanism and extended for interactions of the virus with the membrane surface and other species or conditions in the feed. During the FI, adsorptive interactions between the virus and the membrane surface as well as the protein present in the solution probably lead to a lower effective diffusion rate and, consequently, a significantly reduced LRV decay. The data also indicate that robustness against LRV decays can be achieved by reduction of the maximum pore diameters (and the share of non-retentive pores). This strategy was successfully incorporated in the development of the second-generation of commercial VFM, which exhibit high overall retention levels and high retention robustness with respect to varying solution and process conditions.

Acknowledgements

The authors thank Tabea Streil, Pia-Vanessa Lehmann, Miriam Börger and Andreas Schwerdt from the Sartorius phage lab team for their support conducting the phage filtration experiments.

References

Aranha-Creado H, Brandwein H. 1999. Application of bacteriophages as surrogates for mammalian viruses: a case for use in filter validation based on precedents and current practices in medical and environmental virology. *PDA J Pharm Sci Tech* **53**:75–82.

Asper M. 2011. Virus Breakthrough after Pressure Release during Virus Retentive Filtration. *Parenter. Drug Assoc. Virus TSE Saf. Forum*. Barcelona, Spain.

Bolton GR, Cabatingan M, Rubino M, Lute S, Brorson K, Bailey M. 2005. Normal-flow virus filtration: detection and assessment of the endpoint in bioprocessing. *Biotechnol. Appl. Biochem.* **42**:133–142.

Brorson K, Shen H, Lute S, Perez JS, Frey DD. 2008. Characterization and purification of bacteriophages using chromatofocusing. *J. Chromatogr. A* **1207**:110–121.

Chen D, Chen Q. 2016. Virus Retentive Filtration in Biopharmaceutical Manufacturing. *PDA Lett.*:20–22.

Dishari SK, Micklin MR, Sung K-J, Zydney AL, Venkiteshwaran A, Earley JN. 2015a. Effects of solution conditions on virus retention by the Viresolve(®) NFP filter. *Biotechnol. Prog.* **31**:1280–1286.

Dishari SK, Venkiteshwaran A, Zydney AL. 2015b. Probing effects of pressure release on virus capture during virus filtration using confocal microscopy. *Biotechnol. Bioeng.* **112**:2115–2122.

Giglia S, Bohonak D, Greenhalgh P, Leahy A. 2015. Measurement of pore size distribution and prediction of membrane filter virus retention using liquid–liquid porometry. *J. Memb. Sci.* **476**:399–409.

Hansmann B, Meyer A, Henning H, Thom V. 2013. Retentive properties of virus filter membranes in challenging experiments – Understanding virus retention by porous membranes. *Parenter. Drug Assoc. Virus TSE Saf. Forum*. Berlin, Germany.

Helling A, Kubicka A, Schaap IAT, Polakovic M, Hansmann B, Thiess H, Strube J, Thom V. 2017. Passage of soft pathogens through microfiltration membranes scales with transmembrane pressure. *J. Memb. Sci.* **522**:292–302.

Hongo-Hirasaki T. 2015. Optimization of Virus Removal Filtration Processes. *Parenter. Drug Assoc. Virus TSE Saf. Forum*. Lisbon, Portugal.

Johnson S, Brorson KA, Frey DD, Dhar AK, Cetlin DA. 2017. Characterization of Non-Infectious

Virus-Like Particle Surrogates for Viral Clearance Applications. *Appl. Biochem. Biotechnol.* **183**:318–331.

Kosiol P, Hansmann B, Ulbricht M, Thom V. 2017. Determination of pore size distributions of virus filtration membranes using gold nanoparticles and their correlation with virus retention. *J. Memb. Sci.* **533**:289–301.

Kosiol P, Müller MT, Schneider B, Hansmann B, Thom V, Ulbricht M. 2018. Determination of pore size gradients of virus filtration membranes using gold nanoparticles and their relation to fouling with protein containing feed streams. *J. Memb. Sci.* **548**:598–608.

Kreil TR, Wieser A, Berting A, Spruth M, Medek C, Pölsler G, Gaida T, Hämmerle T, Teschner W, Schwarz HP, Barrett PN. 2006. Removal of small nonenveloped viruses by antibody-enhanced nanofiltration during the manufacture of plasma derivatives. *Transfusion* **46**:1143–1151.

Lacasse D, Genest P, Pizzelli K, Greenhalgh P, Mullin L, Slocum A. 2013. Impact of Process Interruption on Virus Retention of Small-Virus Filters. *Bioprocess Int.* **11**:34–44.

LaCasse D, Lute S, Fiadeiro M, Basha J, Stork M, Brorson K, Godavarti R, Gallo C. 2016. Mechanistic Failure Mode Investigation and Resolution of Parvovirus Retentive Filters. *Biotechnol. Prog.* **32**:959–970.

Lei J, Ulbricht M. 2014. Macroinitiator-mediated photoreactive coating of membrane surfaces with antifouling hydrogel layers. *J. Memb. Sci.* **455**:207–218.

Lute S, Bailey M, Combs J, Sukumar M, Brorson K. 2007. Phage passage after extended processing in small-virus-retentive filters. *Biotechnol. Appl. Biochem.* **47**:141–151.

Lute S, Riordan W, Pease III LF, Tsai D, Levy R, Haque M, Martin J, Moroe I, Sato T, Morgan M, Krishnan M, Campbell J, Genest P, Dolan S, Tarrach K, Meyer A, Tarlov MJ, Etzel M, Brorson K. 2008. A Consensus Rating Method for Small Virus-Retentive Filters. I. Method Development. *PDA J Pharm Sci Tech* **62**:318–333.

Marichal-Gallardo PA, Álvarez MM. 2012. State-of-the-Art in Downstream Processing of Monoclonal Antibodies: Process Trends in Design and Validation. *Biotechnol. Prog.* **28**:899–916.

Miesegaes G, Lute S, Aranha H, Brorson K. 2013. Virus Retentive Filters. In: Flickinger, MC, editor. *Downstream Industrial Biotechnology*. Hoboken (New Jersey, USA): John Wiley & Sons, pp. 641–654.

Nguyen TH, Easter N, Gutierrez L, Huyett L, Defnet E, Mylon SE, Ferri JK, Viet NA. 2011. The

RNA core weakly influences the interactions of the bacteriophage MS2 at key environmental interfaces. *Soft Matter* **7**:10449–10456.

PDA. 2008. Technical Report No. 41 - Virus Filtration. *PDA J. Pharm. Sci. Technol.* Bethesda, MD: Parenteral Drug Association. Vol. 62.

Peinador RI, Calvo JI, ToVinh K, Thom V, Prádanos P, Hernández A. 2011. Liquid – liquid displacement porosimetry for the characterization of virus retentive membranes. *J. Memb. Sci.* **372**:366–372.

Ray S, Dolan S. 2011. Single-Use Virus Clearance Technologies in Biopharmaceutical Manufacturing: Case Studies. In: Eibl, R, Eibl, D, editors. *Single-Use Technology in Biopharmaceutical Manufacture*. Hoboken (New Jersey, USA): John Wiley & Sons, pp. 311–322.

Shukla AA, Aranha H. 2015. Pharmaceutical Viral clearance for biopharmaceutical downstream processes. *Pharm. Bioprocess.* **3**:127–138.

Strauss D, Goldstein J, Hongo-Hirasaki T, Yokoyama Y, Hirotomi N, Miyabayashi T, Vacante D. 2017. Characterizing the impact of pressure on virus filtration processes and establishing design spaces to ensure effective parvovirus removal. *Biotechnol. Prog.* **33**:1294-1302.

Trilisky EI, Lenhoff AM. 2009. Flow-Dependent Entrapment of Large Bioparticles in Porous Process Media. *Biotechnol. Bioeng.* **104**:127–133.

Wieser A, Berting A, Medek C, Poelsler G, Kreil TR. 2015. The evolution of down-scale virus filtration equipment for virus clearance studies. *Biotechnol. Bioeng.* **112**:633–7.

Woods MA, Zydney AL. 2014. Effects of a Pressure Release on Virus Retention With the Ultipor DV20 Membrane. *Biotechnol. Bioeng.* **111**:545–551.

World Health Organization. 2004. Guidelines on Viral Inactivation and Removal Procedures Intended to Assure the Viral Safety of Human Blood Plasma Products. Technical Report, Series No. 924, Annex 4. Geneva, Switzerland.

Yamamoto A, Hongo-Hirasaki T, Uchi Y, Hayashida H, Nagoya F. 2014. Effect of Hydrodynamic Forces on Virus Removal Capability of Planova Filters. *AIChE J.* **60**:2286–2297.

Zydney AL, Aimar P, Meireles M, Pimbley JM, Belfort G. 1994. Use of the log-normal probability density function to analyze membrane pore size distributions: Functional forms and discrepancies. *J. Memb. Sci.* **91**:293–298.

Supporting information

Table SI. Experimental conditions selected for DoE study.

Experiment condition	pH	Conductivity	Protein concentration	Protein binding capacity	Maximum pore diameter	Number of replicates
1	-	-	-	-	-	4
2	-	-	-	-	+	4
3	-	-	-	+	-	4
4	-	-	-	+	+	4
5	-	-	+	-	-	2
6	-	-	+	-	+	2
7	-	-	+	+	-	2
8	-	-	+	+	+	2
9	-	+	-	-	-	4
10	-	+	-	-	+	4
11	-	+	-	+	-	4
12	-	+	-	+	+	4
13	-	+	+	-	-	2
14	-	+	+	-	+	2
15	-	+	+	+	-	2
16	-	+	+	+	+	2
17	0	-	-	-	-	4
18	0	-	-	-	+	4
19	0	-	-	+	-	4
20	0	-	-	+	+	4
21	0	0	-	-	-	12
22	0	0	-	-	+	12
23	0	0	+	-	-	6
24	0	0	+	-	+	6
25	0	+	-	-	-	4
26	0	+	-	-	+	4
27	0	+	-	+	-	4
28	0	+	-	+	+	4
29	+	-	-	-	-	4
30	+	-	-	-	+	4
31	+	-	-	+	-	4
32	+	-	-	+	+	4
33	+	-	+	-	-	2
34	+	-	+	-	+	2
35	+	-	+	+	-	2
36	+	-	+	+	+	2
37	+	+	-	-	-	4
38	+	+	-	-	+	4
39	+	+	-	+	-	4
40	+	+	-	+	+	4
41	+	+	+	-	-	2
42	+	+	+	-	+	2
43	+	+	+	+	-	2
44	+	+	+	+	+	2

-: lower limit

0: mid-range value

+: upper limit

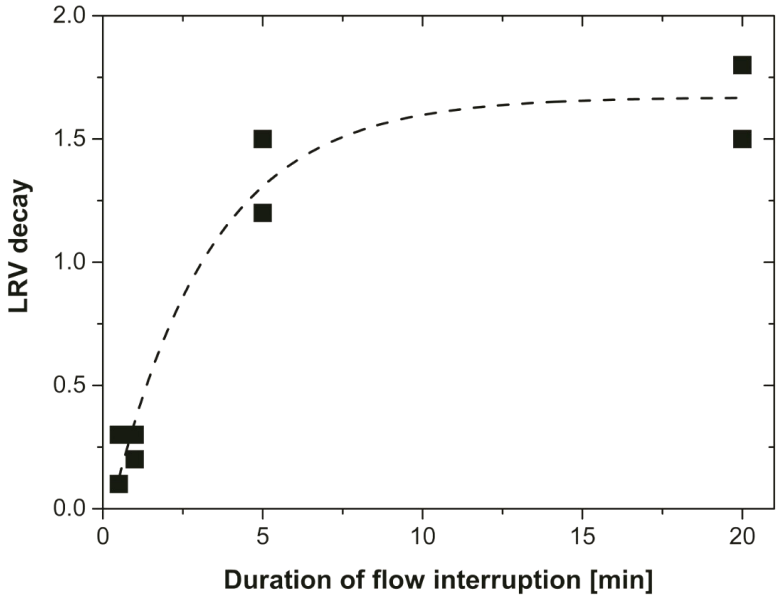

Fig. S1. LRV decay after a FI in dependence of the duration of the FI determined using experimental condition 21 of the DoE study (see Table SI, supporting information). The dashed line represents an empirical fit to the data indicating that the LRV decay after FI is a function of the duration of the FI.

4 Summary and conclusion

Two analytical techniques have been developed that have shown to be capable to determine PSDs and PSGs of VFMs in a quantitative manner. Both techniques are based on retention of GNPs of defined particle diameter in course of filtration experiments. A major drawback, limiting the applicability of nanoparticle retention tests towards low interacting membranes made of RC [16,17,48], originates from GNP adsorption to polymeric materials superimposing retention by size exclusion [43,47,49,55,56]. Based on observations by Liu and Wei, addition of an anionic surfactant to the GNP solution, namely SDS, has shown to minimize adsorption of GNPs to polymeric surfaces [57,58]. In paper 1, the impact of SDS on the retention mechanism of GNPs by porous polymeric membranes was investigated. By increasing the SDS concentration in the equilibration and GNP solution, retention mechanism of GNPs with PES membranes was shifted from an adsorption- to a size exclusion-dominated mechanism. Suppressing GNP adsorption by SDS resolved the main drawback for structural investigations based on GNP retention, extending the applicability towards membranes made from higher interacting materials such as PES. Building on this, in paper 1 PSDs of a broad panel of membranes including commercial and non-commercial VFMs and one UFM were determined by photometrical measurement of the GNP concentrations in the filtrates after separate filtrations using different sized GNPs. Although similar mean pore diameters were found for all membranes, the UFM and the VFMs from first-generation exhibited larger cut-off pore diameters and broader PSDs than the state-of-the-art second-generation VFMs. These results provide a structure-based explanation for the lack of retention robustness often observed for the first-generation VFM [19]. Also, some correlation was observed between the cut-off pore diameter and bacteriophage PP7 retention. This finding is supported by Peinador et al. investigating PSDs of homologous model VFMs, showing that virus retention correlates best with the maximum pore diameters rather than with the mean or minimum pore diameters [34]. A better correlation between pore diameter and virus retention throughout a broad set of different VFMs could be potentially found also using a suitable detergent in the virus containing solution suppressing possible virus adsorption. However, some effort will be required to find a suitable detergent that does not reduce virus infectivity, which is a prerequisite for the virus quantification assay.

Complementary to the analysis of PSDs by determination of GNP concentrations in the filtrates, PSGs were derived within paper 2 from the position of retained particles inside the same membrane samples already used within paper 1. Due to the funnel-like structure of the VFMs with the larger pores facing towards the feed, GNPs of a certain size are retained at a distinct depth of the membrane causing a local discolouration. From microscopic analysis of membrane cross-sections, the position of the discolouration was determined providing information on the effective pore diameter at this depth of the membrane. By using different sized GNPs ranging from 5-50 nm, effective pore diameters were estimated at different depths of the membrane close to the SAL. Quantitative PSGs were obtained as slopes from linear fits of pore diameter against membrane depth. For one membrane type, the PSG was also determined by image analysis of pristine membrane samples by measuring the mean free path lengths, a method adapted from Ziel et al. [69]. Although both techniques provided very similar PSGs, the magnitude of pore diameters estimated from measurement of the mean free path lengths was significantly larger compared to the GNP based technique. This deviation can be easily attributed to the use of the mean free path length as gross simplification of the pore diameter, also measuring other parts of the pore void than the bottleneck pore diameter, which is most relevant for the size exclusion properties. Thereby, based on size exclusion, pore size determinations by GNP retention in general provide results with higher relevance towards the application of these membranes.

In order to link fouling robustness with the membrane structure, the fouling mechanism and the fouling species of IVIG were determined in paper 2. Using DLS for comparing size distributions in feed stream and filtrates, it was found that small aggregates retained by the VFM, probably in the size range of 16-30 nm, are the main cause for fouling and foul the membrane mostly by size exclusion. To further elucidate the nature of the foulants, DLS was applied after fractionation of the IVIG feed stream using HIC. Presence of larger species was observed for fractions containing more hydrophobic species. These results also support the findings by Bolton et al. and Villain that the fouling species in IVIG feed streams are more hydrophobic than the majority of IgG monomers, but contradict these authors with respect to the size of these foulants [94,99]. In a comparable previous experiment by Villain using SEC instead of DLS in combination with HIC, no differences between HIC fractions were observed with respect to aggregate levels [99]. It was already suspected by Villain that disruption of

reversible aggregates might have occurred, which was caused by the SEC procedure. The present DLS results further raise a doubt on the previous SEC based studies.

In context of a fouling mechanism of IVIG mainly caused by size exclusion of small aggregates, protein mass throughputs of all membranes were determined in paper 2 using IVIG. A correlation between protein mass throughput and PSG was observed. VFMs having steep PSGs exhibited by several orders of magnitude lower protein mass throughputs than VFMs having shallow PSGs. These findings are in accordance to the hypothesis of the membrane structure located between the feed and the SAL acting as a depth pre-filter, thereby protecting the SAL from early fouling. This can be explained by the fact that VFMs with more shallow PSGs utilize a larger section of their structure to act as a depth pre-filter for foulants that are retained, similar to viruses, by size exclusion.

Due to the high complexity of virus retention mechanisms, in addition to paper 1, a deeper, holistic investigation was carried out in paper 3. This DoE-based study using model VFMs was conducted to determine the virus retention mechanisms of bacteriophage PP7 during typical process-related flow conditions (initial LRV) and after a FI (LRV decay) as a function of membrane properties and solution conditions. A unique feature of this study is the use of VFMs having specifically designed PSDs and protein binding capacities as measure for the interaction of proteins with the membrane, which is presumably also valid for the interaction between non-enveloped viruses and the membrane. The study supports the current understanding that the initial LRV is dominated by a size exclusion based retention mechanism and thereby is mostly influenced by the maximum pore diameter, as was already observed in paper 1. Further, the LRV decay after a FI is reported by numerous authors to be based on a diffusive reorganization of previously constrained virus particles by retentive pores within the membrane structure with a certain chance for each virus particle to reach a non-retentive pore [87,88]. The results of this study are consistent with the reported diffusion-based mechanism. The current understanding is also extended by the present thesis for interactions of the virus with the membrane surface and other species or conditions in the feed. Biophysical characterization using DLS was carried out to assess virus-virus, virus-protein and protein-protein interactions in solution under the diverse solution conditions including different pH and solution conductivities. During the FI, adsorptive interactions between the virus and the membrane surface as well as the protein present in the solution probably lead to a lower effective diffusion rate of the viruses and, consequently, a significantly reduced LRV

decay. The data also indicate that robustness against LRV decays can be achieved by reduction of the maximum pore diameters (and the share of non-retentive pores). This strategy was successfully incorporated in the development of the second-generation of commercial VFM, which exhibit high overall retention levels and high retention robustness with respect to varying solution and process conditions.

5 References

[1] FDA, Guidance for industry - Q5A viral safety evaluation derived from cell lines of human or animal origin, 1998.

[2] WHO, Guidelines on viral inactivation and removal procedures intended to assure the viral safety of human blood plasma products, Technical report, Series No. 924, Annex 4, 2004.

[3] G. Miesegaes, S. Lute, K. Brorson, Analysis of viral clearance unit operations for monoclonal antibodies, Biotechnol. Bioeng. 106 (2010) 238–246.

[4] G. Miesegaes, S. Lute, H. Aranha, K. Brorson, Virus retentive filters, in: M.C. Flickinger (Ed.), Downstream Industrial Biotechnology, John Wiley & Sons, Hoboken (New Jersey, USA), 2013: pp. 641–654.

[5] R. Esfandiary, D.B. Hayes, A. Parupudi, J. Casas-Finet, S. Bai, H.S. Samra, A.U. Shah, H.A. Sathish, A systematic multitechnique approach for detection and characterization of reversible self-association during formulation development of therapeutic antibodies, J. Pharm. Sci. 102 (2013) 3089–3099.

[6] FDA, Points to consider in the manufacture and testing of monoclonal antibody products for human use, 1997.

[7] V. Bethencourt, Virus stalls Genzyme plant, Nat. Biotechnol. 27 (2009) 681–681.

[8] O.W. Merten, Virus contaminations of cell cultures - A biotechnological view, Cytotechnology. 39 (2002) 91–116.

[9] Reuters staff, Timeline - Key dates in Genzyme's manufacturing crisis, Reuters. (2010). https://www.reuters.com/article/genzyme/timeline-key-dates-in-genzymes-manufacturing-crisis-idUSN1321252820100813 (accessed November 19, 2017).

[10] P.F. Dimond, Genzyme plant shutdown could mean up to $300M in lost sales, Genet. Eng. Biotechnol. News. (2009). https://www.genengnews.com/gen-exclusives/genzyme-plant-shutdown-could-mean-up-to-300m-in-lost-sales/57506615 (accessed November 19, 2017).

[11] EMEA, Guideline on virus safety evaluation of biotechnological investigational medicinal products, 2006.

[12] P.A. Marichal-Gallardo, M.M. Álvarez, State-of-the-art in downstream processing of monoclonal antibodies: process trends in design and validation, Biotechnol. Prog. 28

(2012) 899–916.

[13] A. Manzke, Virus risk mitigation in cell culture media – trends and developments. Presented at Informa viral safety & raw materials congress, Vienna (Austria), (2015).

[14] Y. Hamamoto, S. Harada, S. Kobayashi, K. Yamaguchi, H. Iijima, S. Manabe, T. Tsurumi, H. Aizawa, N. Yamamoto, A novel method for removal of human immunodeficiency virus: filtration with porous polymeric membranes, Vox Sang. 56 (1989) 230–236.

[15] A.J. DiLeo, A.E. Allegrezza Jr., S.E. Builder, High resolution removal of virus from protein solutions using a membrane of unique structure, Nat. Biotechnol. 10 (1992) 182–188.

[16] K. Yamaguchi, Y. Hamamoto, S. Manabe, N. Yamamoto, Microparticle removability of the regenerated cellulose hollow fiber (BMM): an electron microscopic evaluation, J. Electron Microsc. 40 (1991) 337–345.

[17] T. Hongo-Hirasaki, K. Yamaguchi, K. Yanagida, K. Okuyama, Removal of small viruses (parvovirus) from IgG solution by virus removal filter Planova® 20N, J. Memb. Sci. 278 (2006) 3–9.

[18] R. Cameron, K. Smith, Virus clearance methods applied in bioprocessing operations: an overview of selected inactivation and removal methods, Pharm. Bioprocess. 2 (2014) 75–83.

[19] D. Chen, Q. Chen, Virus retentive filtration in biopharmaceutical manufacturing, PDA Lett. (2016) 20–22.

[20] PDA, Technical Report No. 41 - Virus Filtration, Parenteral Drug Association, Bethesda (USA), 2008.

[21] Z.H. Syedain, D.M. Bohonak, A.L. Zydney, Protein fouling of virus filtration membranes: effects of membrane orientation and operating conditions, Biotechnol. Prog. 22 (2006) 1163–1169.

[22] T. Hongo-Hirasaki, M. Komuro, S. Ide, Effect of antibody solution conditions on filter performance for virus removal filter Planova 20N, Biotechnol. Prog. 26 (2010) 1080–1087.

[23] M. Mulder, Basic of Principles of Membrane Technology, 2nd ed., Kluwer Academic Publishers, Dordrecht (The Netherlands), 1996.

[24] E. Drioli, L. Giorno, eds., Comprehensive membrane science and engineering 1, 2nd ed., Elsevier B.V., Oxford (UK), 2017.

[25] M.W. Jornitz, T.H. Meltzer, eds., Filtration and purification in the biopharmaceutical

industry, 2nd ed., informa healthcare, New York (USA), 2008.

[26] Z. Xu, X. Huang, L. Wan, Surface engineering of polymer membranes, 1st ed., Springer Berlin Heidelberg, Berlin (Germany), 2009.

[27] S. Giglia, D. Bohonak, P. Greenhalgh, A. Leahy, Measurement of pore size distribution and prediction of membrane filter virus retention using liquid–liquid porometry, J. Memb. Sci. 476 (2015) 399–409.

[28] A.L. Zydney, P. Aimar, M. Meireles, J.M. Pimbley, G. Belfort, Use of the log-normal probability density function to analyze membrane pore size distributions: Functional forms and discrepancies, J. Memb. Sci. 91 (1994) 293–298.

[29] C. Charcosset, Membrane Processes in Biotechnology and Pharmaceutics, 1st ed., Elsevier B.V., Oxford (UK), 2012.

[30] S.R. Wickramasinghe, E.D. Stump, D.L. Grzenia, S.M. Husson, J. Pellegrino, Understanding virus filtration membrane performance, J. Memb. Sci. 365 (2010) 160–169.

[31] T. Urase, K. Yamamoto, S. Ohgaki, Effect of pore structure of membranes and module configuration on virus retention, J. Memb. Sci. 115 (1996) 21–29.

[32] S. Lute, M. Bailey, J. Combs, M. Sukumar, K. Brorson, Phage passage after extended processing in small-virus-retentive filters, Biotechnol. Appl. Biochem. 47 (2007) 141–151.

[33] K. Tung, K. Chang, T. Wu, N. Lin, K. Lee, J. Lai, Recent advances in the characterization of membrane morphology, Curr. Opin. Chem. Eng. 4 (2014) 121–127.

[34] R.I. Peinador, J.I. Calvo, K. ToVinh, V. Thom, P. Prádanos, A. Hernández, Liquid – liquid displacement porosimetry for the characterization of virus retentive membranes, J. Memb. Sci. 372 (2011) 366–372.

[35] P. Kosiol, B. Hansmann, M. Ulbricht, V. Thom, Structure analysis of virus filters via gold nanoparticles and liquid-liquid displacement porometry. Presented at PDA Virus & TSE Safety Forum, Lisbon (Portugal), (2015).

[36] J.I. Calvo, A. Bottino, G. Capannelli, A. Hernández, Comparison of liquid – liquid displacement porosimetry and scanning electron microscopy image analysis to characterise ultrafiltration track-etched membranes, J. Memb. Sci. 239 (2004) 189–197.

[37] M.W. Phillips, A.J. DiLeo, A validatible porosimetric technique for verifying the integrity of virus-retentive membranes, Biologicals. 24 (1996) 243–253.

[38] I.M. Wienk, B. Folkers, T. van den Boomgaard, C.A. Smolders, Critical factors in the determination of the pore size distribution of ultrafiltration membrances using the liquid displacement method, Sep. Sci. Technol. 29 (1994) 1433–1440.

[39] R.I. Peinador, J.I. Calvo, P. Prádanos, L. Palacio, A. Hernández, Characterisation of polymeric UF membranes by liquid – liquid displacement porosimetry, J. Memb. Sci. 348 (2010) 238–244.

[40] M.L. Méndez, A.I. Romero, V.B. Rajal, E.F. Castro, J.I. Calvo, L. Palacio, A. Hernández, Properties of polyethersulfone ultrafiltration membranes modified with polyethylene glycols, Polym. Eng. Sci. 54 (2014) 1211–1221.

[41] M. Bakhshayeshi, D.M. Kanani, A. Mehta, R. van Reis, R. Kuriyel, N. Jackson, A.L. Zydney, Dextran sieving test for characterization of virus filtration membranes, J. Memb. Sci. 379 (2011) 239–248.

[42] S.R. Wickramasinghe, S.E. Bower, Z. Chen, A. Mukherjee, S.M. Husson, Relating the pore size distribution of ultrafiltration membranes to dextran rejection, J. Memb. Sci. 340 (2009) 1–8.

[43] A. Duek, E. Arkhangelsky, R. Krush, A. Brenner, V. Gitis, New and conventional pore size tests in virus-removing membranes, Water Res. 46 (2012) 2505–2514.

[44] E. Arkhangelsky, V. Gitis, Effect of transmembrane pressure on rejection of viruses by ultrafiltration membranes, Sep. Sci. Technol. 62 (2008) 619–628.

[45] C. Agarwal, A.K. Pandey, S. Das, M.K. Sharma, D. Pattyn, P. Ares, A. Goswami, Neck-size distributions of through-pores in polymer membranes, J. Memb. Sci. 415-416 (2012) 608–615.

[46] E. Arkhangelsky, Y. Sefi, B. Hajaj, G. Rothenberg, V. Gitis, Kinetics and mechanism of plasmid DNA penetration through nanopores, J. Memb. Sci. 371 (2011) 45–51.

[47] E. Arkhangelsky, A. Duek, V. Gitis, Maximal pore size in UF membranes, J. Memb. Sci. 394-395 (2012) 89–97.

[48] T. Tsurumi, N. Osawa, T. Hirasaki, K. Yamaguchi, S. Manabe, T. Yamashiki, Mechanism of removing monodisperse gold particles from a suspension using cuprammonium regenerated cellulose hollow fiber, Polym. J. 22 (1990) 304–311.

[49] T. Mizuno, A. Namiki, S. Tsuzuki, A novel filter rating method using less than 30-nm gold nanoparticle and protective ligand, IEEE Trans. Semicond. Manuf. 22 (2009) 452–461.

[50] H. Susanto, S. Franzka, M. Ulbricht, Dextran fouling of polyethersulfone ultrafiltration

membranes - Causes, extent and consequences, J. Memb. Sci. 296 (2007) 147–155.

[51] A. Helling, A. Kubicka, I.A.T. Schaap, M. Polakovic, B. Hansmann, H. Thiess, J. Strube, V. Thom, Passage of soft pathogens through microfiltration membranes scales with transmembrane pressure, J. Memb. Sci. 522 (2017) 292–302.

[52] M. Ramos, L. Ortiz-Jordan, A. Hurtado-Macias, S. Flores, J.T. Elizalde-Galindo, C. Rocha, B. Torres, M. Zarei-Chaleshtori, R.R. Chianelli, Hardness and elastic modulus on six-fold symmetry gold nanoparticles, Materials (Basel). 6 (2013) 198–205.

[53] T. Hirasaki, T. Noda, H. Nakano, Y. Ishizaki, S. Manabe, N. Yamamoto, Mechanism of removing Japanese encephalitis virus (JEV) and gold particles using cuprammonium regenerated cellulose hollow fiber (i-BMM or BMM) from aqueous solution containing protein, Polym. J. 26 (1994) 1244–1256.

[54] P.L. Roberts, P. Feldman, D. Crombie, C. Walker, K. Lowery, Biologicals Virus removal from factor IX by filtration: Validation of the integrity test and effect of manufacturing process conditions, Biologicals. 38 (2010) 303–310.

[55] D.A. Ladner, M. Steele, A. Weir, K. Hristovski, P. Westerhoff, Functionalized nanoparticle interactions with polymeric membranes, J. Hazard. Mater. 211-212 (2012) 288–295.

[56] S.-C. Chen, D. Segets, T.-Y. Ling, W. Peukert, D.Y.H. Pui, An experimental study of ultrafiltration for sub-10nm quantum dots and sub-150 nm nanoparticles through PTFE membrane and Nuclepore filters, J. Memb. Sci. 497 (2016) 153–161.

[57] G.-T. Wei, F.-K. Liu, Separation of nanometer gold particles by size exclusion chromatography, J. Chromatogr. A. 836 (1999) 253–260.

[58] F. Liu, G. Wei, Effect of mobile-phase additives on separation of gold nanoparticles by size-exclusion chromatography, Chromatographia. 59 (2004) 115–119.

[59] N. Hamasaki, S. Ide, Method for test on integrity of microporous membrane, WO2008/111510 A1, 2008.

[60] B. Hansmann, A. Meyer, H. Henning, V. Thom, Retentive properties of virus filter membranes in challenging experiments – Understanding virus retention by porous membranes. Presented at PDA Virus & TSE Safety Forum, Berlin (Germany), Parenter. Drug Assoc. Virus TSE Saf. Forum. (2013).

[61] T. Burnouf, M. Radosevich, Nanofiltration of plasma-derived biopharmaceutical products, Haemophilia. 9 (2003) 24–37.

[62] D.M. Bohonak, A.L. Zydney, Compaction and permeability effects with virus filtration membranes, J. Memb. Sci. 254 (2005) 71–79.

[63] M. Bakhshayeshi, A.L. Zydney, Effect of solution pH on protein transmission and membrane capacity during virus filtration, Biotechnol. Bioeng. 100 (2008) 108–117.

[64] J.G. Barnard, D. Kahn, D. Cetlin, T.W. Randolph, J.F. Carpenter, Investigations into the fouling mechanism of parvovirus filters during filtration of freeze-thawed mAb drug substance solutions, J. Pharm. Sci. 103 (2014) 890–9.

[65] M. Marroquin, A. Vu, T. Bruce, R. Powell, S.R. Wickramasinghe, S.M. Husson, Location and quantification of biological foulants in a wet membrane structure by cross-sectional confocal laser scanning microscopy, J. Memb. Sci. 453 (2014) 282–291.

[66] D.M. Kanani, X. Sun, R. Ghosh, Reversible and irreversible membrane fouling during in-line microfiltration of concentrated protein solutions, J. Memb. Sci. 315 (2008) 1–10.

[67] S. Nakao, Determination of pore size and pore size distribution, J. Memb. Sci. 96 (1994) 131–165.

[68] I. Masselin, L. Durand-Bourlier, J.-M. Laine, P.-Y. Sizaret, X. Chasseray, D. Lemordant, Membrane characterization using microscopic image analysis, J. Memb. Sci. 186 (2001) 85–96.

[69] R. Ziel, A. Haus, A. Tulke, Quantification of the pore size distribution (porosity profiles) in microfiltration membranes by SEM, TEM and computer image analysis, J. Memb. Sci. 323 (2008) 241–246.

[70] T. Li, X. Lu, B. Wang, Z. Wu, K. Li, D.J.L. Brett, P.R. Shearing, X-ray tomography-assisted study of a phase inversion process in ceramic hollow fiber systems – Towards practical structural design, J. Memb. Sci. 528 (2017) 24–33.

[71] J. Viguié, T. Savart, P. Duru, J.-C. Rouch, J.-C. Remigy, Characterisation of 3D porous macrostructure of hollow fibre membranes using X-ray tomography — Effects of some spinning process conditions, J. Memb. Sci. 435 (2013) 11–20.

[72] H. Reingruber, A. Zankel, C. Mayrhofer, P. Poelt, Quantitative characterization of microfiltration membranes by 3D reconstruction, J. Memb. Sci. 372 (2011) 66–74.

[73] G. Sundaramoorthi, M. Hadwiger, M. Ben-Romdhane, A.R. Behzad, P. Madhavan, S.P. Nunes, 3D membrane imaging and porosity visualization, Ind. Eng. Chem. Res. 55 (2016) 3689–3695.

[74] M. Bakhshayeshi, N. Jackson, R. Kuriyel, A. Mehta, R. Van Reis, A.L. Zydney, Use of

confocal scanning laser microscopy to study virus retention during virus filtration, J. Memb. Sci. 379 (2011) 260–267.

[75] S.K. Dishari, A. Venkiteshwaran, A.L. Zydney, Probing effects of pressure release on virus capture during virus filtration using confocal microscopy, Biotechnol. Bioeng. 112 (2015) 2115–2122.

[76] S.K. Dishari, M.R. Micklin, K.-J. Sung, A.L. Zydney, A. Venkiteshwaran, J.N. Earley, Effects of solution conditions on virus retention by the Viresolve(®) NFP filter, Biotechnol. Prog. 31 (2015) 1280–1286.

[77] E.M. van Voorthuizen, N.J. Ashbolt, A.I. Schäfer, Role of hydrophobic and electrostatic interactions for initial enteric virus retention by MF membranes, J. Memb. Sci. 194 (2001) 69–79.

[78] C.L. Heldt, A. Zahid, K.S. Vijayaragavan, X. Mi, Experimental and computational surface hydrophobicity analysis of a non-enveloped virus and proteins, Colloids Surfaces B Biointerfaces. 153 (2017) 77–84.

[79] G.R. Bolton, M. Cabatingan, M. Rubino, S. Lute, K. Brorson, M. Bailey, Normal-flow virus filtration: detection and assessment of the endpoint in bioprocessing, Biotechnol. Appl. Biochem. 42 (2005) 133–142.

[80] T.R. Kreil, A. Wieser, A. Berting, M. Spruth, C. Medek, G. Pölsler, T. Gaida, T. Hämmerle, W. Teschner, H.P. Schwarz, P.N. Barrett, Removal of small nonenveloped viruses by antibody-enhanced nanofiltration during the manufacture of plasma derivatives, Transfusion. 46 (2006) 1143–1151.

[81] D.M. Strauss, J. Goldstein, T. Hongo-Hirasaki, Y. Yokoyama, N. Hirotomi, T. Miyabayashi, D. Vacante, Characterizing the impact of pressure on virus filtration processes and establishing design spaces to ensure effective parvovirus removal, Biotechnol. Prog. 33 (2017) 1294–1302.

[82] M. Asper, Virus breakthrough after pressure release during virus retentive filtration. Presented at PDA Virus & TSE Safety Forum, Barcelona (Spain), (2011).

[83] T. Hongo-Hirasaki, Optimization of virus removal filtration processes. Presented at PDA Virus & TSE Safety Forum, Lisbon (Portugal), Parenter. Drug Assoc. Virus TSE Saf. Forum. (2015).

[84] D. LaCasse, P. Genest, K. Pizzelli, P. Greenhalgh, L. Mullin, A. Slocum, Impact of process interruption on virus retention of small-virus filters, Bioprocess Int. 11 (2013) 34–44.

[85] D. LaCasse, S. Lute, M. Fiadeiro, J. Basha, M. Stork, K. Brorson, R. Godavarti, C. Gallo, Mechanistic failure mode investigation and resolution of parvovirus retentive filters, Biotechnol. Prog. 32 (2016) 959–970.

[86] M.A. Woods, A.L. Zydney, Effects of a pressure release on virus retention with the Ultipor DV20 membrane, Biotechnol. Bioeng. 111 (2014) 545–551.

[87] E.I. Trilisky, A.M. Lenhoff, Flow-dependent entrapment of large bioparticles in porous process media, Biotechnol. Bioeng. 104 (2009) 127–133.

[88] A. Yamamoto, T. Hongo-Hirasaki, Y. Uchi, H. Hayashida, F. Nagoya, Effect of hydrodynamic forces on virus removal capability of Planova filters, AIChE J. 60 (2014) 2286–2297.

[89] C. Spiess, Q. Zhai, P.J. Carter, Alternative molecular formats and therapeutic applications for bispecific antibodies, Mol. Immunol. 67 (2015) 95–106.

[90] H.L. Perez, P.M. Cardarelli, S. Deshpande, S. Gangwar, G.M. Schroeder, G.D. Vite, R.M. Borzilleri, Antibody-drug conjugates: current status and future directions., Drug Discov. Today. 19 (2014) 869–81.

[91] A. Beck, J.M. Reichert, Antibody-drug conjugates: present and future, MAbs. 6 (2014) 15–7.

[92] A. Buchacher, W. Kaar, Intravenous Immunoglobulin G from human plasma - Purification concepts and important quality criteria, in: J. Bertolini, N. Goss, J. Curling (Eds.), Production of Plasma Proteins for Therapeutic Use, 1st ed., WILEY, Hoboken (USA), 2013.

[93] A. Brown, C. Bechtel, J. Bill, H. Liu, J. Liu, D. Mcdonald, S. Pai, A. Radhamohan, R. Renslow, B. Thayer, S. Yohe, C. Dowd, Increasing parvovirus filter throughput of monoclonal antibodies using ion exchange membrane adsorptive pre-filtration, Biotechnol. Bioeng. 106 (2010) 627–637.

[94] G.R. Bolton, S. Spector, D. LaCasse, Increasing the capacity of parvovirus-retentive membranes: performance of the Viresolve Prefilter, Biotechnol. Appl. Biochem. 63 (2006) 55–63.

[95] R. Reindl, P. Ru, R. Mu, Adsorption behavior of a surfactant and a monoclonal antibody to sterilizing-grade filters, J. Pharm. Sci. 99 (2010) 2620–2627.

[96] J.A. Koehler, M. Ulbricht, G. Belfort, Intermolecular forces between a protein and a hydrophilic modified polysulfone film with relevance to filtration, Langmuir. 16 (2000)

10419–10427.

[97] K. Nakamura, K. Matsumoto, Properties of protein adsorption onto pore surface during microfiltration: Effects of solution environment and membrane hydrophobicity, J. Memb. Sci. 280 (2006) 363–374.

[98] G.A. Truskey, R. Gabler, A. DiLeo, T. Manter, The effect of membrane filtration upon protein conformation, PDA J Pharm Sci Tech. 41 (1987) 180–193.

[99] L. Villain, High capacity membrane design for size exclusion based virus removal, Dissertation, Universität Hannover, 2010.

[100] A.S. Sediq, R.B. van Duijvenvoorde, W. Jiskoot, M.R. Nejadnik, No touching! Abrasion of adsorbed protein is the root cause of subvisible particle formation during stirring., J. Pharm. Sci. 105 (2016) 519–29.

[101] L. Brückl, T. Schröder, S. Scheler, R. Hahn, C. Sonderegger, The effect of shear on the structural conformation of rhGH and IgG1 in free solution., J. Pharm. Sci. 105 (2016) 1810–8.

[102] A.T. Lee, A.J. McHugh, The effect of simple shear flow on the helix – Coil transition of poly-L-lysine, Biopolymers. 50 (1999) 589–594.

[103] I.B. Bekard, P. Asimakis, C.L. Teoh, T. Ryan, G.J. Howlett, J. Bertolini, D.E. Dunstan, Bovine serum albumin unfolds in Couette flow, Soft Matter. 8 (2012) 385–389.

[104] J.S. Bee, J.L. Stevenson, B. Mehta, J. Svitel, J. Pollastrini, R. Platz, E. Freund, J.F. Carpenter, T.W. Randolph, Response of a concentrated monoclonal antibody formulation to high shear, Biotechnol. Bioeng. 103 (2009) 936–943.

[105] J. Jaspe, S.J. Hagen, Do protein molecules unfold in a simple shear flow?, Biophys. J. 91 (2006) 3415–3424.

[106] J. De Souza, K. Scott, P. Genest, Virus-filtration development optimization, Bioprocess Int. 41 (2016) 62–74.

[107] G. Miesegaes, M. Bailey, H. Willkommen, Q. Chen, D. Roush, J. Blümel, K. Brorson, Proceedings of the 2009 Viral Clearance Symposium, Dev Biol. 133 (2010) 3–101.

[108] R. Falkenstein, S. Hepbildikler, W. Kuhne, T. Lemm, H. Rogl, E. Rosenberg, G. Winter, F. Zettl, R. Zippelius, Protein purification and its relation to protein aggregation, in: H.-C. Mahler, W. Jiskoot (Eds.), Analysis of Aggregates and Particles in Protein Pharmaceuticals, 1st ed., WILEY, Hoboken (USA), 2012: pp. 350–354.

[109] B.F. Marques, D.J. Roush, K.E. Goeklen, Virus filtration of high-concentration

monoclonal antibody solutions, Biotechnol. Prog. 25 (2009) 483–491.

[110] S.X. Liu, J.-T. Kim, S. Kim, Effect of polymer surface modification on polymer-protein interaction via hydrophilic polymer grafting, J. Food Sci. 73 (2008) E143–50.

[111] H. Susanto, N. Stahra, M. Ulbricht, High performance polyethersulfone microfiltration membranes having high flux and stable hydrophilic property, J. Memb. Sci. 342 (2009) 153–164.

[112] V. Kochkodan, D.J. Johnson, N. Hilal, Polymeric membranes: Surface modification for minimizing (bio) colloidal fouling, Adv. Colloid Interface Sci. 206 (2014) 116–140.

[113] D. Rana, T. Matsuura, Surface modifications for antifouling membranes, Chem. Rev. 110 (2010) 2448–2471.

[114] K.C. Khulbe, C. Feng, T. Matsuura, The art of surface modification of synthetic polymeric membranes, J. Appl. Polym. Sci. 115 (2009) 855–895.

[115] J. Ayyavoo, T.P.N. Nguyen, B.-M. Jun, I.-C. Kim, Y.-N. Kwon, Protection of polymeric membranes with antifouling surfacing via surface modifications, Colloids Surfaces A Physicochem. Eng. Asp. 506 (2016) 190–201.

[116] G.R. Bolton, J. Basha, D.P. Lacasse, Achieving high mass-throughput of therapeutic proteins through parvovirus retentive filters, Biotechnol. Prog. 26 (2010) 1671–1677.

[117] W.J. Rayfield, D.J. Roush, R.A. Chmielowski, N. Tugcu, S. Barakat, J.K. Cheung, Prediction of viral filtration performance of monoclonal antibodies based on biophysical properties of feed, AIChE J. 31 (2015) 765–74.

6 Appendix

6.1 List of abbreviations

AEX	anion exchange chromatography
CA	cellulose acetate
CEX	cation exchange chromatography
DF	diafiltration
DLS	dynamic light scattering
DNA	deoxyribonucleic acid
DoE	Design of Experiment
FDA	Food and Drug Administration
FI	flow interruption
Fig.	Figure
GLDP	gas-liquid displacement porometry
GNP	gold nanoparticle
HIC	hydrophobic interaction chromatography
IVIG	intravenous immunoglobulin
LLDP	liquid-liquid displacement porometry
LRV	$\log_{10}$ reduction value
PC	polycarbonate
PDA	Parenteral Drug Association
PES	polyethersulfone
PSD	pore size distribution
PSG	pore size gradient
PVDF	polyvinylidene fluoride
RC	regenerated cellulose
SAL	separation-active layer
SDS	sodium dodecyl sulfate
SEC	size exclusion chromatography
SEM	scanning electron microscopy
TEM	transmission electron microscopy

TFF	tangential flow filtration
UFM	ultrafiltration membrane
UV-Vis	ultraviolet and visible
VFM	virus filtration membrane

6.2 List of figures

6.3 List of tables

6.4 List of publications

Journal articles

P. Kosiol, B. Hansmann, M. Ulbricht, V. Thom, Determination of pore size distributions of virus filtration membranes using gold nanoparticles and their correlation with virus retention, J. Memb. Sci. 533 (2017) 289–301. doi: 10.1016/j.memsci.2017.03.043.

P. Kosiol, M.T. Müller, B. Schneider, B. Hansmann, V. Thom, M. Ulbricht, Determination of pore size gradients of virus filtration membranes using gold nanoparticles and their relation to fouling with protein containing feed streams, J. Memb. Sci. 548 (2018) 598–608. doi: 10.1016/j.memsci.2017.11.048.

P. Kosiol, C. Kahrs, V. Thom, M. Ulbricht, B. Hansmann, Investigation of virus particle retention by size exclusion membranes under different flow regimes, Biotechnol. Prog. (2018) (under revision).

Oral presentations

P. Kosiol, B. Hansmann, M. Ulbricht, V. Thom, Structure analysis of virus filters via gold nanoparticles and liquid-liquid displacement porometry. Presented at PDA Virus & TSE Safety Forum, Lisbon (Portugal), (2015).

P. Kosiol, B. Hansmann, V. Thom, M. Ulbricht, Determination of pore size distributions and pore size gradients of virus filtration membranes via filtration of gold nanoparticles. Presented at Euromembrane, Aachen (Germany), (2015).

P. Kosiol, C. Kahrs, B. Hansmann, M. Ulbricht, V. Thom, Investigation of virus retention mechanisms by size exclusion membranes: The role of membrane properties and solution conditions in different flow regimes. Presented at ACS, San Francisco (USA), (2017).

Poster presentations

P. Kosiol, M. Ulbricht, B. Hansmann, V. Thom, Characterization of virus retentive membranes via filtration of gold nanoparticles. Presented at Gordon Research Conference - Membranes: Materials & Processes, New London (USA), (2014).

P. Kosiol, B. Hansmann, V. Thom, M. Ulbricht, Charakterisierung virus-rückhaltender Membranen mittels Filtration von Goldnanopartikeln und flüssig-flüssig Porometrie. Presented at ProcessNet – Jahrestreffen der Fachgruppen “Fluidverfahrenstechnik” und “Membrantechnik”, Bremen (Germany), (2015).

P. Kosiol, C. Kahrs, B. Hansmann, M. Ulbricht, V. Thom, Mechanistic study of virus particle retention by size exclusion membranes: The interplay of size exclusion and adsorptive action under different flow regimes. Presented at Recovery of Biological Products, Bermuda (UK), (2016).

C. Kahrs, P. Kosiol, B. Hansmann, M. Ulbricht, V. Thom, The influence of flow interruptions on the retention mechanisms of virus particles by virus filters used in downstream processing of biopharmaceuticals: The interplay of size exclusion and adsorptive action under different flow regimes. Presented at Aachener Membran Kolloquium, Aachen (Germany), (2016).

M. Bieberbach, P. Kosiol, M. Bennecke, B. Hansmann, V. Thom, S. Hepbildikler, Mechanisms of virus retentive filter fouling. Presented at ACS, San Francisco (USA), (2017).

6.5 Declaration of own and co-authors' contributions

All experiments were planned, executed, evaluated and processed into manuscripts for publication by Peter Kosiol under supervision of Prof. Dr. Ulbricht (Duisburg-Essen University), Dr. Hansmann (Sartorius) and Dr. Thom (Sartorius). Exceptions to this are summarized below.
For paper 1, execution of virus filtration experiments using bacteriophage PP7 was carried out by staff from the Sartorius microbiology department (Fig. 12) and corresponding experiments using mammalian viruses PCV-2, MVM and HAV were conducted by a third party contract laboratory (Fig. 11).
For paper 2, execution and evaluation of exemplary SEM image analysis of pristine membranes (Fig. 6) were carried out by Dr. Schneider (Sartorius). Execution and evaluation of HIC fractionation (Fig. S1), SEC (Fig. 8), DLS of IVIG solutions (Fig. 9, 10) and flux measurements with IVIG solutions (Fig. 10) were carried out by Ms Müller (master student) under supervision of Peter Kosiol.
For paper 3, execution and evaluation of membrane surface modification, protein binding capacity determination (Table II), virus filtration (Fig. 2, 4, 5, 6, 7) and DLS experiments (Fig. 3) using bacteriophage PP7 were carried out by Ms Kahrs (master student) under supervision of Peter Kosiol. First preliminary results of this study were processed by Ms Kahrs under supervision of Peter Kosiol and presented at the Aachener Membran Kolloquium 2016 (poster) by Ms Kahrs. Ms Kahrs also contributed to the paper manuscript by providing a first draft for the introduction and for the materials and methods sections.

6.6 Curriculum vitae - Peter Kosiol

Der Lebenslauf ist in der Online-Version aus Gründen des Datenschutzes nicht enthalten.